ISSN 1880-6503

Sustainable Humanosphere

BULLETIN OF
RESEARCH INSTITUTE FOR SUSTAINABLE HUMANOSPHERE
KYOTO UNIVERSITY

No. 15 September 2019

PUBLISHED BY
RESEARCH INSTITUTE FOR SUSTAINABLE HUMANOSPHERE
KYOTO UNIVERSITY
UJI, KYOTO 611-0011, JAPAN

‘Sustainable Humanosphere’ is a serial publication issued annually by the Research Institute for Sustainable Humanosphere (RISH) of Kyoto University, which aims to provide a report on the ongoing research at our Institute along with new research field of sustainable humanosphere. This journal will be distributed free of charge and prefers to exchange similar articles with scientific institutions and libraries throughout the world. All communications concerning ‘Sustainable Humanosphere’ should be addressed to Research Institute for Sustainable Humanosphere (RISH), Kyoto University, Gokasho, Uji 611-0011, Japan.
(Email: edit-e-journal@rish.kyoto-u.ac.jp)

CONTENTS

Note

Recent research activities

Abstracts (Ph.D. thesis)

Abstracts (Master thesis)

NOTE

Biological and molecular characterization of Citrus tatter leaf virus in Taiwan

(Center for Exploratory Research on Humanosphere, RISH, Kyoto University)

Chun-Yi Lin

Citrus tatter leaf virus (CTLV) causes chlorotic leaves with bud union incompatibility in citrus scion and its current incidence in Taiwan is 65%. However, the burden of infection has long been underestimated due to its common latency and the serious threat of tatter leaf disease should be investigated and addressed without delay. Here, we evaluated the biological characteristics and genome sequences of Taiwanese isolates. Three full-length sequenced local isolates and phylogenetic analyses revealed similarities with isolates from neighbouring countries, indicating the possible origins of local isolates. Two mild isolates obtained from Liuchen sweet orange (LCd-NA-1) and Kumquat (Kq-6-2-46) were inoculated on indicator plants and exhibited differences in foliar symptom expression and temperature tolerance compared with foreign isolates causing severe disease. In summary, the study provided comprehensive information and a foundation for citrus virus management or further research.

Introduction

Citrus tatter leaf was first reported in latently infected Meyer lemon trees (*Citrus limon* L. Burm.f.) in California imported from China [1]. Typical local chlorotic lesions and systemic mosaic symptoms on the leaves of herbaceous plants have been observed following mechanical CTLV inoculation [2, 3, 4]. CTLV inoculation also causes tattered and chlorotic leaves with bud union incompatibility in citrus scion grafted on *Citrus excelsa*, Rusk trifoliate and Troyer citranges or swingle citrumelos [5]. CTLV is primarily transmitted via mechanical inoculation and infected bud propagation, but no insect vectors have been identified [6].

CTLV is a member of the genus *Capillovirus* (family *Betaflexiviridae*), which includes two species, *Cherry virus A* (CVA) and *Apple stem grooving virus* (ASGV) [7]. The single-stranded, positive-sense genomic CTLV RNA is 6496 nt in length with a 5' cap and 3' poly adenine tail. This sequence contains two open reading frames (ORF1 and ORF2), and multiple functional proteins are translated to perform biological functions.

Tatter leaf disease, one of the four major systemic and endemic citrus diseases in Taiwan, has long been present and is commonly detected up to 50% of total citrus plants in field surveys [8]. Because of its latent infection characteristics, the severity of tatter leaf disease has been underestimated, and few CTLV-related studies have been conducted worldwide. Here, we determined the biological characteristics of different isolates from Rusk citrange or *C. quinoa*. This study provides comprehensive and basic information for CTLV management and further research.

Symptom expression as determined in the CTLV bioassay

In the Rusk citrange test, the indicator plants were more susceptible to Chinese isolates (Table 1). The Sat-HY-2 (Chinese) isolate caused severe leaf curling and chlorosis, whereas the Cal-KS-1 isolate induced severe tatter and distorted leaves 4-8 weeks after inoculation. In contrast, the LCd-NA-1 (Taiwanese) isolate caused mild symptoms, including slight leaf curl, while the Kq-6-2-46 isolate caused severe, obviously chlorotic spots accompanied by leaf distortion (Fig. 1a). In the *C. quinoa* test, the indicator plants were more sensitive to Chinese isolates at two temperatures (Table 1). Under high temperature conditions, symptoms developed more rapidly (5-10 days) following infection with the two Chinese isolates than with the Taiwanese isolate (6-12 days). The Chinese isolates both caused obvious local chlorotic lesions with clear edges on inoculated leaves; the Cal-KS-1 isolate also induced heightened mosaic, chlorotic, curling and epinasty symptoms on systemic top leaves compared with Sat-HY-2 infection. The Kq-6-2-46 isolate caused mild local lesions on inoculated leaves, whereas few chlorotic spots were observed on LCd-NA-1-infected leaves. Moreover, only LCd-NA-1 induced mosaic chlorotic spots on systemic top leaves (Fig. 1b). Symptom development is slowed under low temperature conditions (20-22 days).

NOTE

Table 1. Comparison of symptom expression on Rusk citrange and *Chenopodium quinoa* infected by four citrus tatter leaf virus (CTLV) isolates.

	CTLV isolate[a]							
Indicator plant	Sat-HY-2 (C)		Cal-KS-1 (C)		LCd-NA-1 (T)		Kq-6-2-46 (T)	
Rusk citrange (leaf)	++[b]		++		++		++	
Chlorotic spots	3		2		1		3	
Leaf distortion	3		2		1		0	
Leaf tattering	3		3		0		1	
C. quinoa	30 °C	22 °C	30 °C	22 °C	30 °C	22 °C	30 °C	22 °C
Inoculated leaves	++	+	++	+	+	+++	++	+
Local lesions	3	3	3	3	1	1	2	1
Uninoculated leaves	–	++	++	+	+	+	+	+
Mottling	0	3	3	0	1	2	0	2
Epinasty	0	3	3	0	0	2	0	2
Leaf curling	0	3	3	0	0	2	0	2

Symptom index: 0, symptomless; 1, mild; 2, moderate; 3, severe. Symptom expression on Rusk citrange was recorded 3 months after inoculation by bud grafting.

[a](C), Chinese isolate; (T) Taiwanese isolate.

[b]RT-PCR detection of CTLV. Pixel value index of the CTLV-specific band on agarose gel measured by a densitometer: –, <30; +, 30–79; ++, 80–129; +++, 130–180.

Obvious partially chlorotic spots were observed on both Chinese isolate-infected leaves, while larger and expanded spots were observed on Sat-HY-2 infected leaves. The opposite results were shown in systemic symptoms. Severely mosaic, chlorotic leaves with curling and distortion were observed on the Sat-HY-2 infected plants, whereas no systemic symptoms were observed with the Cal-KS-1 infection. The two Taiwanese isolates caused no obvious symptoms on inoculated leaves but did cause distortion and curling symptoms on systemically infected leaves (Fig. 1b).

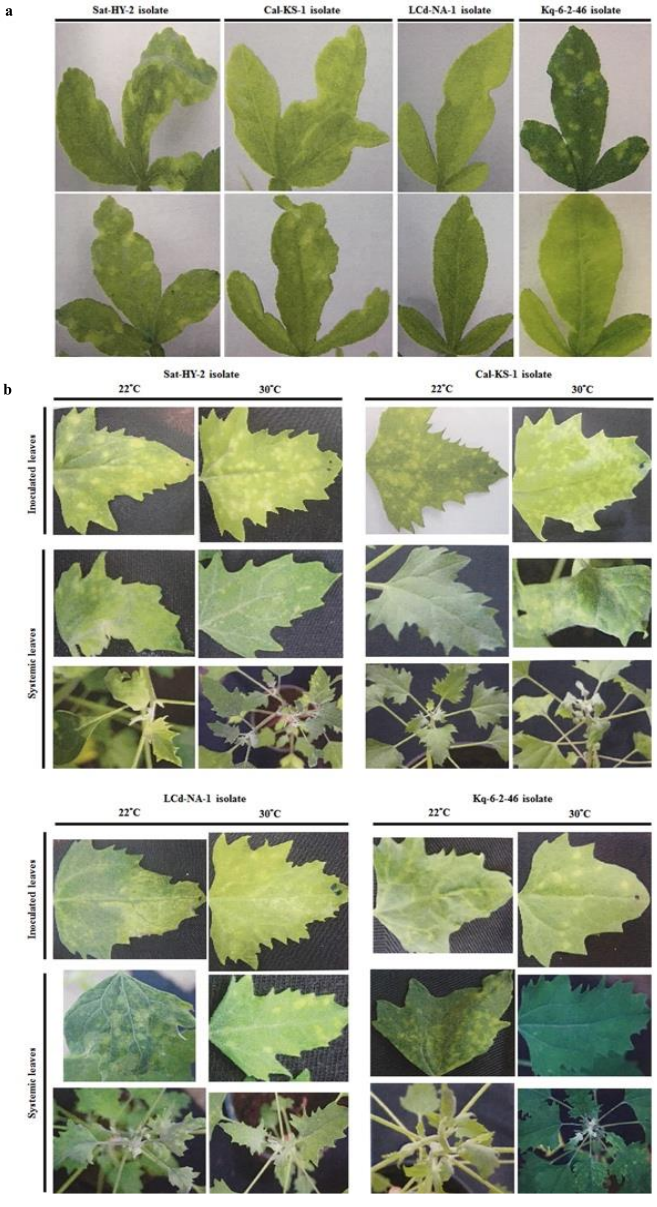

Figure 1. Comparison of foliar symptoms on Rusk citrange (a) and *C. quinoa* (b) following infection with four distinct CTLV isolates. Symptom expression on Rusk citrange and *C. quinoa* was observed at six weeks and one week after inoculation, respectively. CTLV inoculation tests on *C. quinoa* were conducted in greenhouses at 22°C and 30°C. Sat, Satsuma mandarin; Cal, Calamondin; LCd, Liuchen sweet orange; Kq, Kumquat.

NOTE

CTLV distribution in different citrus tissues

RT-PCR detection was performed on different tissues from two CTLV-infected citrus cultivars (Kumquat and Minneola tangelo). Strong CTLV signals were detected in mature and young leaves and stem bark, whereas moderate signals were present in the root, midrib and fruit. No signals were detected in flower tissues (Fig. 2).

Figure 2. Analysis of CTLV distribution in different citrus tissues by RT-PCR. (a) CTLV-infected Minneola tangelo cultivated in the citrus nursery of Chiayi Agriculture Experiment Station (CAES). (b) RT-PCR assay for CTLV detection in different tissues of host citrus plants. The product size was 527 bp. Lane 1, root; 2, mature leaf; 3, young leaf; 4, midribs; 5, bark; 6, flower; 7, fruit transportation tissue. M, 100-bp DNA ladder marker.

Genomic, amino acid and phylogenetic analyses of CTLV

As shown in Table 2, 79.4-94% similarity was observed for nucleotide alignment when compared to CTLV-Pk. Amino acid (aa) alignment demonstrated high similarities for the ORF1 (85.3-95.8%), CP (92-95.8%) and MP (93.4-99.1%) sequences compared to CTLV-Pk. Obvious variations in variable regions I (14.3-18.2%) and II (56.3-63.6%) exist among the isolates from Taiwan and other countries (Table 2). Based on phylogenetic analyses of the ORF1 genome sequences (Fig. 3a), the Taiwanese isolates were similar to isolates from the USA (CTLV-ML) and China (CTLV-SO). In addition, phylogenetic analysis based on aa sequences indicated the Taiwanese isolates were similar to the Chinese isolates which comes from the same group, whereas the Japanese isolates belong to another group (Fig. 3b).

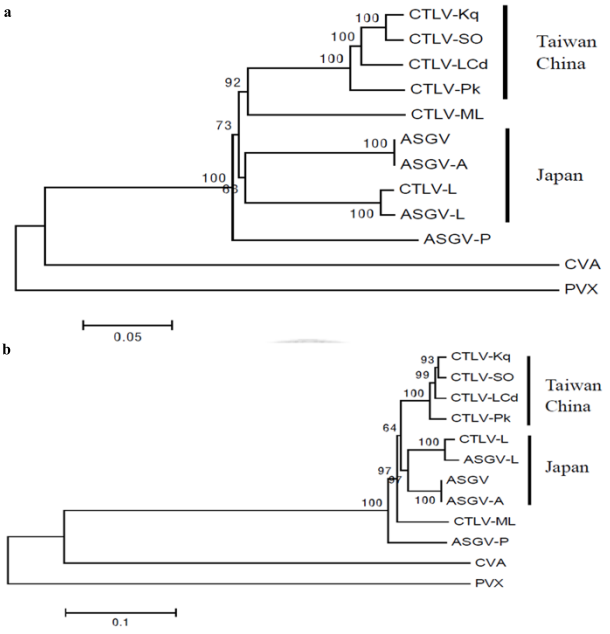

Figure 3. Phylogenetic trees derived from full-length genome sequences (a) and ORF1 aa sequences (b) of citrus tatter leaf virus (CTLV) isolates from Ponkan mandarin (CTLV-Pk) and other capilloviruses. Trees were constructed with MEGA 5.0 using the UPGMA method with 1000 bootstrap replications. Potato virus X (PVX) (JF430080) was used as the out-group. Bars indicate numbers of nucleotide substitutions per site.

NOTE

Table 2. Comparison of genome sequences and amino acid (aa) identities (%) of open reading frame (ORF1) polyprotein, coat protein (CP), movement protein (MP) and variable regions (VRI and VRII) among Ponkan isolate of citrus tatter leaf virus (CTLV-Pk) and other capilloviruses.

Sequence	CTLV-Pk	CTLV-Kq	CTLV-LCd	CTLV-ML	CTLV-L	ASGV	ASGV-P	CVA
Genome	100	94.0	93.9	81.9	81.7	81.7	79.4	42.9
ORF1 aa	100	95.0	95.8	86.9	86.9	87.6	85.3	22.7
CP aa	100	95.4	95.8	92.0	94.5	93.7	92.0	25.5
MP aa	100	99.1	98.1	95.9	96.9	95.6	93.4	20.1
VRI aa	100	70.0	80.0	14.3	23.8	14.3	18.2	nd
VRII aa	100	85.0	87.4	63.6	56.3	57.0	57.7	nd

CTLV from Ponkan mandarin (CTLV-Pk), kumquat (CTLV-Kq), Liuchen sweet orange (CTLV-LCd), Meyer lemon (CTLV-ML), lily (CTLV-L); apple stem grooving virus from apple (ASGV), pear black necrotic leaf spot isolate of ASGV (ASGV-P); cherry virus A (CVA).
nd, not determined.

Conclusion

In this study, we focused on the biological and molecular characterisation of CTLV isolates and improved the sensitivity and specificity of available detection methods. Standard protocols, including a bioassay and molecular detection, are essential tools to prevent infection by exotic and frequently severe isolates, and permit the early detection and removal of local latent infections. In the future, the construction of an infectious CTLV clone could represents a useful tool for further functional and genetic research on virus replication, movement and pathogenicity. The artificial clone will also benefit the development of a virus-induced gene silencing (VIGS) vector for further *in planta* studies. The study provides basic biological results which may help industry to select tolerant cultivars to prevent viral infection and construct suitable environmental factors to growth virus-free citrus seedlings. Uneven distributions of CTLV in different citrus tissues could give important suggestion to establish standard operation procedure in quarantine protocol. The study provides valuable aspects for citrus management strategy to citrus industry and government people.

Acknowledgements

We thank the kind supply of several citrus cultivars and samples by the farmers of Taiwan to complete the field survey. The authors also thank Prof. Hong-Ji, Su from National Taiwan University for collecting foreign isolates and giving advices on the manuscript.

References

[1] Wallace, J. M., and R. J. Drake, “Tatter-leaf, a previously undescribed virus effect on citrus”, *Plant Disease Reporter*, vol. 46, 211-212, 1962.

[2] Yarwood, C. E., “Mechanical transmission of a latent lemon virus”, *Phytopathology*, vol. 53, pp. 1145, 1963.

[3] Fulton, R. W., “Mechanical transmission of tatter leaf virus from cowpea to citrus”, *Phytopathology*, vol. 56, pp. 575-576, 1966.

[4] Garnsey, S.M., “Mechanical transmission of a virus that produces tatter leaf symptoms in *Citrus excelsa*”, In: Weathers LG, M Cohen, eds. *Proceeding of the 6th Conference of the International Organization of Citrus Virologist*. IOCV: University of California Riverside, USA, pp. 137, 1974.

[5] Zhang, T.M., X. Y. Liang, and C. N. Roistacher, “Occurrence and detection of citrus tatter leaf virus (CTLV) in Huangyan, Zhejiang Province, China”, *Plant Disease*, vol. 72, pp. 543-545, 1988.

[6] Miyakawa, T., and C. Matsui, “A bud-union abnormality of Satsuma mandarin on *Poncirus trifoliata* rootstock in Japan”, In: Calavan EC, ed. *Proceeding of the 7th Conference of the International Organization of Citrus Virologist*. IOCV: University of California Riverside, USA, pp. 125-131, 1976.

[7] Martelli, G.P., M. J. Adams, J. F. Kreuze, V. V. Dolja, “Family Flexiviridae: A case study in virion and genome plasticity”, *Annual Review of Phytopathology*, vol. 45, pp. 73-100, 2007.

[8] Tsai, C.H., H. J. Su, Y. C. Feng, and T. H. Hung, “Study of citrus Huanglongbing and its complex infection with Citrus tristeza closterovirus and Citrus tatter leaf capillovirus in Taiwan”, *Plant Pathology Bulletin,* vol. 16, pp. 121-129, 2007.

RECENT RESEARCH ACTIVITIES

Visualization of cellulose molecules in synthesis with time-resolved SAXS

(Laboratory of Biomass Morphogenesis and Information, RISH, Kyoto University)

Tomoya Imai, Hirotaka Tajima, and Paavo A. Penttilä

Purpose of the study

Cellulose is one of the sustainable materials to be used in near future given its high renewability. The major reason why cellulose could be such a useful material is that cellulose has a solid structure with fiber morphology, in which polymeric straight molecules of cellulose are crystallized (cellulose microfibril). Such a molecular assembly together with its molecular conformation provides the toughness with cellulose microfibril. The protein that produces such an excellent super-molecular structure is cellulose synthase, an enzyme embedded in cell membrane. We have not yet successfully reconstituted the native cellulose synthase activity *in vitro* despite many trials for as long as 10 years. In those experiments, cellulose polymer was successfully synthesized. However the synthesized product was no longer microfibril as found in nature, but globular aggregation as reported previously [1]. For clarifying this error in the reaction, we tried to understand what happens in this "abnormal" *in vitro* reaction with small angle X-ray scattering (SAXS), which allowed cellulose molecular seembling process to be visualized *in situ* in the reaction.

Experiments and results

In vitro reaction by crude enzyme of cellulose synthase, which was prepared from a bacterium *Komagataeibacter xylinus* [1], was observed by time-resolved SAXS experiment at BL40B2 in SPring-8 (Hyogo, Japan): details of the experiments are found in our published paper [2]. Briefly, SAXS pattern was recorded from the *in vitro* reaction every 5 min after starting the reaction, and azimuthally integrated to convert the scattering pattern to 1-D data with scattering vector q (= $(4\pi \cdot \sin\theta)/\lambda$) and scattering intensity I: θ is a half of scattering angle and λ is X-ray wavelength. Scattering signal from the cellulose synthesized by the reaction was approximately visualized by subtracting the 1st frame data of a time-resolved measurement (Figure 1). The scattering at q = 0.05 nm^{-1} started being apparent after 16 min of the reaction, while the one at q = 0.25 nm^{-1} was found already at very beginning of the reaction. Given that the former represents larger structure, it was shown that the synthesized cellulose molecules formed smaller structure at first, and subsequently those primitive aggregations were packed to form larger aggregates. This is the behavior of cellulose molecules synthesized by partially denatured cellulose synthase in our *in vitro* system.

Acknowledgements

This study was performed in collaboration with Professor Y. Yuguchi and Ms. K. Yamamoto at Osaka Electro-Communication University. SAXS experiment was performed at BL40B2 in SPring-8, Hyogo, Japan with the approval of JASRI (Proposal No. 2016A1069, 2017A1049, and 2017B1094). This work was financially supported by Mission Research Grant in part.

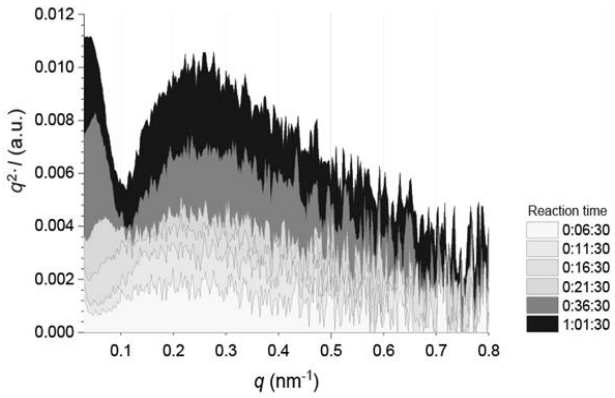

Figure 1.Typical time-resolved SAXS data for the *in vitro* synthesis of cellulose represented by Kratky plot: q vs q^2I. Scattering intensity indicates the existence of structure at the corresponding q, inversely indicating the size of structure.

References

[1] Hashimoto, A., Shimono, K., Horikawa, Y., Ichikawa, T., Wada, M., Imai, T., Sugiyama, J. "Extraction of cellulose-synthesizing activity of *Gluconacetobacter xylinus* by alkylmaltoside", *Carbohydr.Res.* **346,** 2760-2768, 2011.

[2] Tajima, H., Penttilä, P.A., Imai, T., Yamamoto, K., Yuguchi, Y. "Observation of *in vitro* cellulose synthesis by bacterial cellulose synthase with time-resolved small angle X-ray scattering", *Int.J.Biol.Macromol.* **130,** 765-777, 2019.

RECENT RESEARCH ACTIVITIES

Screening and identification of useful enzymes from biphenyl/PCB-degrading bacteria that metabolize lignin-derived aromatic compounds

(Laboratory of Biomass Conversion, RISH, Kyoto University)

Takahito Watanabe

A variety of microorganisms play a significant role in the mineralization of plant lignin. The lignin-derived aromatic compounds are further degraded by soil bacteria. So far, a number of biphenyl/polychlorinated biphenyls (PCB)-degrading bacteria have been isolated from various environmental samples and characterized in terms of biochemical and genetic aspects [1]. Recently, the genome analyses of ten biphenyl/PCB-degrading bacteria, isolated from biphenyl-contaminated soil in Kitakyushu, Japan, were performed [2-3]. Interestingly, some of these biphenyl/PCB-degrading bacteria grew well on lignin-derived aromatic compounds as the sole sources of carbon and energy, as well as xenobiotic compounds like PCB. This finding implies that biphenyl/PCB-degrading bacteria may be a type of terminal lignin-degrading bacterium.

To globally screen and identify expressed proteins involved in the metabolism of lignin-derived aromatic compounds from these biphenyl/PCB-degrading bacteria, a proteomic approach is needed. On the other hand, I have already optimized a fluorescence two-dimensional difference gel electrophoresis (2D-DIGE) method for a white-rot fungus surrounded by polysaccharide sheath [4]. Therefore, I tried to modify this method for biphenyl/PCB-degrading bacteria and to perform 2D-DIGE using intracellular proteins prepared from *Pseudomonas furukawaii* (formerly *P. pseudoalcaligenes*) KF707 [5]—one of the best-characterized biphenyl/PCB-degrading bacteria—grown in the presence and absence of biphenyl. As a result, I successfully detected the difference in protein expression under the two culture conditions and also identified up-regulated, constantly expressed, and down-regulated proteins by peptide mass finger printing. These results show that using proteomic and genomic approaches, I can efficiently screen and identify candidate proteins and genes involved in the metabolism of lignin-derived aromatic compounds from biphenyl/PCB-degrading bacteria. These approaches can also lead to the production of useful aromatic compounds from wood biomass.

References

[1] Furukawa, K., Fujihara, H., "Microbial degradation of polychlorinated biphenyls: biochemical and molecular features". *J. Biosci. Bioeng.* **105,** 433-449 (2008).

[2] Suenaga, H., Fujihara, H., Kimura, N., Hirose, J., Watanabe, T., Futagami, T., Goto, M., Shimodaira, J., Furukawa, K., "Insights into the genomic plasticity of *Pseudomonas putida* KF715, a strain with unique biphenyl-utilizing activity and genome instability properties". *Environ. Microbiol. Rep.* **9,** 589-598 (2017).

[3] Hirose, J., Fujihara, H., Watanabe, T., Kimura, N., Suenaga, H., Futagami, T., Goto, M., Suyama, A., Furukawa, K., "Biphenyl/PCB degrading *bph* genes of ten bacterial strains isolated from biphenyl-contaminated soil in Kitakyushu, Japan: comparative and dynamic features as integrative conjugative elements (ICEs)". *Genes* **10,** 404 (2019).

[4] Watanabe, T., Yoshioka, K., Kido, A., Lee, J., Akiyoshi, H., Watanabe, T., "Preparation of intracellular proteins from a white-rot fungus surrounded by polysaccharide sheath and optimization of their two-dimensional electrophoresis for proteomic studies". *J. Microbiol. Methods* **142,** 63-70 (2017).

[5] Kimura, N., Watanabe, T., Suenaga, H., Fujihara, H., Futagami, T., Goto, M., Hanada, S., Hirose, J., "*Pseudomonas furukawaii* sp. nov., a polychlorinated biphenyl-degrading bacterium isolated from biphenyl-contaminated soil in Japan". *Int. J. Syst. Evol. Microbiol.* **68,** 1429-1435 (2018).

RECENT RESEARCH ACTIVITIES

Structure, biosynthesis, and bioengineering of lignocellulose and phenylpropanoid metabolites for future biorefinery

(Laboratory of Metabolic Science of Forest Plants and Microorganisms, RISH, Kyoto University)

Toshiaki Umezawa, Yuki Tobimatsu, Shiro Suzuki, and Masaomi Yamamura

It is becoming increasingly important to establish a sustainable society by reducing our excessive reliance on fossil resources and mitigate global climate change. As lignocellulosic biomass represents the most abundant renewable and carbon-neutral resources on earth, technologies to improve their utilizations are key for realizing the goal. In this context, we investigate the structure, biosynthesis and bioengineering of lignocellulose using various model plants and biomass crops. In addition, we are interested in understanding the biosynthesis of plant-derived phenylpropanoid metabolites with useful biological activities. Our program typically integrates research ideas and approaches based on chemistry, biochemistry, and plant molecular biology.

Among a wide variety of biomass feedstocks, grass biomass crops, such as *Erianthus*, *Sorghum*, sugarcane and bamboo, have attracted particular attention due to their high biomass productivity and superior environmental adaptability. To explore new breeding strategies to improve the production of useful fuels and materials from grass biomass, we seek to develop transgenic rice plants that produce biomass with improved utilization properties. Our research particularly focuses on manipulating lignin, a phenylpropanoid polymer accounting for 15-30 wt% of lignocellulosic biomass. We have developed various rice transgenic lines in which specific genes encoding enzymes and transcription factors functioning in the lignin biosynthetic pathway are down- and/or up-regulated. Some of our developed transgenic lines display notably improved biomass utilization properties. In parallel, we are also working on selective breeding of grass crop varieties, such as *Erianthus* spp. and *Sorghum* spp., with superior lignins suited for bioenergy and biomaterial productions. In addition, aiming at biological production of useful phytochemicals, we have been characterizing plant and microbial enzymes/genes involved in formations of bioactive phenylpropanoids such as lignans and norlignans. Our recent projects include elucidation of the biosynthesis of antitumor podophyllotoxin in *Anthriscus sylvestris*, unravelling crystal structures of hinokiresinol synthases, unique enzymes responsible for the enantioselective formation of bioactive norlignans, and identification of enzymes/genes involved in the formation of estrogenic mammalian lignans (enterolignans) via human intestinal bacteria.

Selected Publications (FY2018)

[1] Takeda Y et al. (2018) Downregulation of p-*COUMAROYL ESTER 3-HYDROXYLASE* in rice leads to altered cell wall structures and improves biomass saccharification. *The Plant Journal* 95: 796-811.
[2] Miyamoto et al. (2018) Comparative analysis of lignin chemical structures of sugarcane bagasse pretreated by alkaline, hydrothermal, and dilute sulfuric acid methods. *Industrial Crops and Products* 121: 124-131.
[3] Umezawa T. Lignin modification *in planta* for valorization. *Phytochemistry Reviews* 17: 1305-1327.
[4] Takeda Y et al. (2019) Lignin characterization of rice *CONIFERALDEHYDE 5-HYDROXYLASE* loss-of-function mutants generated with the CRISPR/Cas9 system. *The Plant Journal* 97: 543-554.
[5] Takeda Y et al. (2019) Comparative evaluations of lignocellulose reactivity and usability in transgenic rice plants with altered lignin composition. *Journal of Wood Science* 65:6.
[6] Tobimatsu Y. and Schuetz M. (2019) Lignin polymerization: how do plants manage the chemistry so well? *Current Opinion in Biotechnology* 56:75-81.
[7] Miyamoto T et al. (2019) OsMYB108 loss-of-function enriches p-coumaroylated and tricin lignin units in rice cell walls. *The Plant Journal,* in press (DOI: 10.1111/tpj.14290).
[8] Lam PY et al. (2019) Recruitment of specific flavonoid B-ring hydroxylases for two independent biosynthesis pathways of flavone-derived metabolites in grasses. *New Phytologist*, in press (DOI:10.1111/nph.15795).
[9] Suzuki S et al. (2019) *De novo* transcriptome analysis of needles of *Thujopsis dolabrata* var. *hondae. Plant Biotechnology*, in press.

RECENT RESEARCH ACTIVITIES

Discovery of a cadmium transporter for phytoremediation

(Laboratory of Plant Gene Expression, RISH, Kyoto University)

Kazufumi Yazaki and Akifumi Sugiyama

Plants chose sessile life style during the evolution since the land plant colonization 500 million years ago. This means that once plants germinate, they complete their entire life duration at the same location where they anchored their roots. Because of the life style, plants have developed a variety of stress response mechanisms to resist and/or tolerate inferior or unfavorable environments. Heavy metal stress is one of them. Because of the economic activities of humans, if particular areas are heavily polluted with heavy metals, such as Pb, or Cd, plants cannot, however, escape from those polluted area, when they started to grow. Thus, plants have developed various heavy metal tolerant mechanisms, and heavy metal transporters are representatives of them.

Transition metal cations play an important role in plant growth and development. For instance, iron (Fe) is an essential element because it acts as a structural and functional component of many biological molecules such as nitrogenase in nodules [1]. In contrast, cadmium (Cd) is a toxic metal that is not required for any physiological functions. Typical cadmium toxicity for plants results in some serious symptoms e.g., chlorosis, growth retardation, and browning of the root tips, which may cause death at a high concentration. Transition metal cations are absorbed with water by root tissues from the soil, and then are circulated in the plant body via vascular tissue and transporter proteins. If the soil contains not only essential metals but also non-essential toxic metals, the uptake of metals may be managed under competition, which is the phenomenon known as inducible deficiency.

We selected a metal accumulater plant, *Crotalaria juncea* (Fabaceae). *C. juncea* has been reported as a plant species to show strong tolerance to Cd, and to accumulate this toxic metal in high concentrations in its leaves (118 mg kg^{-1} DW) in addition to Fe. This is an attractive plant to study metal transporters involved in Cd accumulation because of its high tolerance for Cd and also because of its preference to translocate these metals into the aerial part of the plant. We have isolated a cDNA, belonging to the metal transporter NRAMP family from this plant.

The membrane localization analysis of CjNRAMP1 showed as being the plasma membrane of plant cells. Complementation experiments using yeast strains, in which metal transport systems were impaired, showed that CjNRAMP1 transported both Fe and Cd in an inward direction within the cells. Transgenic Arabidopsis plants overexpressing *CjNRAMP1* gained high tolerance to Cd; notably, the Cd translocation from roots to leaves was dramatically enhanced compared to the wild type plants. The overexpression of *CjNRAMP1* resulted in a higher accumulation of Fe in both the shoots and roots, suggesting that CjNRAMP1 recognizes Fe and Cd as substrates, and that the high Cd tolerance of CjNRAPM1 is due to its strong Fe uptake activity even under the high Cd concentrations in the rhizosphere.

References

[1] Takanashi, K., Yokosho, K., Saeki, K., Sugiyama, A., Sato, S., Tabata, S., Ma, JF., Yazaki, K., "LjMATE1, a citrate transporter responsible for iron supply to nodule infection zone of *Lotus japonicus*" Plant Cell Physiol., 54 (4), 585-594, 2013.

[2] Nakanishi-Masuno, T., Shitan, N., Sugiyama, A., Takanashi, K., Inaba, S., Kaneko, S., Yazaki, K., "The *Crotalaria juncea* metal transporter CjNRAMP1 has a high Fe uptake activity, even in an environment with high Cd contamination" Intl. J. Phytoremed., 20 (14): 1427-1437 (2018).

RECENT RESEARCH ACTIVITIES

Mie–Raman lidar techniques using the UV laser for profiling atmospheric constituents in the atmospheric boundary layer

(Laboratory of Atmospheric Sensing and Diagnosis, RISH, Kyoto University)

Masanori Yabuki

Atmospheric constituents in the atmospheric boundary layer (ABL), which present in the lowest part of the Earth's atmosphere, play a key role in air pollution, local weather, and climate change. Their spatial and temporal distributions near the surface are highly variable, because of the complex turbulent flow over the surface and the rapid interactions of each species. Therefore, innovative techniques for observing the distributions of atmospheric constituents with good spatio-temporal resolution are required. The Mie–Raman lidar is a laser-based remote sensing instrument that is used for profiling aerosols, ozone, water vapor, and temperature. Although the operation of the lidar system using ultraviolet (UV) optical components including the deep UV (DUV) wavelength range of 200–300 nm is not easy in comparison with systems using the visible wavelengths, the unique characteristics of the UV light have led to the development of new lidar observation methods.

Here, we introduce our four recently developed lidar systems: (1) In terms of the light scattering by particles, shorter wavelengths can be used to obtain information on small particles. A lidar with a multiple field-of-view receiver employing lasers of 266 nm and 355 nm wavelengths was developed for detecting multiple scattering effects to acquire quantitative information concerning the aerosol size distribution within the sub-micrometer and smaller size range. (2) Characteristics of the strong UV light absorption by ozone molecules in the troposphere can be used to obtain information on the ozone profile. Figure 1 shows a time–height cross section of ozone concentration observed by our Raman differential absorption lidar with a 266 nm laser. (3) The use of the deep UV wavelengths is convenient for lidar observation because of the low background noise during daytime, as most of the solar radiation in the wavelength range below 300 nm is absorbed by the ozone layer in the stratosphere. By use of this feature, we constructed a UV Raman lidar for long-term monitoring of water vapor mixing ratio profiles in the ABL for 24 hours. (4) With regard to eye safety, the UV laser has an advantage over instruments using wavelengths in the visible range because the maximum permitted exposure in the UV region is larger than that in the visible region. Highly eye-safe UV laser can be applied to the scanning lidar. We constructed a scanning Raman lidar to observe the cross-sectional distribution of water vapor mixing ratio and aerosols near the Earth's surface, which are difficult to observe when a conventional Raman lidar system is used [1].

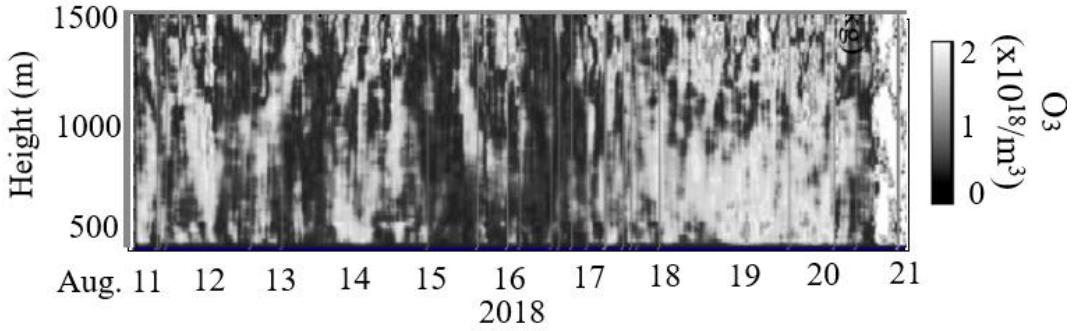

Figure 1. Time–height cross sections of the ozone profiles observed by the Raman lidar at Shigaraki, Japan, from August 11 to 21, 2018.

Reference

[1] Yabuki, M., Matsuda M., Nakamura T., Hayashi T., and Tsuda T, A scanning Raman lidar for observing the spatio-temporal distribution of water vapor, *J. Atmos. Sol. Terr. Phys.*. 59, 150-151, pp. 21-30, 2016. doi.10.1016/j.jastp.2016.10.013

RECENT RESEARCH ACTIVITIES

A proposal for satellite observation of the whole atmosphere – superconducting submillimeter-wave limb-emission sounder (SMILES-2)

(Laboratory of Atmospheric Environmental Information Analysis, RISH, Kyoto University)

Masato Shiotani

Background

In the middle atmosphere the ozone layer shielding harmful ultraviolet radiation enables life on Earth. In the upper atmosphere high energy radiation with shorter wavelength such as X-ray and extreme ultraviolet is absorbed to produce plasma particles. It is recognized that the middle and upper atmosphere is susceptible to anthropogenic perturbations, such as the release of chlorofluorocarbons resulting in ozone destruction and the increase in greenhouse gases bringing about cooling there. The middle and upper atmosphere is also known to be sensitive to variability in solar activities such as explosions on Sun's surface (e.g. flare), 27-day solar rotation, and the 11-year solar cycle.

The region around the mesopause, including the upper mesosphere and the lower thermosphere (MLT), is an important transition layer where atmospheric characteristics change in terms of both physics and chemistry. The thermal and dynamical structure in the middle atmosphere, mostly determined by a radiative balance with time scale longer than a day, is characterized by the background states varying with a seasonal time scale and the disturbances with periodicities over 24 hours. In contrast, in the upper atmosphere temperature variations show a distinctive diurnal cycle mostly driven by changing solar radiation due to the earth's rotation. The diurnal variations in the upper atmosphere are highly affected by atmospheric waves propagating from the middle atmosphere and by electromagnetic energy inputs from the magnetosphere. However, the lacking of global observations in the MLT region seriously hinders us from investigating the underlying coupling processes between the lower and upper atmosphere.

Mission objectives

On the basis of the heritage of the Superconducting Submillimeter-Wave Limb-Emission Sounder (SMILES) on the International Space Station, we propose a satellite mission "SMILES-2" to observe temperature and wind fields, and distributions of atmospheric trace gases for the full diurnal cycle from the middle atmosphere to the upper atmosphere. SMILES-2 observations will enable us to obtain global information with unprecedented accuracy on the whole atmosphere including the MLT where observation data have been lacking. We set the following four science objectives for the SMILES-2 mission: (1) To investigate the 4-D space-time structure of the diurnal variations (atmospheric tides) in view of dynamics, chemistry, and electromagnetic processes; (2) To unveil the vertical propagation of synoptic-to-planetary scale disturbances from the middle atmosphere (non-migrating tides and stratospheric sudden warming events) to the upper atmosphere; (3) To understand atmospheric variations due to energy inputs from the magnetosphere (particle precipitation and magnetic storm); (4) To provide benchmarks for whole atmosphere models and climate models with detailed description of the background thermal structure and distribution of minor species.

From those views we will be able to grasp the upward and downward coupling processes in the 4-D dynamical structure of diurnal variations which are one of the most essential characteristics in the earth's atmosphere. These outcomes including the atmospheric trace gas data will greatly contribute to improve the reliability of chemistry climate models for future projection and the accuracy of prediction models for space weather.

Acknowledgements

The full mission proposal was prepared by the SMILES-2 mission team, and I thank all members of the SMILES-2 mission team. The proposal was sent to ISAS/JAXA in response to Announcement of Opportunity for competitive M-class missions.

RECENT RESEARCH ACTIVITIES

International Equatorial Atmosphere School 2019

(Laboratory of Radar Atmospheric Science, RISH, Kyoto University)

Tatsuhiro Yokoyama and Mamoru Yamamoto

The equatorial atmosphere generates the strongest convection in the world and affects the global atmospheric circulation as well as the local weather and climate. To further strengthen the collaboration between Japan and the equatorial countries such as Indonesia, it is very important to promote education and research activity in these countries. To this end, we held the first International Equatorial Atmosphere School on March 18-22, 2019 at the Aerospace Research Institute (LAPAN) in Bandung, Indonesia in partnership with Humanosphere Asia Research Node (ARN). 109 researchers and students from Japan, Indonesia and surrounding countries participated at LAPAN, and 61 students in three different institutes participated online, so the total number of participants was 170.

RISH, Kyoto University and LAPAN collaborate and conduct the equatorial atmospheric research for a long time. Since 2001, we have been successfully operating the Equatorial Atmosphere Radar (EAR) at Kototabang, West Sumatra, and continue the long-term observations. We proposed an international school for the study of the equatorial atmosphere. This school event was aimed to benefit young scientists and researchers who are interested in this field to have a good summary of the study techniques and recent topics. Also, this event helped accelerate our big research project to establish the Equatorial MU Radar (EMU) that is the full-spec atmospheric radar in the near future right next to the EAR.

Figure 1. Lecture scene at the school.

The lecture topics in the school are: 1) Introduction and basics of the Earth's atmosphere, 2) Atmospheric radar basics and advanced, 3) Equatorial rainfall and global climate, 4) Climate-biogeosphere-humanosphere interaction, 5) Atmospheric waves and coupling processes, 6) Upper atmosphere basics and observations, 7) Radio Acoustic Sounding System (RASS), 8) GNSS measurement of the atmosphere, 9) Numerical models in Japan and Indonesia, 10) Numerical simulation techniques for atmosphere, and 10) Hands-on training of IUGONET data analysis for promotion of atmospheric science.

Figure 2. Group photo of all participants.

All lectures and school events were successfully completed with a great help of LAPAN staff. Participants learned the basics and research techniques of the equatorial atmosphere, and the importance of the EMU project to further understand the whole atmospheric dynamics. We hope to hold the school regularly to maintain the research activity in Southeast Asia.

Acknowledgements

The first International Equatorial Atmosphere School was supported by Kyoto University, JSPS, Nagoya University, LAPAN, and RISTEKDIKTI, Indonesia.

RECENT RESEARCH ACTIVITIES

Modification of fibrous material by radiation technique

(Laboratory of Fiber Multiplication, RISH, Kyoto University)

Satoko Okubayashi

As polymer materials and vinyl monomers are irradiated with an electron beam (EB) that is a type of radiations, ionization and excitation occur locally and instantaneously to generate radicals in the molecules. The radicals induce hydrogen abstraction reaction, addition reaction to a double bond, crosslinking by radical recombination, decomposition, oxidation, etc., which change the properties of polymer material. Mainly two procedures, simultaneous irradiation and pre-irradiation are frequently applied for experimental operation. The polymer material pre-coated with monomers is irradiated with electron beam by the simultaneous treatment while the polymer is exposed to electron beam and then coated with the monomer by the pre-irradiation. The monomer and its polymer are immobilized to the material by chemical bonding, which is called EB-graft polymerization. New properties can be added to the base material by the EB-grafting. Recently, equipment of electron beam irradiation has been developing, and the process is widely used in industrial fields such as film and rubber. However, only a few applications to fiber materials has been reported in textile industry.

In this paper, we examined EB-graft polymerization of glycidyl methacrylate (GMA) which is a scaffolding material for incorporation of ionic groups, to non-woven and woven fabrics of modacrylic fiber consisting of vinyl chloride-acrylonitrile copolymer (provided by Kaneka Co., Ltd.) by pre-irradiation method for the purpose to prepare ion exchange fabrics.

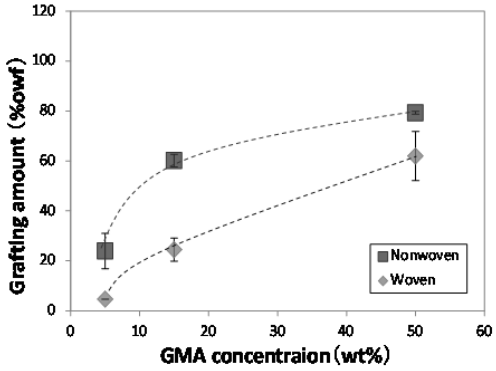

Figure 1. Effects of monomer concentration and fabric structure on grafting amount of GMA.

Table 1. Amount of radical generated on modacrylic fiber by EB irradiation.

Fabric structure	Basis weight (g/m^2)	Amount of radical (g^{-1} of fiber)x10^{18}
Woven fabric	225	3.68
Non-woven fabric	160	3.28
	221	3.40

As shown in Figure 1, weight gain indicating the grafting amount of GMA at 300 keV of accelerating voltage and 100 kGy of absorbed dose to both the non-woven and woven fabrics increased with increasing the GMA concentration, while higher grafting amount was obtained with non-woven fabric having low fiber density as compared with the woven fabric. In order to clarify the difference in the grafting amount in more detail, the amount of radicals generated in woven and non-woven fabrics after EB irradiation were colorimetrically determined using 1, 1-diphenyl-2-picrylhydrazyl free radical (DPPH). It was found that 3.3 to 3.7×10^{18} radicals were generated per fiber weight, regardless of the fabric structure and fabric thickness (Table 1). Considering the same amount of radicals generated by EB irradiation for different fabric structures, and no difference in the grafting amount at the initial stage of grafting in woven and non-woven fabrics (the results are not shown in this report), it is suggested that monomer diffusion to fiber surface and into fiber are retarded after some degree of grafting progressed for dense fabric. Finally the higher grafting amount can be obtained with a fabric having the lower fiber density.

The fabric is three dimensional unstable porous material consisting of a plenty of thin fibers. Many parameters affect monomer diffusion and reaction on and in solid fiber surface, so that the reproducibility is insufficient. This may delay its commercialization in the industry. However, the processing principle is very simple, and it is a very unique method that can provide various functions in an instant with just a few seconds of irradiation. We will continue to seek new seeds for the use of electron EB in fiber processing.

RECENT RESEARCH ACTIVITIES

Joint force to battle the red imported fire ants in Japan: a multi-institution collaborative framework supported by the Ministry of the Environment

(Laboratory of Urban Pestology, RISH, Kyoto University)

Chin-Cheng Scotty Yang

Overview of the joint project

Discovery of red imported fire ants (hereinafter referred to as fire ant) was first reported in mainland Japan in the year of 2017. While detections of fire ant have increased since then, research effort is surprisingly limited. To prevent establishment of fire ant, a total of four Japanese research institutions, namely University of the Ryukyus, Kyoto University, Okinawa Institute of Science and Technology Graduate University (OIST), and National Institute for Environmental Studies, have teamed up to assemble a research platform that offers multiple knowledge-based strategies against future invasions of fire ant in Japan.

The role of each participating institution

Financially supported by the Ministry of the Environment, each institution is granted with 3-year funding that allows them to carry out the proposed research. The principle investigators have different yet equally important role in this team project: Prof. Kazuki Tsuji (University of the Ryukyus) is aiming to put together a novel technology of baiting that is expected to perform more efficiently than any contemporary bait products available. Dr. Kouichi Goka, (National Institute for Environmental Studies) attempts to develop an efficient, easy tool to detect and control fire ant and eventually distribute the tool, once available, nationwide to allow both early warning and rapid response possible. Dr. Yoshimura (OIST) will target on elevating public awareness of fire ant and would like to approach it by developing a citizen-science network to facilitate education, information distribution and involvement of general public into local fire ant monitoring projects.

Dr. Chin-Cheng Scotty Yang (Kyoto University) participates in the team project as principle investigator to characterize the potential impacts of pathogens (virus as focal group) on foraging behaviors of fire ant and, based on the results (which are being generated), attempts to improve the current baiting and luring systems. The virus-infected fire ants have been shown to display decreased foraging activity and a shift of macronutrient preference (from lipid/protein to carbohydrate, Figure). Consequences of such behavioral alterations include 1) use of conventional food lures may result in underestimating actual fire ant numbers; 2) current low-toxicity bait products may not be as attractive as expected. Various approaches will be tested to confirm if declined foraging patterns in virus-infected fire ants can be restored, and will be applied to develop an enhanced food lure/bait system.

Acknowledgements

The author acknowledges Mr. Hung-Wei Hsu, Dr. Ming-Chung Chiu and Prof. Chow-Yang Lee for their contributions to this joint project. Gratitude also goes to the Ministry of the Environment for financial support.

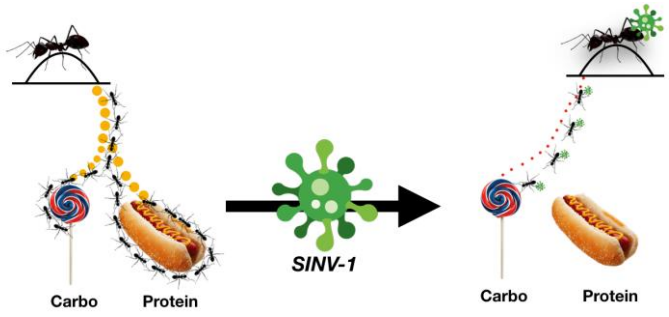

Figure. Illustrations to explain the potential impacts of the virus (SINV-1) on foraging behaviors of fire ant. Note: “Carbo” denotes Carbohydrate; the dot size corresponds to the foraging intensity.

RECENT RESEARCH ACTIVITIES

Cellulose nanofiber-based hydrogels with improved mechanical properties

(Laboratory of Active Bio-based Materials, RISH, Kyoto University)

Yang Xianpeng, Kentaro Abe, and Hiroyuki Yano

Hydrogels are wet and soft materials, comprising hydrophilic polymer networks, which hold large amounts of water and have similar wet properties to human tissues. One of the most important issues for synthesized hydrogels is to improve the mechanical properties. Cellulose nanofibers (CNFs) are hydrophilic natural materials, which are extremely stiff and strong and are thus widely used to reinforce hydrogels. However, problems remain. First, the stiffness of CNFs in wet conditions is lost because of disengagement of interfibrillar hydrogen bonds. Second, it is difficult to increase the CNF content owing to the high viscosity. Third, the interactions between CNFs and the polymer matrix are weak under wet conditions. Therefore, we recently tried to composite a wet CNF cake, which has a high CNF content, with polymers to fabricate composite hydrogels with improved mechanical properties.

CNF/poly(vinyl alcohol) hydrogels [1]

It will be convenient if CNFs can be combined with polymer directly to prepare hydrogels. Poly(vinyl alcohol) (PVA) is considered because PVA is a water soluble, crystallizable, biodegradable and nontoxic polymer with good mechanical properties, even in a hydrated state. In detail, a CNF suspension with a concentration of 0.1 wt% was filtrated to form a CNF cake with a solid content of around 10 wt%. Then, CNF/PVA hydrogels were prepared by immersing the CNF cake in PVA aqueous solution followed by the treatment of drying, annealing and rehydration. The resulted sample, with a water content of 66.8%, had an elastic modulus and fracture strength of 47.92 ± 0.99 MPa and 15.91 ± 0.48 MPa, which were almost comparable to skin and cartilage (Fig. 1). It was revealed that both the PVA networks and the interactions between the CNFs and PVA were maintained well in the hydrated state. This study may suggest a simple and versatile method for preparation of load-bearing hydrogels from nanocelluloses.

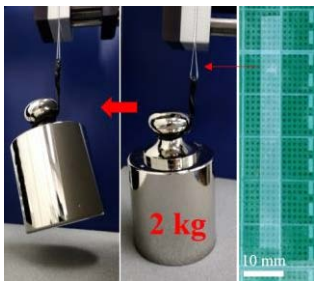

Fig. 1 CNF/PVA hydrogels. A small hydrogel sheet with width of 5 mm and thickness of 0.25 mm could hold a 2-kg weight.

Modified CNF-based hydrogels [2]

We also used the surface modified CNFs to prepare hydrogels, expecting to improve the interactions between CNFs and polymer matrix. To simplify the modification process, we used a CNF cake as a reactor, where nanochannels formed with a large aspect ratio. The flow in the nanochannels under the force of a vacuum might show a negligible back-mixing phenomenon. When the reactant was filtrated through, the water in the CNF cake was replaced by the reactant mixture gradually and the reaction occurred. After the reaction, the cake was washed by passing ethanol and water through the cake. As a result, the degree of substitution of maleic acid monoester-modified CNFs reached 0.14 at room temperature within 25 min. The crystallinity and morphology of modified CNFs were well maintained. Then, the modified CNFs were used to form composites with poly(acrylamide-co-acrylic acid) networks, which were further cross-linked by Fe^{3+}. The elastic modulus of the nanocomposite hydrogels increased considerably from 10.27 ± 0.48 MPa to 24.67 ± 0.53 MPa after slight surface modification. The additional cross-linking enhanced the friction force between nanofibers and matrix, resulting in increased modulus. Our modification method is simple but effective. It shows potential for preparing a range of CNF-based functional nanocomposite materials. The stiffened composite hydrogels also proved the importance of interfacial design for CNF-based hydrogels.

References

[1] X. Yang, K. Abe, S. K. Biswas and H. Yano, *Cellulose*, 2018, 25, 1-10.

[2] X. Yang, S. K. Biswas, H. Yano and K. Abe, *ACS Sustainable Chemistry & Engineering*, 2019, 7, 9092-9096.

RECENT RESEARCH ACTIVITIES

Evaluation of NO_2 sorption ability of cedar wood

(Laboratory of Sustainable Materials, RISH, Kyoto University)

Miyuki Nakagawa, Kenji Umemura, and Kozo Kanayama

Introduction

Nitrogen dioxide (NO_2) is a criteria air pollutant and affects human health, particularly the lungs and breathing passages. As representative materials for NO_2 removal, it is known that activated carbon, photocatalyst and terpenes from leaf oil have a high NO_2 sorption ability. However, use of these materials is limited by the problems of time-consuming production, decline in function depending on the weather and time, and waste liquid and residue disposal. Recently, it's known that Japanese cedar wood (*Cryptomeria Japonica*) has especially high NO_2 sorption ability compared with other wood species. Cedar wood is available itself as NO_2 removing material without any chemical or industrial treatment. Therefore, it has a great potential as a material for NO_2 removal. It is considered that NO_2 sorption ability of cedar wood is influenced by the structural features of tissues, moisture content and extractives. However, influences of each factor have not been evaluated in detail so far. We are trying to elucidate the influence on NO_2 sorption ability under various conditions focused on each factor by using a new system (Figure 1) for measuring NO_2 sorption volume developed by ourselves.

Experiment

In an incubator at 20±1 ˚C, Japanese cedar wood having different form and drying condition were aerated with concentrated NO_2 (1000 ppb, flow velocity: 560 ml/min). NO_2 concentration before and after passing through the specimens were monitored with a NOx monitoring devices. The amount of NO_2 sorption were calculated and compared among various specimens.

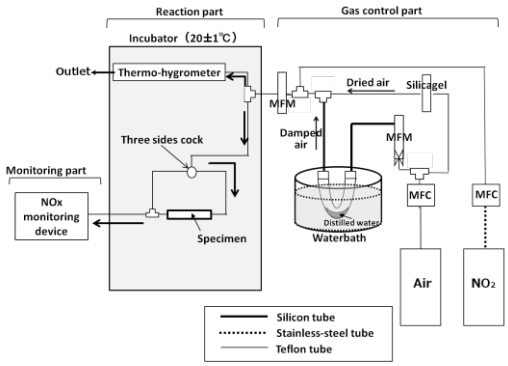

Figure 1. Experimental system for NO_2 sorption test. MFC means the mass flow controller which control flow rate. MFM means the mass flow meter which monitor flow rate [1)].

Results and discussion

When the NO_2 gas flowed over the surface of transverse section of specimen, the NO_2 sorption volume depended on the thickness of longitudinal direction and NO_2 sorption effect was high especially in the range of ca. 3 mm from the surface of transverse section. This range was almost same average length to the cedar tracheid. Also, NO_2 sorption volume depended on the interface area of the specimen which can contact with NO_2. These results show that the interface area which the structure of tracheid contributed was influenced to the NO_2 sorption ability. Furthermore, the average NO_2 sorption volume was the greatest in the specimen of natural drying and decreased as drying temperature was high. Because NO_2 sorption volume in extraction-treated specimen decreased to almost same values regardless of the drying temperature and it is reported that drying temperature is influenced to the amount of extractives in the wood by previous studies, the differences of amount of extractives by drying treatment seem to be influenced to the NO_2 sorption volume. We will examine the influence of moisture content as a next step.

Reference

[1] Miyuki Nakagawa, Akitaka Kimura, Kenji Umemura, Shuichi Kawai "Evaluation of NO_2 sorption of cedar wood with difference of the specimen size and contact condition between NO_2 gas and specimen using new test system", *Journal of Wood Science*, vol. 64, no. 3, pp. 318-325, 2018.

RECENT RESEARCH ACTIVITIES

Lateral Performance of the frame with upper mud wall in Japanese traditional residential houses

(Laboratory of Structural Function, RISH, Kyoto University)

Hiroshi Isoda and Zherui Li

1. Introduction

Facing the severe challenge from earthquakes, the lateral behavior of Japanese traditional timber structure has been highly regarded based on its long-term practical experience. In the current structural calculation method for the timber frames with upper mud wall that is applied for Japanese traditional residential houses, the shear resistance of mud wall is mainly considered. While the moment resistance of end joints between columns and beams is not taken into account in the overall lateral performance of the frame. In order to clarify the contribution of the moment resistance from each column and beam end joint, experimental study with numerical analysis have been carried out on the performance of column and Sashi-gamoi tie beam frame under both conditions with and without mud wall. Simultaneously individual joint rotation test was conducted to improve the estimating theories of traditional column-tie beam frame.

Figure 1. Experiment examples by research subjects

2. Research subjects

The research of frame with upper mud wall system is focused along following subjects for example (Figure 1).

1) **Performance of frame based on the column and beam joint rotation** is estimated by conducting the cyclic loading test of each joint type and the whole frame with same scale (as shown in Figure 2). The different moment resistance of the side T-shape joint and center X-shape joint from push to pull side due to the unsymmetrical structure and working mechanism is clarified. From this research, the lateral performance of the frame is confirmed by overlying the moment of all the joints, and it fits well with the numerical results on the elastic deformation part.

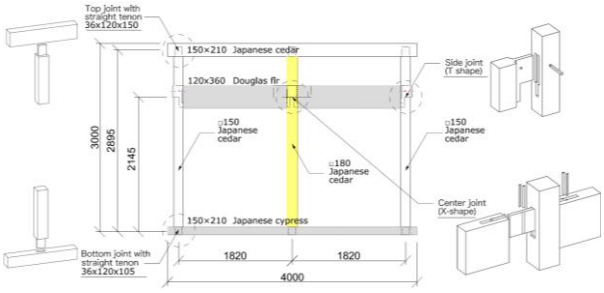

Figure 2. Structural details of joints and the frame

2) **Performance of frame with hanging mud wall**. By contrasting the lateral resistance of the frame with and without mud wall, the overall performance of frame with mud wall in practical design can be considered as the assembly of rotational resistance calculation of all the tenon-mortise joints, the diagonal compression axial force, with the addition of shear resistance of mud wall. The overlying result is a little larger in elastic deformation part, and the effect of large bending deformation of columns that bearing the shear force from mud wall is the main reason.

3. Future plan

Based on current research, the diagonal compression effect of Sashi-gamoi tie beam will be evaluated accurately, along with the influence of columns' combination including their elastic modulus and cross-sections. What's more, several different parameters, including the position and cross-section of beams, the diameter of the dowels and the dimension lost of the columns are expected to be considered in the further frame tests and numerical analysis, aimed to improve the estimating theories of Japanese traditional residential frame system with hanging wall.

RECENT RESEARCH ACTIVITIES

Relaxation effects in the scent of *Lilium japonicum*

(Laboratory of Innovative Humano-habitability, RISH, Kyoto University)

Aya Yanagawa

Lillium japonicum has been a sacred flower of Miwa shrine in Nara for over 1300 years. It has been symbolized for disease resistance, and dedicated to the gods who controls disease epidemics. Japanese people traditionally come to pray in this shrine with the wishes of disease healing. The shrine holds two annual ceremonies, which called as Chinka-festival (flower comforting festival) and Saikusa-festival (Yuri festival) to placate the ancient gods and sprits. Saikusa festival is called also as Lily festival since *L. japonicum* has been dedicated to the guardian god. In this study, to approach the pharmaceutical reason behind the dedication of this flower, the questionnaire-based investigation has been conducted to learn the influence of its scent on human physiological condition.

Materials and methods

The questionnaire was designed by the physiological and psychological parameters (Miyazaki 1997; Higuchi et al., 2002). The survey was conducted at the lily garden in Miwa shrine, Nara, from 27th May to 18th June 2017 during the annual opening time of the lily garden. The questionnaire was provided randomly to visitors. A volunteered visitor cooperated to the survey. We have collected the answer from 239 visitors including 165 females and 65 males. Nine people did not provide the information of their gender.

Suggested physiological effects of the scent of *Lilium japonicum*

Subjective appraisal	Mark	Physiological response		psychological response		
		Sympathetic nerve	Parasympathetic nerve	affirmative	contra diction	rest
Depression or Dejection (Q4)	Low		O	O		
Anger or Hospitality (Q5)	Low		O	O		
Tension or Anxiety (Q7)	Low		O	O		
Vigor or Activity (Q8)	High	O		O		
Fatigue or Inertia (Q9)	Low		O	O		
Confusion or Bewilderment (Q10)	Low		O	O		
Others						
Preference (Q2)	High		O	O		
Happiness (Q3)	Mid	△	△	△		
Calmness (Q6)	high		O			O

Questionnaire

Q1. Please described the impression of this flower's scent in a few words.
Q2. You like the scent.
Q3. This scent makes you happy.
Q4. This scent makes you depressed.
Q5. This scent makes you irritated.
Q6. This scent makes you feel calm/relaxed.
Q7. This scent makes you feel nervous/anxious.
Q8. This scent refresh you.
Q9. This scent makes you tired.
Q10. This scent makes you feel confused.

Fig. 1 The suggested physiological effects of the lily scent.

Results and discussions

Three most-frequently-appeared sense-descriptive adjectives of the lily scent (Q1) were 'gentle', 'sweet' and 'elegant'. The subjective appraisals (Q2-Q10) indicated that the lily scent enhanced the activity of parasympathetic nerves (Fig. 1). The results indicated that the scent of the sacred flower, *L. japonicum* has relaxation effects on human.

Acknowledgements

The author deeply appreciate to the corporation of Miwa shrine, Nara. The author is grateful to Mr. Arai, S. (Miwa shrine) and Dr. Nakamura, M. (Kyoto University) for their helps and thoughtful discussions. This research had been conducted in the corroboration project with Ms. Fujisawa, M., Mr. Hanasaki, N., Dr. Takikawa, Y., Dr. Matsukawa, T., Prof. Akino, T. and Prof. Kajiyama, S.. The results have been published in the Jpn. J. Pharmacol. 73(2), 1-6. (in Japanese with English summery)

References

[1] Miyazaki, Y., "The relationship netween subjective evaluation and physiological response.", *Jpn. J. Sens. Eval.* vol. 1, pp37-42, 1997.(in Japanese with English summery)

[2] Higuchi, T., Shouji, K. and Hatayama, T. "A psychological study of sense-descriptive adjectives for characterizing fragrance", *Jpn. J. Res. Emotions* vol. 8, pp45-59, 2002.

RECENT RESEARCH ACTIVITIES

Simulations and modeling of geospace environment

(Laboratory of Computer Simulation for Humanospheric Sciences, RISH, Kyoto University)

Yoshiharu Omura and Yusuke Ebihara

We numerically obtained Green's functions to model evolution of the electron distribution function after all of the possible interactions with the waves. In both wave models with and without subpackets, electrons undergoing the cyclotron resonance with the waves are efficiently accelerated by nonlinear wave trapping. Modifying the numerical Green's function method with the simplified model of chorus waves uniform in longitude, we compute the formation process of the outer radiation belt electron fluxes induced by the interaction with the chorus waves localized in longitude. The formation of MeV electron fluxes is characterized by large acceleration rates and butterfly pitch angle distributions [1]. We performed test particle simulations with parameters at L = 5 and a small wave normal angle 10 degrees to study the wave-particle interactions via the Landau resonance. We show that effective wave damping occurs near half the electron gyrofrequency. This nonlinear wave damping is contributed by Landau resonance rather than cyclotron resonance. This damping is dominated by perpendicular components of the wave electric field [2]. By analyzing the induction coil magnetometer data in Antarctica, we have found that amplitude-frequency dependence of EMIC subpacket structures is unaltered during their propagation to the ground. EMIC waves observed on the ground are mainly (>70%) associated with right-handed elliptical polarization. Duration of subpacket structure is found to be proportional to its maximum amplitude [3].

The Earth receives energy from the Sun in different forms. The solar wind and the magnetic field are known to drive the magnetic storms and substorms that are major disturbances in near-Earth space. On the basis of the results obtained by global magnetohydrodynamics (MHD) simulation, we found that 37-88% of the magnetic energy coming into the magnetosphere originates from the solar wind kinetic energy. This is fully different from the previously believed idea. The amount of stored/released energy in the tail region is also found to depend on the solar wind condition. This is different from the previous view that the stored/released energy cannot be predicted. The magnitude of the westward auroral electrojet and the Joule heating rates during the substorm expansion phase are correlated with the amount of intake magnetic energy, suggesting that the magnitude of the substorm expansion can be predicted [4]. We also calculated the geomagnetically induced current (GIC) flowing in the Japanese power grid on the basis of 3-dimensional Finite Difference Time Domain method. The simulated GIC is well consistent with the observation conducted at substations [5].

References

[1] Kubota, Y., & Y. Omura, Nonlinear dynamics of radiation belt electrons interacting with chorus emissions localized in longitude. J. Geophys. Res. Space Physics, 123, 4835-4857, 2018.

[2] Hsieh, Y.-K., & Y. Omura, Nonlinear damping of oblique whistler mode waves via Landau resonance. J. Geophys. Res. Space Physics, 123, 7462-7472, 2018.

[3] Kakad, B., Y. Omura, A. Kakad, A. Upadhyay, & A. K. Sinha, Characteristics of subpacket structures in ground EMIC wave observations. J. Geophys. Res. Space Physics, 123, 8358-8376, 2018.

[4] Ebihara, Y., T. Tanaka, and N. Kamiyoshikawa, New diagnosis for energy flow from solar wind to ionosphere during substorm: Global MHD simulation, J. Geophys. Res. Space Phys., 124, 360-378, doi:10.1029/2018JA026177, 2019.

[5] Nakamura, S., Y. Ebihara, S. Fujita, T. Goto, N. Yamada, S. Watari and Y. Omura, Time domain simulation of geomagnetically induced current (GIC) flowing in 500 kV power grid in Japan including a three-dimensional ground inhomogeneity, Space Weather, 16, 1946-1959, doi:10.1029/2018SW002004, 2018.

RECENT RESEARCH ACTIVITIES

Development of microwave irradiation applicators for sustainable chemistry

(Laboratory of Applied Radio Engineering for Humanosphere, RISH, Kyoto University)

Tomohiko Mitani, Naoki Shinohara, Junji Miyakoshi, Shin Koyama, and Yohei Ishikawa

Microwave heating has been expected as one of the energy-and-cost-saving processes for chemical reactions and other applications, owing to its features of rapid and selective heating. Numerous studies on microwave processing of biomass for bioenergy production have been reported [1], and woody biomass conversion by using microwave irradiation has been studied for producing bioenergy and value-added chemical products as an interdisciplinary study in RISH. Here we introduce microwave irradiation applicators for chemical reactions recently developed by our laboratory.

Figure 1 shows a wideband microwave applicator used within the 915 MHz and 2.45 GHz ISM (Industrial, Scientific and Medical) frequency bands [2]. The applicator structure incorporated a coaxial cable, and a liquid sample (volume: 360 ml) was placed in the space between the inner and outer conductors. A truncated cone-shaped polytetrafluoroethylene (PTFE) device was inserted for reducing microwave reflection over a wide frequency range. Microwave heating experiments using the applicator showed that it could heat liquid samples of water or NaOH solution at 915 MHz, 1.7 GHz and 2.45GHz, with estimated microwave absorption efficiencies varying between 28 and 66% depending on the frequency, sample type and heating duration.

Figure 2 shows a downsized microwave applicator (volume: 20 ml) for chemical reactions [3]. The key component of the applicator is a tapered section composed of PTFE and alumina. Insertion of the tapered section between the input port and the applicator vessel realizes reduction of reflected power from the applicator. From microwave heating experiments, the heating rate of the applicator was roughly estimated as 63 to 69 K for a 5-minute 2.45-GHz microwave irradiation at the input power of 100 W. These developed applicators will contribute to the next generation of green and sustainable chemistry.

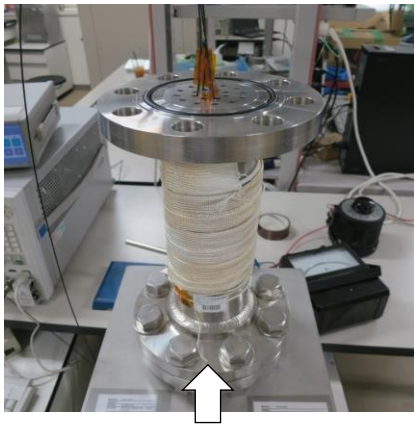

Figure 1. Wideband microwave applicator.

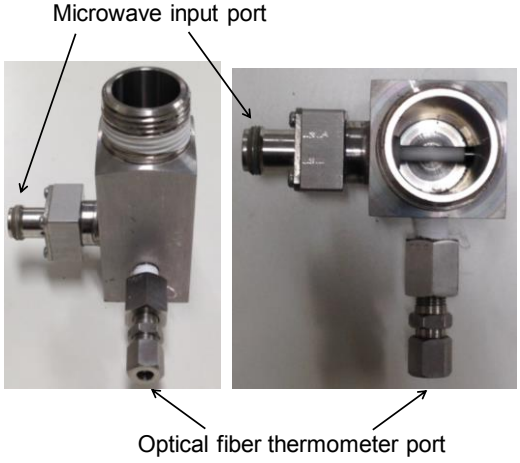

Figure 2. Downsized microwave applicator.

References

[1] T. Mitani, “Recent Progress on Microwave Processing of Biomass for Bioenergy Production”, *Journal of the Japan Petroleum Institute*, vol. 61, no. 2, pp. 113-120, 2018.

[2] T. Mitani, N. Hasegawa, R. Nakajima, N. Shinohara, Y. Nozaki, T. Chikata, T. Watanabe, “Development of a wideband microwave reactor with a coaxial cable structure”, *Chemical Engineering Journal*, vol. 299, pp. 201-216, 2016.

[3] T. Mitani, R. Nakajima, N. Shinohara, Y. Nozaki, T. Chikata, T. Watanabe, “Development of a Microwave Irradiation Probe for a Cylindrical Applicator”, *Processes*, vol. 7, no. 3, paper no. 143, 2019.

RECENT RESEARCH ACTIVITIES

Novel space environment monitor, instrument, and space mission concepts

(Laboratory of Space Electromagnetic Environment Exploration, RISH, Kyoto University)

Hirotsugu Kojima and Yoshikatsu Ueda

Space debris observation, modelling, and mitigation

The space debris problem is tackled from observation (space situational awareness), trajectory evolution, and mitigation points of view. 1) A method to identify the size, shape, and rotation features, and to determine the trajectory of known space debris using range Doppler data of MU (Middle and Upper) Radar, RISH, Kyoto Universiry, is investigated with successful observation results. 2) A study to investigate space debris trajectory evolution focusing on objects smaller than 1 cm has been started to shed light on geomagnetic field effects.

Exploration of electromagnetic space environments

The dominant phenomena in space plasmas are electromagnetic. The medium that transfers kinetic energies of plasma particles in space plasmas is plasma waves, because space plasmas are essentially collisionless. The energy transfer process taking place in space is so-called wave-particle interaction. Exploring electromagnetic environments in space is to investigate wave-particle interactions. The present research focuses on plasma wave observations via scientific satellites. The Exploration of the terrestrial radiation belts by the Arase satellite is the most recent activity. Plasma waves are believed to have significant roles for the generation and loss of high energy particles in the radiation belts. Plasma waves observed by the Arase satellite are extensively analyzed consulting particle measurement data. The results have been showing the detailed and quantitative processes of wave-particle interactions in the radiation belts. Another exploration got started in October 20, 2018. It is the BepiColombo mission targeting the Mercury. Plasma wave instruments onboard the spacecraft will reveal the wave-particle interactions that no one has seen before around the Mercury after 6years' cruising.

Miniaturization of plasma wave receiver system

Plasma wave receiver is one of the essential instruments for space environment exploration; however, conventional receiver has a problem in its large weight and size. In order to overcome this problem, we have been miniaturized plasma wave receiver by developing Application-Specific Integrated Circuits (ASIC) for plasma wave receivers. We succeeded in developing miniaturized plasma wave receiver by realizing analog circuit, which is especially large part of the receiver, using ASIC. This miniaturized receiver will be onboard the SS-520-3 sounding rocket, which will launch in the not-too-distant future to resolve the cause of ion outflow phenomena at the cusp region. In addition, we aim to develop a mixed-signal ASIC chip for one-chip plasma wave receiver. The mixed-signal ASIC chip includes all analog and digital circuits for plasma wave receiver. One-chip plasma wave receiver allows to reduce weight and size of the instruments drastically, and it will contribute for increasing opportunities of plasma wave observation.

Theoretical study of fine bubble and its application research

Fine bubble (FB, less than 1 micro meter) technology is standardized as ISO/TC 281 and its basic and application research is conducted by many researchers. Basic properties and assumed generation mechanisms are now making clear. There is still remained problems of integrated theory of FB such as generation and stabilization. And we also need to apply FB technology to various application field with its detailed theory. As for integrating basic properties, we conduct various measurement such as ultrasonic attenuation of FB water, as measuring electrical potential of FB and as comparison with nano-particles in water. We also try to do application experiment in agricultural field as international collaboration study.

PRIZE

Drs. Hwang Sungwook, Kayoko Kobayashi, Zhai Shengcheng and Professor Junji Sugiyama were awarded the Journal of Wood Science Best Paper Award by Japan Wood Research Society on 15 March 2019

Drs. Hwang Sungwook, Kayoko kobayashi, Zhai Shengcheng and Professor Junji Sugiyama were awarded the Journal of Wood Science Best Paper Award by Japan Wood Research Society on 15 March 2019 for their novel paper titled "Automated identification of Lauraceae by scale-invariant feature transform", Journal of Wood Science, Vol.64, No.2.

Dr. Kayoko Kobayashi was awarded the Encouragement Award by the Cellulose Society of Japan on 5 July 2018

Dr. Kayoko Kobayashi was awarded the Encouragement Award by the Cellulose Society of Japan on 5 July 2018 for her novel research "Structure and properties of hydrated crystalline polysaccharides".

Mr. Yuki Tokunaga was awarded the Poster Prize Award by the 63rd Lignin Symposium

On 2 November 2018, Mr. Yuki Tokunaga was presented with the Poster Prize Award at the 63rd lignin symposium for his presentation on NMR analysis of adsorption between lignin and carbohydrate-binding module of cellulase.

Mr. Chihiro Kimura was awarded the Student Poster Competition Award by the WST/JWRS International Convention

On 9 November 2018, Mr. Chihiro Kimura was presented with the 2nd Place Student Poster Competition Award at the 2018 Society of Wood Science and Technology (SWST)/the Japan Wood Research Society (JWRS) International Convention for his study on production of antiviral compounds from sugarcane bagasse by microwave reaction.

Dr. Yuri Takeda was awarded the Japan Wood Research Society Outstanding Woman Student Award for 2018 by the Japan Wood Research Society

On 26 January 2019, Dr. Yuri Takeda was awarded the Japan Wood Research Society Outstanding Woman Student Award for 2018 for her outstanding research achievements related to metabolic engineering studies toward elucidation of the relationship between lignin aromatic composition and lignocellulose usability.

Mr. Subir Kumar Biswas won 1st Prize in the Student Poster Competition, 2018 Joint Convention of the Society of Wood Science and Technology, USA (SWST) and the Japan Wood Research Society (JWRS)

Mr. Subir Kumar Biswas won 1st Prize in the Student Poster Competition in the Joint Convention of the Society of Wood Science and Technology, USA (SWST) and the Japan Wood Research Society (JWRS) held in Nagoya in November 2018 for the poster titled "Transparent Polymer Nanocomposites Reinforced with Immiscible Nanocelluloses Fabricated via a Water-Based Pathway".

Mr. Subir Kumar Biswas was awarded the Student Travel Grant by the Society of Wood Science and Technology, USA (SWST)

The Student Travel Grant was awarded to Mr. Subir Kumar Biswas by the Society of Wood Science and

Technology, USA (SWST) to present his poster titled “Transparent Polymer Nanocomposites Reinforced with Immiscible Nanocelluloses Fabricated via a Water-Based Pathway” in the Joint Convention of the Society of Wood Science and Technology, USA (SWST) and the Japan Wood Research Society (JWRS) held in Nagoya in November 2018.

Professor Hiroshi Isoda and his laboratory received 8th Seismic Retrofitting Architectural Excellence Award from Japan Building Disaster Prevention Association

On 19 February 2019, Professor Isoda and his laboratory received 8th Seismic Retrofitting Architectural Excellence Award from Japan Building Disaster Prevention Association by seismic retrofitting design and construction of Shima Kanko Hotel “The Classic and The Club”. They were historically valuable buildings originally designed by the Architect, Togo Murano.

Dr. Seiji Zenitani received Tanakadate Award from Society of Geomagnetism and Earth, Planetary and Space Sciences

On May 23, 2018, Dr. Seiji Zenitani received Tanakadate Award from Society of Geomagnetism and Earth, Planetary and Space Sciences (SGEPSS) for study of micro physical processes in magnetic reconnection employing new approaches.

Mr. Takeshi Nogi received ISSS Prize

On September 13, 2018, Mr. Takeshi Nogi was awarded ISSS Prize for his outstanding presentation on two-dimensional particle simulation of whistler mode chorus wave damping through Landau resonance in ISSS-13 (The 13th International School/Symposium for Space Simulations).

Mr. Ryo Mochizuki was awarded the Best Presentation Award at Thailand Japan Microwave 2018 (TJMW2018)

On June 27-29, 2018, Mr. Ryo Mochizuki was awarded the Best Presentation Award for his poster presentation titled “Novel Length Independent Beltrami Resonators Using Corrugated Reflectors” at Thailand Japan Microwave 2018 (TJMW2018).

Mr. Yuta Nakamoto was awarded the Best Presentation Award at Thailand Japan Microwave 2018 (TJMW2018)

On June 27-29, 2018, Mr. Ryo Mochizuki was awarded the Best Presentation Award for his poster presentation titled “Study on a Microwave Power Transfer System to a Stratospheric Platform Airship” at Thailand Japan Microwave 2018 (TJMW2018).

Mr. Isami Sato was awarded WTC (Wakate Technical Committee) Best Presentation Award at 2018 English Presentation Workshop by IEEE Microwave Theory and Technique Society (MTT-S) Kansai Chapter

On October 13, 2018, Mr. Isami Sato was awarded WTC (Wakate Technical Committee) Best Presentation Award for his presentation titled “Basic Study for Wireless Power Transfer to a Pipeline Inspection Robot” at 2018 English Presentation Workshop by IEEE Microwave Theory and Technique Society (MTT-S) Kansai Chapter.

PRIZE

Mr. Takashi Hirakawa was awarded the Student Award, at 2018 Asia Wireless Power Transfer Workshop

On November 2-4, 2018, Mr. Takashi Hirakawa was awarded the Student Award for his presentation titled "Theoretical Analysis of the Simple Single Shunt Rectifier" at 2018 Asia Wireless Power Transfer Workshop.

Mr. Seishiro Kojima was awarded the Best Presentation Award at IEEE AP-S Kansai Joint Chapter Workshop

On December 8, 2018, Mr. Seishiro Kojima was awarded the Best Presentation Award for his poster presentation in Japanese titled "Low Side Lobe Flat Beamforming by Synthesizing Chebyshev Beams for High Efficient Microwave Power Transfer" at IEEE AP-S Kansai Joint Chapter Workshop.

Mr. Taichi Sasaki was awarded the Best Presentation Award at IEEE AP-S Kansai Joint Chapter Workshop

On December 8, 2018, Mr. Taichi Sasaki was awarded the Best Presentation Award for his poster presentation in Japanese titled "Study on Multipath Retrodirective for Microwave Power Transmission" at IEEE AP-S Kansai Joint Chapter Workshop.

Mr. Tatsumasa Hagiwara was awarded the Best Student Paper Award at the Asia-Pacific International Symposium on Aerospace Technology, 2018

On October 17, 2018, Mr. Tatsumasa Hagiwara was awarded the Best Student Paper Award for his presentation titled "Performance Evaluation of Magnetic Nozzle by using thermal plasma" at the Asia-Pacific International Symposium on Aerospace Technology.

ABSTRACTS (PH D THESIS)

Generation of transgenic rice with altered lignin composition and comparative characterization of their biomass utilization properties

(Graduate School of Agriculture, Laboratory of Metabolic Science of Forest Plants and Microorganisms, RISH, Kyoto University)

Yuri Takeda

Lignocellulose, a complex bio-composite composed of lignin, cellulose, and hemicelluloses, constitutes the secondary cell walls of vascular plants and accounts for the highest proportion of terrestrial biomass on Earth. Hence, sustainable production and utilization of lignocellulosic biomass are crucial. Trees and grass biomass crops represent major lignocellulose feedstocks. While the annual biomass production of typical tree species is estimated to be less than 20 t ha^{-1} $year^{-1}$, some large-sized grass biomass crops, such as *Sorghum*, sugarcane, and *Erianthus*, produce several-fold higher biomass yields compared with those of typical trees [1]. In addition, delignification of grass lignocellulose is generally easier than that of wood lignocellulose [1]. These characteristics render grass biomass crops potential materials for biochemical and thermochemical platforms and/or combustion use, although trees are indispensable for wood-based materials and for pulp and paper production.

Lignin is mainly composed of three different types of aromatic component, *p*-hydroxyphenyl (H), guaiacyl (G), and syringyl (S) units. Lignin aromatic composition, i.e., H/G/S lignin unit ratio, has been considered to be an important structural trait that affects the physico-chemical properties of lignocellulosic biomass. However, our knowledge regarding the relationship between the lignin aromatic composition and biomass utilization characteristics is yet considerably limited especially in monocotyledonous grass species. The main objectives of this PhD research were therefore to generate novel transgenic rice plants that produce lignocellulose with distinct lignin aromatic composition and then, through comparative characterization of their lignocellulose properties, to elucidate the effect of lignin composition on the utilization properties of grass lignocellulose as a source of biofuels and biomaterials.

First, transgenic rice lines augmented with G and S lignin units were successfully obtained through manipulating coniferaldehyde 5-hydroxylase (*CAld5H*) gene expression. Among three *CAld5H* genes identified in rice, *OsCAld5H1* appeared to be predominantly expressed in lignin-producing rice vegetative tissues. RNAi-mediated down-regulation of *OsCAld5H1* resulted in altered lignins largely enriched in G units, whereas up-regulation of *OsCAld5H1* under the control of a modified ubiquitin promoter resulted in lignins substantially enriched in S units, as demonstrated by a series of wet-chemical and NMR structural analyses. The results collectively demonstrate that *OsCAld5H1* expression is a key factor controlling the S/G lignin composition in rice cell walls [2].

To further investigate the effect of *OsCAld5H1*-suppression on rice lignin structure, the author characterized loss-of-function mutants of *OsCAld5H1* generated by the CRISPR/Cas9 genome editing system. A series of cell wall analysis demonstrated that, although lignins in the mutant were predictably enriched in G units, all tested mutant lines produced considerable amounts of S units. Intriguingly, lignin *γ*-*p*-coumaroylation analysis by the DFRC method revealed that the enrichment of G lignin units in the *OsCAld5H1*-knockout mutants was limited to the non-γ-*p*-coumaroylated lignin units, whereas grass-specific γ-*p*-coumaroylated lignin units were apparently unaffected. These data suggested that CAld5H is mainly involved in the production of non-γ-*p*-coumaroylated S lignin units, common in both eudicots and grasses, but not in the production of grass-specific γ-*p*-coumaroylated S units in rice [3].

Second, transgenic rice lines augmented with H lignin units were successfully obtained through manipulating p-*coumaroyl ester 3-hydroxylase* (*C3'H*) gene expression. *C3'H*-knockdown lines generated via RNAi-driven gene silencing, with about 0.5% of the residual expression levels, reached maturity and set seeds, whereas *C3'H*-knockout rice mutants generated via the CRISPR/Cas9-mediated targeted mutagenesis were severely dwarfed and sterile. Cell wall analysis of the mature *C3'H*-knockdown RNAi lines revealed that their lignins were largely enriched in H units while being substantially reduced in the normally dominant G and S units. Interestingly, however, lignin *γ*-*p*-coumaroylation analysis by the DFRC

method revealed that the enrichment of H units was limited to the non-acylated lignin units, with grass-specific γ-*p*-coumaroylated lignin units remaining apparently unchanged. These data suggested that, similar to what the author has shown for CAld5H, C3′H is mainly involved in the production of non-γ-*p*-coumaroylated lignin units, but not in the production of grass-specific γ-*p*-coumaroylated lignin units in rice. Suppression of *C3'H* also resulted in a substantial reduction in wall cross-linking ferulates. These results demonstrate that *C3'H* expression is an important determinant not only of lignin content and composition but also of the degree of cell wall cross-linking in grasses [4].

The author further characterized the CRISPR/Cas9-mediated *C3'H*-knockout mutants. In line with their severely impaired growth phenotype, the *C3'H*-knockout lines appeared to show irregular vasculature and ectopic lignification in culm and root. Transcriptomic analysis data suggested that, along with altered expressions of the phenylpropanoid biosynthetic genes, gene expressions related to various biological processes were perturbed in the *C3'H*-knockout lines. Lignin analysis of the mutant cell walls demonstrated that, as observed in the *C3'H*-knockdown lines, H lignin units were substantially increased but the augmentation of H lignin units in the mutants were limited to non *γ-p*-coumaroylated lignin units, with grass-specific *γ-p*-coumaroylated lignin units being mostly unaffected, further supporting the author's notion that there is C3′H-independent metabolic pathway(s) responsible for the production of grass-specific *γ-p*-coumaroylated lignin units.

Lastly, the author used the above-described transgenic rice lines to study the impact of the altered lignin composition on the chemical reactivity, enzymatic saccharification efficiency and calorific value of rice lignocellulose. It was suggested that H and G lignins are more susceptible to acid-induced condensation reactions than S lignins. The H-lignin-enriched transgenic rice was shown to display significantly enhanced biomass saccharification efficiency without any pretreatment or with alkali and acid pretreatments, whereas the S-lignin-enriched transgenic rice showed further enhanced saccharification efficiency after liquid hot water pretreatment. While no significant differences in the biomass heating values were observed between the transgenic rice materials tested, analysis of synthetic lignins comprising only H, G or S units suggested that increasing H or G units may be beneficial to increase the heating value of biomass [5].

Acknowledgements

The author thanks Professor Dr. Toshiyuki Takano and Dr. Masahiro Sakamoto, Graduated school of Agriculture, Kyoto University, Dr. Taichi Koshiba and Dr. Shinya Murakami, RISH, Kyoto University, Professor Dr. John Ralph and Dr. Steven D. Karlen, University of Wisconsin, Professor Dr. Keishi Osakabe, Dr. Yuriko Osakabe and Dr. Takefumi Hattori, Tokushima University, Professor Dr. Hironori Kaji and Ms. Ayaka Maeno, Institute for Chemical Research (ICR), Kyoto University, and Dr. Kazuaki Katagiri, Mr. Shimpei Yamaguchi and Mr. Takuya Ehiro, Osaka Research Institute of Industrial Science and Technology, for their scientific advices and technical supports. The author also thanks Dr. Masaharu Kuroda, National Agriculture and Food Research Organization, Professor Dr. Ko Shimamoto and Dr. Daisuke Miki, Nara Institute of Science and Technology, and Professor Dr. Seiichi Toki, Dr. Masaki Endo and Mr. Masafumi Mikami, NARO, for providing transformation vectors. The author acknowledges the Japan Society for the Promotion of Science (JSPS) for financial supports (#17J09654). Part of this study was conducted using the facilities in the DASH/FBAS at RISH, Kyoto University, and the NMR spectrometer in the JURC at ICR, Kyoto University.

Reference

[1] Umezawa (2018) *Phytochem. Rev.* 17:1305-1327; [2] Takeda *et al.* (2017) *Planta* 246:337-349; [3] Takeda *et al.* (2018) *Plant J.* 95:796-811; [4] Takeda *et al.* (2019) *Plant J.* 97:543-554; [5] Takeda *et al.* (2019) *J. Wood Sci.* 65:6.

ABSTRACTS (PH D THESIS)

Characteristics of tropical tropopause and stratospheric gravity waves analyzed using high resolution temperature profiles from GNSS radio occultation

(Graduate School of Science, Laboratory of Atmospheric Sensing and Diagnosis, RISH, Kyoto University)

Noersomadi

The tropical tropopause at 12–19 km altitude functions as a boundary between the upper troposphere and lower stratosphere (UTLS), typically at altitudes of 10−30 km. Various coupling processes occur across this region which influence mixing between the troposphere and stratosphere, primarily through the activity of atmospheric gravity waves (GWs). The routine radiosonde observations are mostly undertaken from continental locations, so they are not sufficient for describing the global distribution of meso-scale atmospheric perturbations.

Global Navigation Satellite System – radio occultation (GNSS-RO) refers to limb soundings of radio waves transmitted by navigation satellites passing through the Earth's ionosphere and atmosphere, which arrive at an onboard GNSS receiver. Since April 2006, the Constellation Observing System for Meteorology, Ionosphere and Climate (COSMIC), working in conjunction with NSPO Taiwan and UCAR has been retrieving between 1500−2000 atmospheric profiles per day. COSMIC provides global temperature profiles with a precise vertical resolution that is comparable to radiosonde measurements. The objective of this study was to utilize COSMIC data to investigate the temperature structure and perturbations in the UTLS.

There are two fundamental GNSS-RO retrieval methods called the geometrical optics (GO), which is the time derivative of the instantaneous phase variation, and wave optics (WO) which inverts the occulted radio signal in the multipath region due to sharp gradient temperature and water vapor. The GO- and WO-based profile provides ~1.5 km and ~0.1 km vertical resolution, respectively. We conducted validation study to discuss different GNSS-RO retrievals derived from GO and WO, then studied the tropical tropopause and stratospheric GWs using WO-based temperature profiles. We processed the retrieval program at RISH, Kyoto University, adopting one of WO methods called full spectrum inversion (*rishfsi*), which was modified from the retrieval scheme at UCAR. We obtained a good vertical resolution (about 100 m near the tropopause) of temperature profiles for altitudes of up to 30 km. The upper limit of the *rishfsi* datasets is ~28 km.

The combined GO-based and WO-based profile occurring at a certain height is known as the transition height or sewing height. UCAR retrieved two sets of dry atmosphere temperatures (*T*) from COSMIC, which are called atmPrf2010 and atmPrf2013. In atmPrf2010, the sewing height varies between 10 and 20 km, but it is fixed at 20 km for atmPrf2013. The height resolution of atmPrf2010 depends on the sewing height, while the *T* profiles of atmPrf2013 are smoothed over 500 m. We examined a possible discrepancy in the statistical results of the cold point tropopause (CPT) and the lapse rate tropopause (LRT) among the three datasets, two UCAR retrievals and *rishfsi*, in addition to comparing them with radiosonde data from the CINDY DYNAMO 2011 campaign for October 2011 to March 2012. Comparison between the three GNSS-RO retrievals showed that the mean difference of temperature in UTLS between atmPrf2010 and atmPrf2013 is almost zero, while the results of *rishfsi* were colder (warmer) than the UCAR retrievals below (above) the tropopause. Throughout the CINDY-DYNAMO period, we found 134 radiosonde soundings that coincided with GNSS-RO within ±3 hours and they were collocated within 200 km from GNSS-RO. The *rishfsi* is consistent with radiosonde readings below LRT, while both atmPrf2013 and atmPrf2010 show a positive bias of 0.2 K. *T* at CPT of the *rishfsi* data is colder, while that of the UCAR profiles is warmer than the radiosonde soundings, within ±0.4 K. The vertical wavenumber spectral density of the temperature gradient, $\partial T/\partial z$, is in good agreement between the *rishfsi* and the radiosonde measurements for the short wavelength range (< 0.5 km).

Further, we continued our study by utilizing the *rishfsi* dataset to investigate two scientific subjects, which are tropical tropopause and stratospheric GWs.

ABSTRACTS (PH D THESIS)

We investigated the structure of the tropopause for the period January 2007 to December 2016. We investigated the global distribution of static stability (N^2) and the characteristics of the tropopause inversion layer in the tropics, where a large change in temperature gradient occurs associated with sharp variations of N^2. When the N^2 profiles are averaged relative to CPT height, there is a very thin (<1 km) layer with average maximum N^2 in the range 11.0–12.0 × 10^{-4} s^{-2}. The mean of the tropopause sharpness, defined as the difference between the maximum N^2 and minimum N^2 within ±1 km of the CPT, is (10.5 ± 3.7) × 10^{-4} s^{-2}. We focused on the variation of tropopause sharpness in two longitude regions, 90°–150°E (Maritime Continent; MC) and 170°–230°E (Pacific Ocean; PO), which have different land-sea distributions. The sharpness anomaly was out-of-phase with the outgoing longwave radiation (OLR) anomaly in both the MC and PO. The correlation between the sharpness anomaly over MC and PO and the sea surface temperature (SST) Niño 3.4 index was –0.66 and +0.88, respectively. This means that during La Niña (SST Nino 3.4 < –0.5 K) in the MC, and El Niño (SST Nino 3.4 > +0.5 K) in the PO, warmer SSTs in the MC and PO produce more active deep convection that tends to force the air upwards to the tropopause layer causing an increase the temperature gradient. The intra-seasonal variation in the sharpness anomaly during slow and fast episodes of the Madden–Julian oscillation demonstrates that eastward propagation of a positive sharpness anomaly is associated with deep convection. This suggests that convective activity in the tropics is a major control on variations in tropopause sharpness at intra-seasonal to interannual timescales.

We studied the characteristics of temperature perturbations in the stratosphere at 20–27 km altitude caused by the atmospheric GWs. This altitude range does not include a sharp jump in the background N^2 near the tropopause, and it was reasonably stable regardless of season and latitude. We analyzed the vertical wavenumber spectra of GWs with vertical wavelengths ranging from 0.5 to 3.5 km, and we integrated the (total) potential energy E_p^T. Another integration of the spectra from 0.5 to 1.75 km was defined as E_p^S for short vertical wavelength GWs, which was not studied with the conventional GO retrievals. We also estimated the logarithmic spectral slope (*p)* for the saturated portion of spectra with a linear regression fitting from 0.5 to 1.75 km. Latitude and time variations in the spectral parameters were investigated in two longitudinal regions: (a) 90–150°E, where the topography was more complicated, and (b) 170–230°E, which is dominated by oceans. We compared E_p^T, E_p^S, and p, with the mean zonal winds (U) and OLR. We also investigated the ratio E_p^S : E_p^T and discussed that the generation source of E_p^S, E_p^T and p clearly showed an annual cycle, with maximum values in winter at 30–50°N in region (a), and 50–70°N in region (b), which was related to topography. At 30–50°N in region (b), E_p^T and p exhibited some irregular variations in addition to an annual cycle. In the southern hemisphere, we also found an annual oscillation in E_p^T and p, but it showed a time lag of about 2 months relative to U. Characteristics of E_p^T and p in the tropical region seem to be related to convective activity. The ratio of E_p^T to the theoretical model value, assuming saturated GWs, became larger in the equatorial region and over mountainous regions.

We have demonstrated the advantages of high vertical resolution temperature profiles, retrieved from GNSS-RO using *rishfsi,* for understanding the global characteristics of UTLS. We investigated the characteristics of the stability profile of the tropical tropopause, and studied the behavior of the very thin enhanced layer within it. We also analyzed the wave energy of stratospheric GWs with vertical wavelengths from several kilometers to as short as approximately 500 m, which were not captured with the conventional GO retrieval of GNSS-RO data. As evidenced, the *rishfsi* dataset with superior vertical resolution (~0.1 km) is useful for studying meso-scale temperature perturbations in the UTLS. Therefore, we encourage the international scientific community to utilize the *rishfsi* dataset, which is now freely available on the inter-university upper atmosphere global observation network (IUGONET) system, the metadata database of the Japanese inter-university research program (www.iugonet.org).

Acknowledgement
Noersomadi would like to thank the Program of Research and Innovation in Science and Technology (RISET-Pro), Ministry of Research, Technology and Higher Education (RISTEKDIKTI) of Indonesia. This study was partially supported by JSPS KAKENHI Grant Number 22253006, JP15H03724, JP18K03741, and RISH, Kyoto University (Mission 5-3).

ABSTRACTS (PH D THESIS)

Study on miniaturization of plasma wave measurement system

(Graduate School of Engineering, Laboratory of Space Electromagnetic Environment Exploration, RISH, Kyoto University)

Takahiro Zushi

Interplanetary space is filled with plasma, mostly generated by the solar wind. In the near-Earth region, the Earth's magnetosphere is formed by the interaction of the geomagnetic field and the solar wind. The magnetosphere is divided into several regions depending on the characteristics of the plasma and the various phenomena occurring in each of these regions. In addition, the magnetosphere experiences the phenomenon of magnetic storms, in which disturbances are caused by the Sun throughout these regions. Magnetic storms have various influences on the whole magnetosphere. Although these characteristics and various phenomena in the Earth's magnetosphere are well understood, there are many unexplained phenomena. For this reason, observations of the space electromagnetic environment are still being made by satellites.

Since the kinetic energy of the collisionless space plasma is exchanged through plasma waves, observations of plasma waves are important for understanding the behavior of space plasma. Hence, plasma wave instruments are essential for exploring the space electromagnetic environment and magnetospheric exploration satellites carry plasma wave instruments. Plasma wave instruments necessarily include large electric circuits because they require wide frequency range, high gain, and low noise analog circuits and digital signal processors for onboard calculations. The present thesis focuses on the miniaturization of plasma wave instruments. Science missions are restricted by limitations on resources in spacecraft. Thus, miniaturization allows plasma wave instruments to be included on new scientific missions and can be expected to lead to new discoveries.

For miniaturization of plasma wave receivers, application-specific integrated circuits (ASICs) are used in this study. An ASIC is an integrated circuit specialized for a particular use. A full custom design is used for developing analog ASICs and a standard cell design is used for digital ASICs.

In the present study, an ASIC for a waveform capture (WFC) receiver is developed, which improves on three points that are unsatisfactory in conventional ASICs: a high offset voltage in the main amplifier, high harmonic distortion in the switched capacitor (SC) filter, and narrow input/output range over the circuit. The main amplifier often has a high offset voltage for a gain setting of 20 dB or 40 dB. To address this problem, an offset adjustment circuit is added. An SC filter is used as an anti-aliasing filter in a WFC receiver. SC filters exhibit high harmonic distortion due to charge injection effects. The harmonic distortion of the SC filter is reduced by the following three improvements: increasing the capacitance, changing the switching sequence, and changing the transfer function. To narrow the dynamic range of the ASIC, a rail-to-rail opamp. is designed. Finally, rail-to-rail of the whole WFC receiver is realized by replacing the Gm-C filters.

The application of an ASIC for a WFC receiver, plasma wave instruments on board a sounding rocket, and a small sensor probe for multiple point observations are developed. SS-520-3 is a sounding rocket experiment for clarifying the ion outflow phenomenon in the polar cusp region. In order to measure wave-particle interactions, which are considered the primary mechanism of the ion acceleration, a plasma wave instrument called the low frequency analyzer system (LFAS) is installed in the rocket. The LFAS has two receivers for electric sensors, and pre-amplifiers. In addition, LFAS has a circuit for software-type wave-particle interaction analyzer calculations that allows the measurement of waveforms and plasma particles synchronously with high time resolution.

Since conventional one-point observations of plasma phenomena in space cannot distinguish between time and spatial variations, missions based on multiple-point observations have become the trend. A new system for multiple-point observations, referred to as the monitor system for space electromagnetic environments (MSEE), is proposed. The MSEE consists of small sensor probes that can measure

electromagnetic waves and transfer received data to a central station through wireless communication. A prototype model of the MSEE sensor probe is developed. The sensor probe includes a plasma wave receiver, microcontroller, wireless communication module, and battery in a 75-mm cubic housing. In addition, loop antennas, dipole antennas, and actuators to expand the dipole antennas are attached on the housing. The total mass of the sensor probe is 692 g and the total power consumption is 462 mW. In the function test, it was found that the analog components had sufficient characteristics to measure electric fields, and the A/D conversion and wireless transmission worked correctly. For the whole performance in an electric field, the sensor probe had an equivalent noise level of -135 dBV/m/sqrt(Hz).

Recent scientific satellites have carried fast Fourier transform (FFT)-based spectrum receivers. However, such receivers have a disadvantage in that they use a wideband analogue component. A new receiver which overcomes this disadvantage of previous receivers is proposed. The new receiver includes band-limiting in the first stage of the analogue component, and it covers the entire observation frequency range of each band by switching its cutoff frequency. To miniaturize the circuit size, the new receiver uses an ASIC and a field-programmable gate array (FPGA). The ASIC chip includes the analogue component of the receiver and the analogue-to-digital converter, and the FPGA includes an FFT module and the controller of the receiver. The proposed spectrum receiver was successfully implemented with a size of 55 mm x 80 mm x 35 mm and a total power consumption of 948.3 mW. The time resolution of the receiver was 112 ms, and the frequency resolutions for frequency bands 10 Hz to 1 kHz, 1 kHz to 10 kHz, and 10 kHz to 100 kHz were 13 Hz, 130 Hz, and 1.3 kHz, respectively.

In conclusion for the present thesis, the miniaturization of the plasma wave observation systems was achieved successfully.

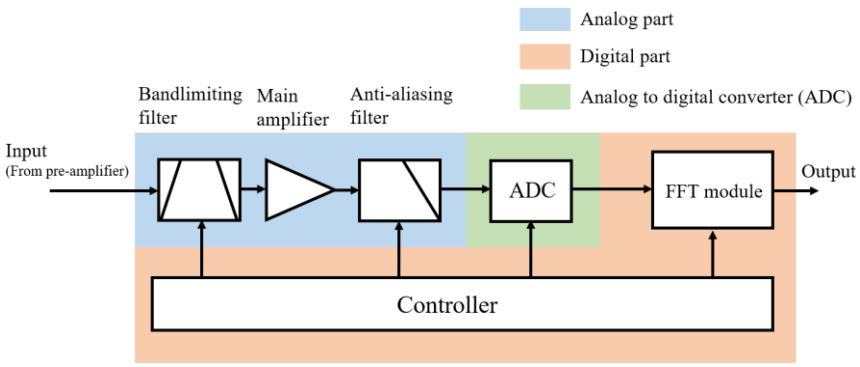

Figure 1. Block diagram of the new type of the spectrum receiver.

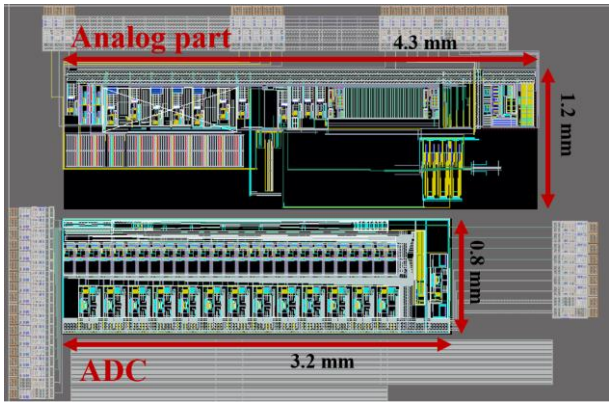

Figure 2. Chip layout of the new type of the spectrum receiver.

ABSTRACTS (MASTER THESIS)

Research on the morphosis of gravitropic bending using a model plant

**(Graduate School of Agriculture,
Laboratory of Biomass Morphogenesis and Information, RISH, Kyoto University)**

Nanako Matsunaga

Introduction

The plant shoot grows upwards by the gravity sensing. While reaction wood is the characteristic wood formed as part of the gravitropic response of trees, primary tissues such as herbaceous plants and young shoots of trees bend upward by differential growth. It is understood that differential growth is caused by different growth rates between upper and lower side of stem. Despite the stem under the apical meristem grows well, there is no clear evidence of where the bending occurs in the stem. Therefore, I examined if the elongation growth occurred at the bending zone by gravitropism.

Methods

Inflorescence stems of *Arabidopsis thaliana* grown on 10 to 20 cm were marked at intervals of 3 mm from the base of the flower and then inclined at 55 °. Photographs were taken after inclination and 24 hours after inclination. The distance between the marks was measured by image processing software; ImageJ. We hereby confirmed the distance of the elongating growth zone from the top of the stem. The bending point was defined as the center of an arc of an inscribed circle to the bending zone.

Next, using a dental impression silicon, replicas of epidermis cells of inflorescence stems were made, and changes of same cell shapes before and after bending were confirmed. Replicas were made from upper and lower side from 3 zones; above bending zone, bending zone, and below bending zone, and observed with a light microscope.

Furthermore, in order to suppress the auxin-induced elongating growth, the polar transport inhibitor; NPA (*N*- (1-Naphthyl) phthalamic acid) 0.1% lanolin paste was applied on above bending zone. These experiments were carried out similarly on no-inclination condition.

Results and discussions

From the measurement of surface extension (marking experiment), it was confirmed that the elongating rate gradually decreased from the shoot tips to the basal of stem, and at the macroscopic level, no elongation was observed in the bending zone. In addition, regardless of the inflorescence stem length, the bending positions were 3 to 4 cm from the tips.

As a result of surface replicas observation, at above bending zone, only longitudinal cell elongation was confirmed. On the other hand, at bending zone, while epidermis cells on upper side did not change in any direction, the cells on lower side expanded in the longitudinal direction and also in the tangential direction. Furthermore, gravitropic bending also occurred even though auxin transport was inhibited, and similar changes in cell shape were observed in epidermal cells of bending zone.

These lines of experiments, it is suggested that the gravitropic bending of inflorescence stem of *Arabidopsis thaliana* is not due to the differential growth induced by auxin.

ABSTRACTS (MASTER THESIS)

Bioethanol production process incorporating expression of laccase bearing lignin-binding peptide

**(Graduate School of Agriculture
Laboratory of Biomass Conversion, RISH, Kyoto University)**

Kento Masuda

In recent year, production of bioethanol and chemicals from lignocellulosic biomass attracts a great deal of interest due to global warming caused by excess usage of fossil fuels. Process of bioethanol production from lignocellulosics consists of pretreatment, saccharification and fermentation. In the conversion process, lignin hiders access of (hemi)celluolytic enzymes to the cell wall polysaccharides, and the residual lignin adsorbs non-productively onto (hemi)cellulase to lose hydrolytic activity of the enzyme. In addition, pretreatments under harsh conditions produce enzyme and fermentation inhibitors. Therefore, removal of the lignin fragments and inhibitors is necessary to improve the bioethanol yield. For this purpose, we planned to develop the conversion process incorporating expression of laccase bearing lignin-binding peptide sequence C416 which had been found by phage display technique [1]

First, we expressed laccase from *Trametes versicolor* bearing the tandem dimer of lignin-binding peptide C416 [2] at N- or C-terminal end in *Saccharomyces cerevisiae* to assess the effects of mutant enzyme on bioethanol production. Next, we expressed the recombinant laccase in *Pichia pastoris*, and effects of the addition of mutant enzyme on bioethanol fermentation was evaluated. In pre-saccharification and simultaneous fermentation (PSSF) process using the laccase bearing the tandem dimer of lignin-binding peptide C416 at C-terminal end, ethanol production was increased compared with PSSF process using the laccase without the lignin biding peptide sequence.

References

[1] Yamaguchi, A., Isozaki, K., Takaya, H., Watanabe, T., “Discovery of 12-mer peptides that bind to wood lignin”, *Scientific Reports*, **6**, 21833, 2016.

[2] Oshiro, S., Yamaguchi, A., Watanabe, T., “Binding behaviour of a 12-mer peptide and its tandem dimer to gymnospermae and angiospermae lignins”, *RCS Advance*, **7**, 31338-31341, 2017.

ABSTRACTS (MASTER THESIS)

Production of antiviral compounds from sugarcane bagasse by microwave reactions

**(Graduate School of Agriculture,
Laboratory of Biomass Conversion, RISH, Kyoto University)**

Chihiro Kimura

Lignocellulosic biomass is renewable carbon source and its efficient conversion is crucial for establishing sustainable society due to its huge quantity, non-competitiveness with food supply and mitigation effects on increasing atmospheric carbon dioxide concentration. Therefore, a large number of studies have been conducted to produce biofuels, platform chemicals and materials from lignocelluloses. So far, a number of natural products have been extracted from plants and identified as bioactive agents including antiviral compounds [1]. However, only a limited number of reports can be found for production of bioactive agents by chemical degradation of plant biomass. According to the IPCC report, global warming attacks human health by direct heat effects and indirect acceleration effects on spread of infectious diseases [2]. Therefore, a novel strategy protecting human life and global environment by the use of plant biomass is strongly required.

In the present study, we studied production of antiviral compounds from sugarcane bagasse using microwave reactions. Sugarcane bagasse is one of the most abundant agro-industrial lignocellulosic residues [3], and microwave irradiation is known as efficient heating methods in polar solvents. Sugarcane bagasse was decomposed by microwave acidic solvolysis and the degradation products were subjected to viral replication inhibition assay against encephalomyocarditis virus (EMCV), which is a nonenveloped single strand RNA virus classified as the family Picornaviridae. As results of the screening, we found an acidolysis reaction producing strong anti-EMCV compounds from sugarcane bagasse. After purification, the antiviral compounds were subjected to the analyses of chemical structure and emerging mechanisms of the antiviral activity. The production of antiviral compounds increases economic feasibility of lignocellulosic biorefinery and contributes to human health and establishment of sustainable society.

References

[1] Kurokawa, M., Ochiai, H., Nagasaka, K., Neki, M., Xu, H., Kadota, S., Sutardjo, S., Matsumoto, T., Namba, T., Shiraki, K., “Antiviral traditional medicines against herpes simplex virus (HSV-1), poliovirus, and measles virus in vitro and their therapeutic efficacies for HSV-1 infection in mice”, *Antiviral Res.*, **22**, 175-188, 1993.

[2] Confalonieri, U., Menne, B., Akhtar, R., Ebi, K.L., Hauengue, M., Kovats, R.S., Revich, B., Woodward, A., Human health. Climate Change 2007: Impacts, Adaptation and Vulnerability. Contribution of Working Group II to the Fourth Assessment Report of the Intergovernmental Panel on Climate Change, Parry, M.L.; Canziani, O.F.; Palutikof, J.P.; van der Linden, P.J.; Hanson, C.E., Eds., Cambridge University Press, Cambridge, UK, 391-431, 2007.

[3] Pandey, A., Soccol, C.R., Nigam, P., Soccol, V.T., “Biotechnological potential of agro-industrial residues. I. Sugarcane bagasse”, *Biores. Technol.*, **74**, 69-80, 2000.

ABSTRACTS (MASTER THESIS)

Characterization of *O*-methyltransferases involved in antitumor lignan biosynthesis in *Anthriscus sylvestris*

(Graduate School of Agriculture, Laboratory of Metabolic Sciences of Forest Plants and Microorganisms, RISH, Kyoto University)

Keisuke Kobayashi

Lignans are typical plant secondary metabolites and distribute widely in vascular plants. Lignans are phenylpropanoid dimers that are linked at C8 position of their propyl side chain. Various lignans are known for having various biological effects, e.g., antitumor, antioxidative, and antiviral effects. Podophyllotoxin is known as an antitumor lignan and used as a precursor for the chemical synthesis of the anticancer drugs such as etoposide, teniposide, and etopophos. Podophyllotoxin for commercial use is mainly isolated from *Podophyllum hexandrum*. However, the overexploitation of the podophyllotoxin producing engendered plant species necessitates an alternative way to stably supply the lignan, that is, a biological production system of podophyllotoxin. To establish the biological production system, it is necessary to elucidate the genes involved in podophyllotoxin biosynthesis. Previous studies of podophyllotoxin biosynthesis used several plant species and some biosynthesis pathways were proposed [1]. There are several *O*-methylation steps in the podophyllotoxin biosynthetic pathways, while eight *O*-methyltransferases (OMTs) that are involved in *O*-methylation of various lignans have so far been identified from several plants [1-4]. Phylogenetic tree analysis using these lignan OMTs and plant OMTs (Pl-OMT II families) indicated that the lignan OMTs was widely spread in various clades, not grouped into a small clade, suggesting that the lignan OMTs were evolved by a convergent evolution [1]. Recently, the research group of the author found that four amino-acid residues are conserved among lignan OMTs by an evolutionary trace method, though homologies of whole amino acid sequences of the lignan OMTs was not high. However, effects of these amino-acid residues on lignan OMT activity have not been examined.

In this study, four mutant proteins of 5-*O*-methylthujaplicatin *O*-methyltransferase (5MTJOMT), where the four conserved amino acid residues were mutated individually, were prepared with single amino-acid residue substitution (K33H, K143R, A199S, and L318C) and subjected to the 5MTJOMT activity assay to examine whether each amino-acid residue affects lignan OMT activity or not. All mutant proteins showed 5MTJOMT activity, while their specific activities significantly differed among all mutant proteins and original 5MTJOMT (WT): 5MTJOMT specific activity was 1.58 ± 0.02 nmol/μg in WT, 0.93 ± 0.05 nmol/μg in K33H, 1.70 ± 0.11 nmol/μg in K143R, 0.09 ± 0.01 nmol/μg in A199S, and 0.36 ± 0.03 nmol/μg in L318C, respectively. Compared with the specific activity of WT (100%), those of K33H and K143R were slightly lower (59.1%) or almost same (107.5%), respectively. Interestingly, the specific activities of A199S and L318C significantly decreased to 5.6% and 23.0%, respectively, suggesting that amino-acid residues, A199 and L318, might contribute to an expression of lignan OMT activity.

References

[1] Umezawa, T., Yamamura, M., Ono, E., Shiraishi, A., Ragamustari, S. K. Recent advances in lignan OMT studies. *Mokuzai Gakkaishi* 65, 1-12, 2019.

[2] Ragamustari, S. K., Nakatsubo, T., Hattori, T., Ono, E., Kitamura, Y., Suzuki, S., Yamamura, M., and Umezawa, T. A novel *O*-methyltransferase involved in the first methylation step of yatein biosynthesis from matairesinol in *Anthriscus sylvestris*. *Plant Biotechnology* 30, 375-384, 2013.

[3] Ragamustari, S. K., Yamamura, M., Ono, E., Hattori, T., Suzuki, S., Suzuki, H., Shibata, D. and Umezawa, T. Substrate-enantiomer selectivity of matairesinol *O*-methyltransferases. *Plant Biotechnology* 31, 257-267, 2014.

[4] Lau, W. and Sattely, E. S. Six enzymes from mayapple that complete the biosynthetic pathway to the etoposide aglycone. *Science* 349, 1224-1228, 2015.

ABSTRACTS (MASTER THESIS)

Characterization of geranyl diphosphate synthase from *Lithospermum erythrorhizon*

**(Graduate School of Agriculture,
Laboratory of Plant Gene Expression, RISH, Kyoto University)**

Hayato Ueoka

Plants have evolved secondary (specialized) metabolisms, which appeared to be non-essential for their life, in addition to primary metabolism ubiquitously found in all organisms. It has been recently recognized that specialized metabolites have important functions in the adaptation to their environment, including pollinator attraction, pest repellent, and plant-plant interactions. Several compounds in specialized metabolism have been used for human life, such as natural dyes, flavors, fragrances, spices, and medicines as well. Based on the chemical structures and biosynthetic pathways, those metabolites are classified into three major classes, i.e. terpenoids, alkaloids, and phenols. Among them, terpenoids represents the largest class, with over 60,000 compounds described to date. According to the number of carbon atoms, terpenoids are subdivided into mono- (C10), sesqui- (C15), di- (C20), sester- (C25), tri- (C30), tetra- (C40), and polyterpenoid (>C40). All terpenoids are constructed from universal building blocks, isopentenyl diphosphate (C5) and its allylic isomer dimethylallyl diphosphate (C5), both of which are provided either *via* mevalonate (MVA) pathway in the cytosol or methylerythritol phosphate (MEP) pathway in plastids. In general, each terpenoid is produced in specific subcellular compartment, i.e. monoterpenoid and diterpenoid are formed in plastids *via* MEP pathway, while sesquiterpenoid is formed in the cytosol *via* MVA pathway. Besides these typical terpenoids, natural products with combined structures of terpenoid and other class compounds are called meroterpenoids.

A medicinal herbal plant, *Lithospermum erythrorhizon*, produces shikonin derivatives, red meroterpenoid pigments. Because of their anti-inflammatory and anti-microorganism effects and their beautiful purple color by co-pigmentation with aluminum, they have been used as ointment and natural dyes in Asian countries, including Japan, China, and Korea. For the mass production of shikonin derivatives, two-step culture system was established using cell suspension cultures of this plant, leading to the stable and rapid production of those valuable compounds (approximately 2 g/l shikonin in culture tank at two weeks) [1]. The development of cell culture system also advanced the study of shikonin biosynthetic pathway at molecular level. One of the rate-limiting steps of shikonin biosynthesis is the formation of *m*-geranyl-*p*-hydroxybenzoic acid (GBA), in which geranyl diphosphate (GPP, C10), a common precursor of monoterpenoid, is attached to *p*-hydroxybenzoic acid.

With respect to the GPP formation, Sommer et al. (1995) reported that GPP synthase activity was mainly detected in the cytosol fraction, not in plastids where GPP and monoterpenoids are commonly formed [2]. Li et al. (1998) also reported that the geranyl moiety of shikonin is derived from the MVA pathway in the cytosol [3]. These reports suggest that GPP synthase of *L. erythrorhizon* (LeGPPS) is exceptionally localized in the cytosol. Toward the elucidation of shikonin biosynthetic pathway, we aimed to identify *LeGPPS* gene through EST- and BLAST-based approaches. Through a series of analyses, we could identify a putative *GPPS* gene. Focusing on this candidate, further biochemical analyses will be performed to uncover the novel GPPS in plants.

References

[1] Yazaki K (2017) *Lithospermum erythrorhizon* cell cultures: Present and future aspects. Plant Biotechnol 34: 131-142.

[2] Sommer S, Severin K, Camara B, Heide L (1995) Intracellular localization of geranylpyrophosphate synthase from cell cultures of *Lithospermum erythrorhizon*. Phytochemistry 38: 623-627.

[3] Li SM, Hennig S, Heide L (1998) Shikonin: A geranyl diphosphate-derived plant hemiterpenoid formed via the mevalonate pathway. Tetrahedron Lett 39: 2721-2724.

ABSTRACTS (MASTER THESIS)

Purine permiases of *Coffea canephora*, CcPUP1 and CcPUP5, are involved in the uptake of adenine

**(Graduate School of Agriculture,
Laboratory of Plant Gene Expression, RISH, Kyoto University)**

Hirobumi Kakegawa

Purine permeases (PUPs) are a large plasma membrane-localized transporter family in plants. These transporters have been shown to function in the proton-coupled uptake of various nucleotide bases and their derivatives, including adenine, cytokinins, and nicotine. Arabidopsis PUP1 was the first member of PUP family identified as the gene which complements the growth of a yeast mutant of adenine uptake. It was shown that the adenine uptake activity of AtPUP1 is inhibited by carbonyl cyanide m-chlorophenyl hydrazine (CCCP). These results suggest the function of AtPUP1 as proton symporter. The adenine uptake activity was shown to be competitively inhibited by the addition of purine derivatives such as cytokinins and caffeine. These results implicate that AtPUP1 mediates the uptake of a broad range of substrates. Arabidopsis contains 21 PUP members in the genome. To date, only four PUP genes have been analyzed.

Rice (*Oryza sativa*) contains 12 PUP family proteins. However, only one member, OsPUP7, was characterized. OsPUP7 was shown to be involved in growth and development. Direct transport assay was not shown, but this transporter possibly mediates the cytokinin transport. Although the direct transport activity is not measured as well, OsPUP7 conferred yeast the sensitivity to caffeine. These results suggest the caffeine uptake activity of OsPUP7 [1].

Nicotine and caffeine are nucleotide base derivatives found in plants. The nicotine uptake activity was reported in a tobacco PUP, NtNUP1 of *Nicotiana tabacum*. NtNUP1 was reported to be involved in the uptake nicotine from the apoplast. Direct uptake activity for nicotine was measured in yeast. NtPUP1 is also shown to take up pyridoxamine, pyridoxine, anatabine, in addition to nicotine.

In this study, we hypothesized that purine permeases of *Coffea canephora* have the ability to take up caffeine in addition to adenine. We have identified 15 members of PUP protein in the genome of *C. canephora*. Based on the yeast sensitivity assay, we selected two candidates, i.e. CcPUP1 and CcPUP5. Direct transport assay was conducted with radioactive compounds. It was shown that both CcPUP1 and CcPUP5 are adenine uptake transporters, but not caffeine uptake transporters. Inhibition assay indicated that this transporter was not inhibited by the excess amount of caffeine. We thought insensitivity to caffeine is important for *C. canephora* PUPs, because adenine uptake transporters of *C. canephora* need to distinguish adenine from caffeine to effectively uptake adenine in cells containing high concentration of caffeine. It can be suggested that purine permeases in origin had the uptake ability for both adenine and caffeine, and that these proteins have been evolved to distinguish adenine from caffeine in plants synthesizing caffeine such as *C. canephora*.

Reference

[1] Kakegawa, H., Shitan, N., Kusano, H., Ogita, S., Yazaki, K., Sugiyama, A. Uptake of adenine by purine permeases of *Coffea canephora* Bioscience, Biotechnology, and Biochemistry (in press).

ABSTRACTS (MASTER THESIS)

Analysis of dynamics and function of daidzein in the soybean rhizosphere

**(Graduate School of Agriculture,
Laboratory of Plant Gene Expression, RISH, Kyoto University)**

Fuki Okutani

Rhizosphere is defined as the “area affected by the root of the plant in soil” and previous works have shown that the rhizosphere has the higher microbial activity mainly due to the influence of root exudates. In the rhizosphere of soybean, it has been reported that isoflavones such as daidzein and genistein secreted by soybean root functions as symbiotic signals with rhizobium and also phytoalexins. These are also shown to be involved in the regulation of rhizosphere microbial communities. Rhizosphere is closely related to the plant growth. It is thought that the metabolites from root play important roles in the formation and maintenance of the rhizosphere; however, its dynamics in the rhizosphere is currently unknown. It is difficult to understand the rhizosphere area precisely. The aim of this study is to define the rhizosphere by creating soybean root zone model. The dynamics of daidzein, the major root root-secreted isoflavone, is analyzed both biochemically and soil physically. I also investigated daidzein concentrations that potentially affect rhizosphere microbial community.

First, to know the tendency of daidzein secretion in soybean fields, daidzein secreted from the root of field-grown soybean was quantified using HPLC. The method is as follows: daidzein secreted from root was quantified directly sandwiching the lateral root with a cellulose acetate membrane which is capable of adsorbing isoflavone effectively. As a result, the secretion of daidzein under field conditions was the highest during the vegetative stages and decreased as it shifted to the reproductive stages, which is consistent with the hydroponic conditions.

Based on the simulation of the dynamics of daidzein calculated from the daidzein distribution coefficient and degradation coefficients, it was shown that in soybean field soil daidzein transfer from roots was limited within about 1 mm in 7 days. Daidzein dynamics was also analyzed using Toyoura sands. The field soil contains higher humic substances and clay minerals. They have daidzein adsorption sites, while Toyoura sand is composed of mainly quart, which is characterized to have no organic matter and uniform particle size. In Toyoura sand, daidzein was not degraded. The distribution coefficient was calculated to be about one twentieth of that of the soybean field soil. Based on these parameters it was simulated that the migration of daidzein from the root surface was about 3 mm for 7 days.

Finally, in order to clarify the extent of the influence of daidzein on the rhizosphere microbial communities, the daidzein concentration that affects bacteria in field soil is analyzed. The effect of daidzein was measured by comparing the bacterial community in which daidzein was added with different concentrations. The content of daidzein in each sample was calculated to be 0.8-28.0 nmol / g soil, which corresponds to the rhizosphere concentration at vegetative growth (10-20 nmol/ g soil). Soil DNA was then extracted from each sample and 16S rRNA amplicon sequence was performed using MiSEQ. The sequences were classified into OTU. PCoA analysis indicated that it forms a significantly different bacterial communities.

ABSTRACTS (MASTER THESIS)

Establishment of virus-induced gene silencing method in *Lithospermum erythrorhizon*, a model plant for plant specialized metabolism

**(Graduate School of Agriculture,
Laboratory of Plant Gene Expression, RISH, Kyoto University)**

Natsumi Isaka

Plants produce a large variety of specialized metabolites, which appear non-essential for plant life, while humans utilize many of those natural organic compounds for human life, such as dye, flavor, spice, functional food, and medicines. Recent years, productions of valuable plant metabolites in microorganisms using plant genes are actively studied as being designated synthetic biology. For achievement of synthetic biology, understanding the complete biosynthetic pathway of interest and genes involved in each biosynthetic reaction step is necessary, while there are only a few examples for such valuable metabolites. This is because the elucidation of biosynthetic pathway of a particular compound is still laborious works, and thus there are many targets to study specialized metabolisms in plants.

An effective approach to identify biosynthetic genes in plants is gene silencing via T-DNA tagging, RNAi, genome editing, etc., which all require the stable transformation method of a target plant. However, there is no ubiquitous method for plant stable transformation, rather researchers should pay large efforts to establish the particular protocol to introduce genes to the plant of interest. It is also known that plant species producing a large amount of specialized metabolites are often difficult to be transformed due to the strong biological activities for their own metabolites. Hence, virus-induced gene silencing technology has a strong merit for the application to analyze the gene function. This is a transient system to shut down the expression of target genes and thus the evaluation of gene functions is achieved in much shorter period than stable transformation-mediated methods.

Lithospermum erythrorhizon is a medicinal plant utilized in many Asian countries as a crude drug and natural dye, as well. The biological active compound produced by this plant is a red naphthoquinone pigment, shikonin, which exists as several ester derivatives in the root bark of this plant. We have an appropriate model system of this plant, i.e., shikonin-producing cell cultures and axenic shoot cultures, in which shikonin production is induced. I this study, we have applied a couple of plant viruses including domestic apple latent spherical virus, which shows relative broad infection spectrum for various plant species and does not exhibit pathogenic symptoms, to *L.erythrorhizon* using LeDI2 gene as a trial. It was already reported that the expression of LeDI2 has strong positive correlation with shikonin production, and the suppression of LeDI2 expression by conventional antisense RNA caused decrease in shikonin production [1]. There are some more experimental steps to improve, but basic methodology has nearly been established.

Reference

[1] Yazaki, K., Matsuoka, H., Shimomura, K., Bechthold, A., and Sato, F. (2001). A novel dark-inducible protein LeDI-2 and its involvement in root-specific secondary metabolism in *Lithospermum erythrorhizon*. *Plant Physiol.*, 125, 1831-1841.

ABSTRACTS (MASTER THESIS)

A study on the detailed boundary layer structure calculated by the Large Eddy Simulation in the real meteorological condition

**(Graduate School of Informatics,
Laboratory of Radar Atmospheric Science, RISH, Kyoto University)**

Naohiro Iwamoto

This research investigated the urbanization effect on the structure of atmospheric boundary layer by constructing the simulation environment of Large Eddy Simulation (LES) under the real meteorological condition.

Introduction

Several previous studies emphasized the importance of the detailed boundary layer structure on the generation of the severe meteorological phenomena. However, in the meso-scale numerical forecast model, the boundary layer structure is conveniently calculated by simple parameterization method. The LES has an advantage in the high-horizontal-resolution simulation by explicitly calculating the grid-scale eddy in the governing equations. However, the ideal cyclic boundary condition was used in the most of the conventional LES studies. For realizing the LES calculation in the real atmospheric condition, this study connected the result of the non-hydrostatic numerical forecast model into the initial and boundary condition of LES.

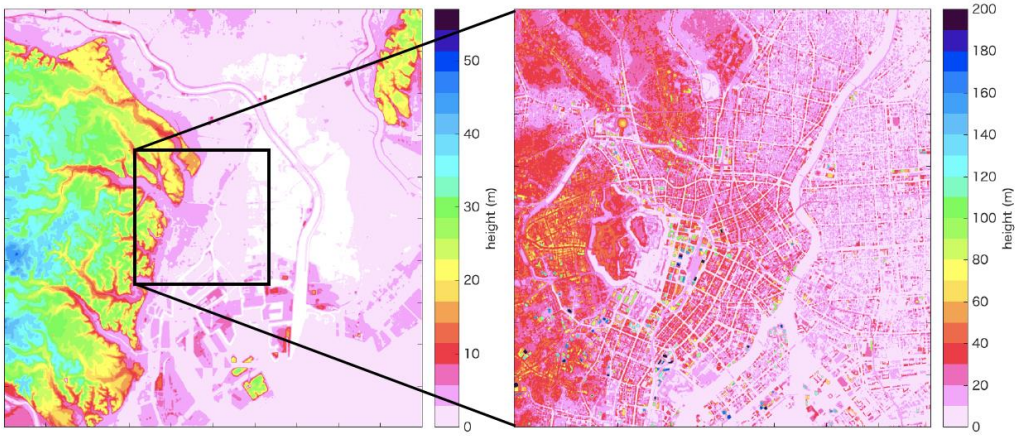

Figure 1. The simulation domain in Tokyo Metropolitan area of LES

Results

The LES environment with the excellent horizontal resolution of five meter was developed by using the high-resolution topographic data in the Tokyo urban regions (Fig. 1). The analysis period was selected on July 11, 2015 by considering the calm meteorological condition.

In the LES simulation, the weak wind region extending to several kilo-meter length was calculated behind the 200m-tall buildings. In this region, the strong vertical wind was analyzed, which implies the strong vertical transport of energy and minor constituent. The simultaneous coherent Doppler lidar observation successfully also showed the similar weak wind region behind the tall buildings. The LES environment in the real weather condition is very useful to elucidate the mechanism of the interaction between the atmospheric boundary layer and the upper free atmosphere.

ABSTRACTS (MASTER THESIS)

Development of high-range resolution lidar for observing aerosol spatial distributions including near ranges

**(Graduate School of Informatics,
Laboratory of Radar Atmospheric Science, RISH, Kyoto University)**

Fumiya Kitafuji

Atmospheric aerosols from nature and anthropogenic sources affect the global climate and local air quality related to human health. A lidar is suitable for observing the spatial distribution of aerosols and conventionally associated with wide-range measurements such as long-range transboundary air pollution. However, the incomplete overlap between the laser beam and field of view of the receiving telescope of the backscatter lidar significantly prevents observation in the near range. In this study, we develop a high-range resolution lidar for observing the detailed aerosol spatial distribution including the near range.

The constructed lidar system can observe aerosol profiles with a maximum range resolution of 18.8 cm by using a short-pulse laser and multispectral detector that can operate at a high sampling rate. Two methods were investigated to observe the near-field range. The first method includes tilting the laser beam axis toward the receiving telescope axis to observe a certain observation range. It is suitable for closed spaces such as the indoors because strong scattering from a hard target (e.g. wall) can be removed. The second method is implemented by slanting a part of the receiving optical axis by the use of several wedge prisms placed in front of the telescope. The advantages of this method are that the observation range in the near field may be modified flexibly. Moreover, the data acquisitions of both the near and far ranges can be achieved within the detector's dynamic range by adjusting the signal power using the wedge prisms. When the telescope diameter was 10 cm (F2) in the Galileo type and 15 cm (F5) in the Newtonian type, this lidar that it can acquire the signal with a statistical uncertainty of less than 10% was 2 m and 5 m, respectively.

Lidar observation on a flat-grassland

Simultaneous measurements between the in-situ instruments using the observation tower and scanning lidar were performed on a flat-grassland in the Miura peninsula in January 2019. We observed that inhomogeneous aerosol spatial distributions varied at a height within several meters under the weak wind condition during nighttime. Figure 1 shows an example of the observation result indicated the inhomogeneous vertical distribution of aerosol backscattering ratio. This is considered to be due to the formation of an aerosol layer caused by a temperature inversion layer under the weak wind conditions during nighttime.

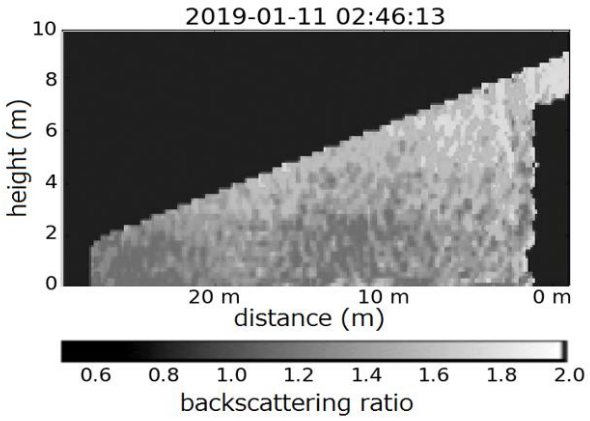

Figure 1. Backscattering ratio of vertical cross section obtained from lidar observation on a flat-grassland in the Miura peninsula at 2:46 JST on January 11, 2019. The vertical and horizontal range resolutions are 0.4 m.

ABSTRACTS (MASTER THESIS)

Functionalization of cellulose nanofiber sheet surface by imprinting method

**(Graduate School of Agriculture,
Laboratory of Active Bio-based Materials, RISH, Kyoto University)**

Kumi Sato

Introduction

Water repellence generated by hierarchical surface structures is known as the “Lotus effect”. In this study, hierarchical structures were formed on cellulose nanofiber (CNF) sheet surfaces by copying a micro-pattern on a silicon wafer onto a CNF sheet. The water repellent performance was studied.

Experiments and results

A silicon wafer template (pattern: $\varphi = 4$ μm, depth = 1 μm, for each 12 μm) was pressed on wet mats of TEMPO-oxidized CNFs swollen with different organic solvents. The mat was dried slowly (Fig. 1). The surface structure of the sheet was observed by FE-SEM and the specific surface area and wettability of the sheet were evaluated.

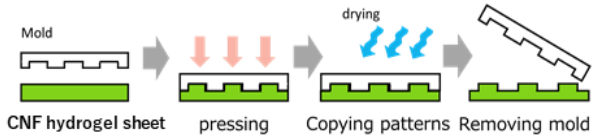

Fig. 1 the procedure of making hierarchical roughness on CNF seats

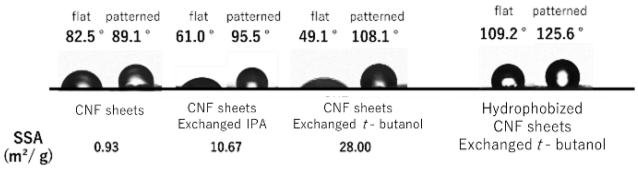

Fig. 2 the result of measurement of contact angles

Fibrous CNF pillars were successfully formed on the surface of the CNF sheet. For a smooth surface, the contact angle of a water droplet on the CNF sheet decreased sharply with increasing specific surface area. This is explained by Wenzel’s formula[1]. In contrast, the contact angle of a CNF sheet with a hierarchical structured pattern increased considerably (Fig. 2), although CNFs are strongly hydrophilic. It is plausible that this is because for the hierarchical surface structure with micro-pillars, water droplets contact not only the CNFs but also the air between the CNF pillars.

On the basis of these results, hydrophobized TEMPO-oxidized CNFs were prepared using tetra-4-butylammonium hydroxide[2] and their water repellent performance was studied. Compared with that of native CNFs, the contact angle of the hydrophobized sheets increased in the cases of both smooth and patterned surface sheets. In particular, the contact angles of surface-patterned hydrophobized CNF sheets increased significantly with increasing surface area and reached a contact angle of 125.6°. The molding strategy developed in this study can be regarded as a simple form of micro- and nano-imprinting lithography techniques. The results of this study will enable the production of unique filters and separators.

Acknowledgements

We would like to express our gratitude to the Daiichi Kogyo Seiyaku Company Limited for the donation of TEMPO-oxidized CNFs and the Nanotechnology Platform, Center for the Promotion Of Interdisciplinary Education and Research, Kyoto University for processing the silicon wafer template.

References

[1] Wenzel R. N., Industrial and Engineering Chemistry, 1936, 28, 988-994.

[2] Shimizu M., *et al*. *Biomacromolecules*, 2014, 15(11), 4320-4325.

ABSTRACTS (MASTER THESIS)

Biomineralization by using cellulose nanofiber gel

**(Graduate School of Agriculture,
Laboratory of Active Bio-based Materials, RISH, Kyoto University)**

Akihiro Matsushita

Introduction

Biominerals are composites of bioorganic polymers such as polysaccharides or proteins and inorganic materials; examples include shells and bones. The process by which organisms create biominerals is called biomineralization. Biominerals can be imitated and used for artificial bones and teeth.

In this study, a strong hydrogel was prepared from cellulose nanofibers (CNFs) and used as a substrate for biomineralization. CNFs, which are the major constituent of plant cell walls, are the most abundant natural nanofibers on earth. Their widths range from 5 to 30 nm and they are highly crystalline materials. The resultant stable structure has outstanding mechanical properties, including a high Young's modulus and a low coefficient of thermal expansion. CNFs therefore have great potential for use as reinforcements in nanocomposites and have attracted a great deal of interest recently. The aim of this study was to imitate a biomineral structure by using a CNF gel and calcium phosphate, to produce a biomaterial for artificial bones.

Experimental

Cellulose was isolated from Japanese cypress wood powder by the Wise method and treatment with 6 wt% potassium hydroxide. A CNF suspension was prepared by grinding the cellulose with a grinder. A CNF/calcium phosphate composite was prepared by dipping the CNF gel (fiber content about 10 wt%, thickness about 500 μm) in 0.6 M diammonium hydrogen phosphate solution (1) and 1.0 M calcium nitrate solution (2). Immersion in (1) and (2) was regarded as one cycle, and 1 to 5 cycles were performed. A tensile test was conducted on a sample conditioned for 1 day in a humidity controller.

Results and discussion

Calcium phosphate was successfully deposited on the surface and inside of the CNF gel. The reaction on the gel surface progressed well, therefore a large amount of calcium phosphate adhered to the gel surface. X-ray diffraction analysis of the obtained composite showed peaks corresponding to hydroxyapatite and octacalcium phosphate. These are two of a number of calcium phosphate types, and are both present in natural and artificial bones. This method therefore has potential applications for use in materials such as artificial bone.

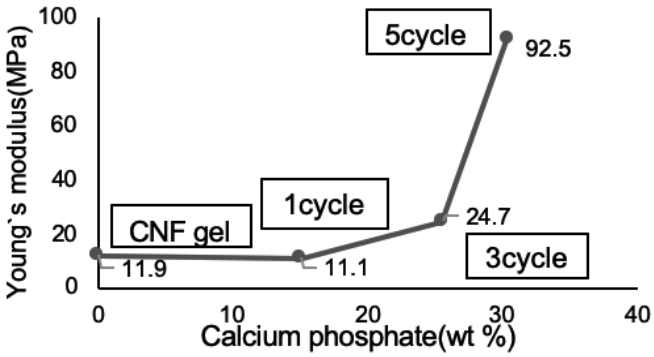

Figure 1. Relationship between Young's modulus and weight percentage of calcium phosphate

Figure 1 shows the changes in Young's modulus with increasing weight ratio of calcium phosphate to composite. This figure shows that the Young's modulus of the composites improved greatly when the weight percentage of calcium phosphate reached about 30%. This suggests that a calcium phosphate network was formed on the surface or inside of the CNF gel when the weight percentage was 30% or more.

ABSTRACTS (MASTER THESIS)

Nanocomposite materials from acrylic resin latex and cellulose nanofibers

**(Graduate School of Agriculture,
Laboratory of Active Bio-based materials, RISH, Kyoto University)**

Tairi Miyake

Introduction

Cellulose nanofibers (CNFs) have outstanding characteristics such as high strength, high elasticity, and low thermal expansion. They have been widely investigated and used as reinforcing components in nanocomposites. A CNF water suspension was uniformly mixed with acrylic resin latex of different droplet sizes. A nanocomposite made of acrylic resin and CNFs was obtained by filtering and drying the mixture. In composites, CNFs form networks on the surfaces of individual resin droplets and bulk networks are formed in nanocomposites. The effect of droplet size on the CNF-reinforced nanocomposites was investigated.

Experimental

Hemicellulose and lignin were removed from cypress wood flour (*Chamaecyparis obtusa*) by the Wise method and alkaline treatment. The refined pulp was mechanically disintegrated with a grinder and diluted with distilled water to prepare a 0.1 wt% CNF water suspension. Three types of acrylic resin latex with different droplet sizes (55, 130, and 527 nm; solid content: 5 wt%) were mixed with the 0.1 wt% CNF water suspension at different ratios. Wet cakes were obtained by vacuum filtration and dried in a vacuum oven at 80 °C for 12 h. Acrylic resin/CNF films were obtained by hot-pressing the dried films at 120 °C and 3 MPa for 5 min (thickness: 200–300 μm). The mechanical properties of the nanocomposites were investigated.

Result and discussion

Optically transparent composites sheets consisting of fine acrylic particles and CNFs were obtained. SEM images of cross sections of the composites showed that the CNFs are homogeneously distributed on the surfaces of the acrylic resin particles and that particles combine to form networks (Fig. 1). The addition of CNFs to the acrylic resin significantly increased the elastic modulus and strength. The reinforcing efficiencies of the CNFs were higher for composites with larger acrylic particles, e.g., of size 527 nm (Fig. 2), than those for composites with smaller acrylic particles. It is considered that the larger particle have larger surface areas, and this restricts the distribution area of CNFs in the composites and enables efficient formation of strong CNF networks.

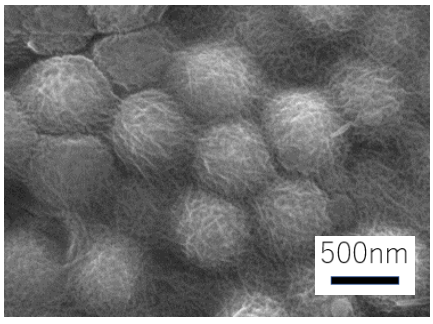

Figure 1. Cross-sectional SEM image of acrylic resin/CNF composite film (CNFs 10 wt%/527 nm acrylic resin particles).

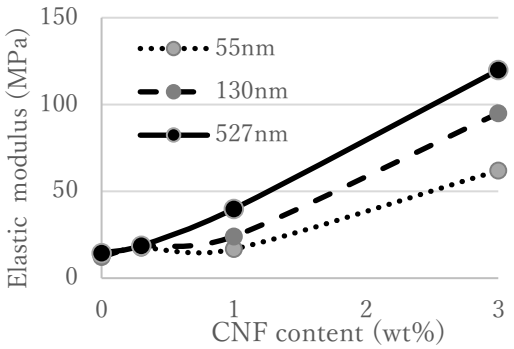

Figure 2. Relationship between Young's modulus of acrylic resin/CNF composites and CNF content.

ABSTRACTS (MASTER THESIS)

Semi-defibration of wood as pretreatment for wood flow forming – The effect of semi-defibration on penetrability of wood

(Graduate School of Agriculture, Laboratory of Sustainable Materials, RISH, Kyoto University)

Rin Matsumoto

Introduction

Wood flow forming is a new method in which wood block is processed into product with three dimensional shape. The forming process includes the heating, pressing, and cooling in a mold. In this process, wood block is separated at around intercellular layer into smaller parts, and subsequently flown into the empty space in the mold. The separated parts are re-bonded to each other and then fixed. The flowability of wood and the physical properties of products, however, is required to be improved. One of the representative techniques to improve such properties is the impregnation of wood with a given resin. It is necessary to solve the isuue as to the irregular distribution of the resin in wood.

Semi-defibration by extrusion of wood before the impregnation is devised to solve this issue. The purpose of this study is to investigate the effect of semi-defibration on penetrability of wood and the influence on the length of cells which largely affect the mechanical properties of products.

Materials and methods

At first, a column specimens (height (R direction) is 50 mm, and diameter (L, and T directions) is 45 mm) was cut from a transverse-heart-wood of yellow cedar (*Chamaecyparis nootkatensis*) whose all dried specific gravity was 0.51. And then, it was treated with the condition of 20℃, 98%RH until specimen's weight became constant. After that, this specimen was steamed for 15 min, and put into a die which is heated to 120℃, then offered to extrusion for semi-defibration. The defibrated wood and column specimens as control were all dried by 105℃ oven drying, and then impregnated the phenol-formaldehyde resin (PF resin, which was prepared for 30 wt% by diluting with water) by vacuuming and compressing. Next of that, resin-impregnated woods were cut at center line, and the cut faces were observed. And more, for investigating the state of destruction of cells, they were separated by Wise method, and measured their length.

Results and discussion

Figure 1 shows the cut faces of PF resin-impregnated woods. In column specimens (a), PF resin was hardly impregnated into wood. On the other hand, in semi-defibrated wood (b), PF resin was impregnated into even inner part. As this reason, it is suggested that semi-defibration was effective for improving the impregnation ability of wood. Also, the average length of cells of column specimen and semi- defibration wood are shown in Table 1. In this table, significant difference is not confirmed between the two values. From this result, it is suggested that notable destruction of cells by conducting semi-defibration was not happened.

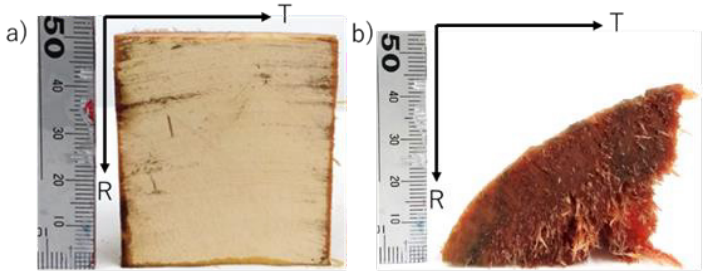

Figure 1. The cross sections of impregnated wood
a) column specimen b) semi-defibrated wood

Table 1. Average length of cells of column specimen and semi-defibrated wood

	Average length of cells (mm)	S.D. (n = 100)
Column specimen	1.99	0.90
Semi-defibrated wood	1.86	0.97

S.D. : standard deviation

ABSTRACTS (MASTER THESIS)

Pretreatment for wood flow forming – Temporal variability of solution distribution in impregnated wood under conditioning

(Graduate School of Agriculture, Laboratory of Sustainable Materials, RISH, Kyoto University)

Masaya Nagai

Introduction

Wood flow forming is a new method in which bulk wood is formed into the product with three dimensional shape. The bulk wood is impregnated with resin for obtaining the stable product. There exists the issue as to the irregular distribution of the resin in cell walls, causing the partial deformation and color change in the product. The impregnated wood is required to be conditioned under controlled atmosphere for promoting the resin diffusion from the cell cavity into the cell walls, leading to the decrease in the irregularity. The solution of the resin should be existed in the cell cavity to cause the diffusion. This has, however, not yet been examined. In this study, the model experiment was performed to understand the flow of the solution distribution in cell cavities during the conditioning.

Figure 1 shows the assumed model of the solution flow in impregnated wood under conditioning. In the model, the solution (liquid phase) is assumed to decrease both from the outside and inside wood. It was, however, difficult to observe directly the solution flow in cell cavities in the impregnated wood. In this study, the PFA micro-tubes are injected with solution and subsequently conditioned to obeserve the solution flow in impregnated wood, and the flow was predicted.

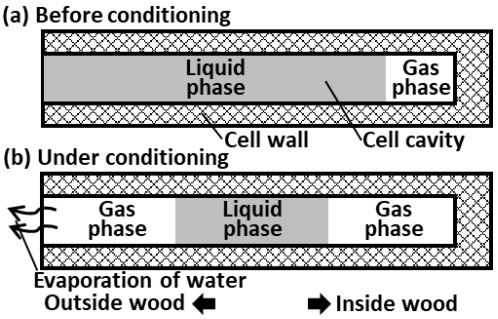

Fig. 1 Predicted solution flow in impregnated wood under conditioning

Materials and methods

Six micro-tubes with 9cm-length and 0.5mm-inner diameter (PFA) were embedded in an acrylic board, and the one side of the tubes were sealed with the adhesive. This preparation is injected with an aqueous solution of patent blue V by vacuuming under a pressure of 3.2kPa, and subsequently by exposing it to an atmosphere. The injected preparations are conditioned under the temperature and relative humidity controlled at several levels. During the conditioning, the picture of the preparation is taken every given times to observe the solution flow in the micro-tubes.

Results and discussion

Figure 2 shows the solution distribution in the micro-tubes under conditioning. The solution was distributed between the opened and closed sides in the micro-tubes, and the distribution varied with evaporation of water. It was also confirmed that the temporal variability of the solution distribution was affected by temperature and RH under the conditioning.

Fig. 2 Solution distribution under conditioning at 74%RH with 60°C
(① Gas phase in opened side, ② Solution (Liquid phase), ③ Gas phase in closed side)

ABSTRACTS (MASTER THESIS)

Estimation of relative displacement of wooden buildings calculated from acceleration using wavelet transform

**(Graduate School of Agriculture,
Laboratory of Structural Function, RISH, Kyoto University)**

Hiroto Yamamoto

Introduction

A technique has been proposed for calculating the relative displacement of each floor acceleration and for automatically determining the residual seismic performance of a building damaged by earthquakes. In this study, in order to apply this technology to wooden buildings, analysis was performed based on the data obtained by the full scale shaking table test.

Analysis method

The relative displacement of each floor is calculated from the acceleration record measured at each floor in the full-scale shaking table experiment by double integral. At this time, since the measurement error such as the baseline deviation included in the acceleration recording increases by integration, the calculated relative displacement does not correspond to the measured displacement. Therefore, the acceleration recording is decomposed into nine components with different frequencies using wavelet transform, and only the main components are selected and added to calculate the displacement from which the measurement error is removed. In this method, the selection of the main components is the main point of analysis accuracy, so the component selection method was examined based on the experimental data of the wooden frame specimen of one story buildings and two story buildings. The calculated displacement (hereinafter, referred to as analysis value) was compared with the displacement actually measured by the displacement meter (hereinafter, referred to as measured value) to evaluate its accuracy. In addition, for the purpose of application to CLT buildings, analysis was conducted using experimental results of two- and five-story CLT specimens.

Consideration and conclusion

In the main component selection, in the previous research, the method of selecting from the transfer function of the analysis floor and the upper floor and the absolute response acceleration-relative displacement relationship of each component was used. When this method was applied to a wooden frame specimen, the average value of the correlation coefficient between the analysis value and the time history waveform of the measured value was 0.864, and the average value of the maximum displacement consistency rate was 0.850. At this time, there were some of data in which the main component could not be selected sufficiently. Therefore, in addition to the component selected by this method, when the component which is superior in the response acceleration Fourier spectrum is selected, the average value of the correlation coefficient can be improved to 0.919 and the average value of the matching rate of the maximum displacement to 0.888.
When the above method was applied to two CLT test specimens, sufficient accuracy could not be confirmed. This result can be considered to be caused by the rocking behavior in the two-story specimen and by the torsional behavior in the five-story specimen. Therefore, we examined a method of calculating relative displacement with higher accuracy by removing these effects.

ABSTRACTS (MASTER THESIS)

Structural performance of steel frame with CLT shear wall

**(Graduate School of Agriculture,
Laboratory of Structural Function, RISH, Kyoto University)**

Kazumi Kanazawa

Introduction

In Japan, Cross Laminated Timber (CLT) is attracting attention as the way of using forest resources that have reached the harvest season. CLT is expected to be used for middle-to-high-rise building with making use of stable in-plane shear performance. In particular, composite structure with steel frame structure or reinforced concrete structure can take advent of respective material properties, and more and more this kind of researches are reported in recent years. A previous research shows the estimation of drift-pin joint with steel plate for fastening CLT and steel frame. This research aims to confirm the structural performance of steel frame with CLT shear wall using drift-pin joint by conducting experiment, and to make analysis model which follows the experimental result.

Method

In this study, one specification of the joint is defined based on the research of Ministry of Agriculture, Forestry and Fisheries conducted in 2016. In this research, the design for this specification, prior analysis for experiment, 1/2 scale experiment, and joint and material test are conducted to understand the structural behavior. After that, analytical model which reproduces the behavior is created. It was assumed to insert CLT into a standard span steel frame at the design stage. In the analysis, finite element analysis software (SNAP) was used to model a steel frame, CLT panel, spring of drift-pin joint, and CLT compression spring, and incremental analysis was conducted. In 1/2 scale experiment, in total of four specimen in different strength grade of CLT or insertion position as parameters are tested.

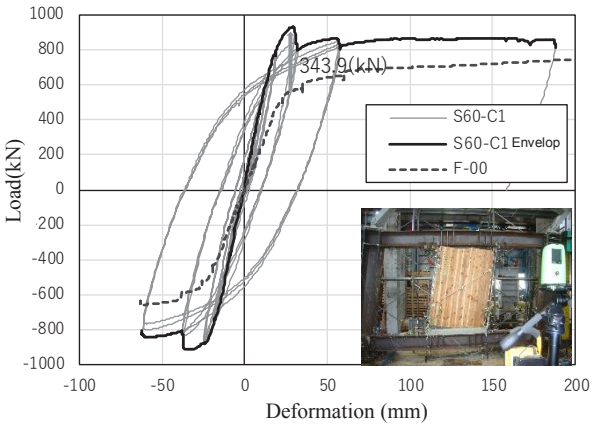

Figure 1. The result of experiment of F-00 and S60-C1

Results and consideration

Fig.1 shows the results of the experiment of steel frame specimen (F-00) and specimen of steel frame with a CLT panel of strength grade S60 inserted at the center (S60-C1). As assumed in the design stage, firstly the steel frame reached the yield point, and then, shear failure of CLT and local buckling of steel frame followed. The maximum load of S60-C1 was 931.7 kN, an increase of 343.9 kN compared to the load at the same deformation of F-00, and the initial stiffness was 1.89 times as F-00. The stiffness of the average shear stress of the CLT almost matched with the shear modulus of the CLT in the material experiment, confirming that the CLT exhibits the maximum performance as a seismic wall.

Fig.2 shows the result of analysis that material property is made from material test. The experimental results and the analytical results were in good agreement, and the behavior was able to be reproduced by the analytical model, comparing the timing of yielding of the members and the stress state at the specific deformation angle.

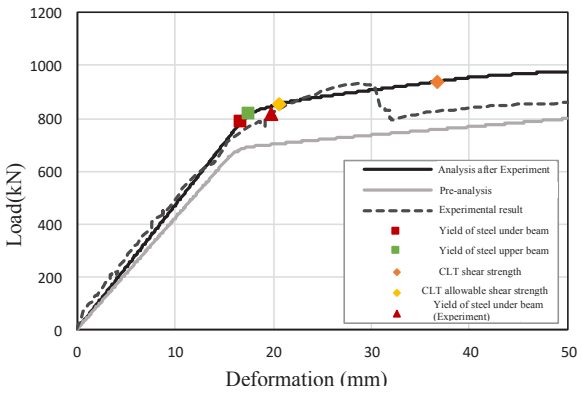

Figure 2. The result of analysis

ABSTRACTS (MASTER THESIS)

Seismic performance of wooden houses required for continuous use after major earthquakes

(Graduate School of Agriculture, Laboratory of Structural Function, RISH, Kyoto University)

Kotaro Sumida

Introduction

In the 2016 Kumamoto earthquakes, not only many wooden houses built according to the current standards were severely damaged, but even in houses that were deemed to be minor, their subsequent use was difficult [1]. In this study, I clarify the seismic performance required for continuous use and explore the possibility of realizing the performance.

Survey of construction situation in Mashiki town two years after the Kumamoto earthquakes

The survey was carried out again two years later on buildings that were completely surveyed just after the 2016 Kumamoto earthquake. The purpose of the survey is to quantify the relationship between damage level, construction year, structure type, etc. and the usage of the buildings after two years.

Analysis for clarification of performance required for continuous use after major earthquakes

A seismic simulation software "wallstat" were used with the purpose of verifying the possibility of continuing use of wooden houses after a severe earthquake. Three-dimensional wooden houses were modeled and time history response analysis were carried out by inputting observed seismic waves. Then, the level of expected damage was estimated from the maximum inter-story deformation.

Shake table tests and comparison with the results from the survey and analysis

Two full-scale wooden houses with different seismic performance were tested on shake table by inputting Kumamoto earthquakes waves, and seismic responses and damages were recorded. Then, obtained results were compared with those of the survey and analysis.

Results and conclusions

The survey revealed that about half of the buildings surveyed areas in Mashiki town do not exist. In addition, it was found that about half of slightly damage buildings considered to experience maximum inter-story deformation of 50 mm are also demolished.

Figure 1. shows the sufficiency ratio of the all analysis models and the maximum response deformation of the first story when 1995 JMA Kobe wave were input. It was found that the maximum response deformation tends to decrease as the sufficiency ratio increases. Against JMA Kobe wave, it is possible to keep the deformation below 50 mm or less and use it continuously if the sufficiency ratio reaches 2.0 or more.

The test building with higher performance survived against three successive Kumamoto earthquakes waves and suffered only tiny damage. This result proved the validity of the analysis.

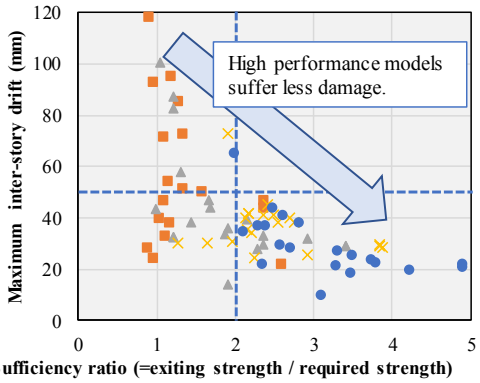

Figure 1. Maximum inter-story drift against a major earthquake (JMA Kobe wave)

Reference

[1] Architectural Institute of Japan, "Report on the Damage Investigation of the 2016 Kumamoto Earthquakes," pp. 29-53, 2018.

ABSTRACTS (MASTER THESIS)

Study of geomagnetically induced current using 3D FDTD method

**(Graduate School of Engineering,
Laboratory of Computer Simulation for Humanospheric Sciences,
RISH, Kyoto University)**

Kazuki Kurisu

We performed numerical simulations by using the three-dimensional finite-difference time domain (FDTD) method to study geomagnetically induced currents (GICs) in terms of the atmosphere-ground-power line coupling. We first conducted numerical experiment to estimate the ground distribution of geomagnetically induced electric field (GIE). We introduced two different ground structures to the simulation system, and imposed a uniform electric field at 60 km altitude. We found that GIE is enhanced near the edge of a bay, whereas, the magnetic field decreases near the coastal lines parallel to the incident electric field. When we introduced a mountain model, GIE has local maxima at foots of a ridge, whereas no significant changes of the magnetic field are observed near the mountain. We confirmed that the local enhancement of GIE is caused by the accumulation of electric charges due to inhomogeneous ground conductivity such as the edge of a bay or foots of the ridge. We also found that the large current flowing on the sea surface contributes to the decrease in the magnetic flux near the coastal lines.

Previously, several electromotive force models have been proposed to explain the generation of GIC. To understand the generation of the electromotive force, we next placed a transmission line on the ground and calculated GIC in the system. We first tested the influence of conductance and shapes of the transmission line on GIC, and the influence of conductance of the ground on GIC. Results show different tendency from conventionally known one. We found that the GIC is correlated with time variation of magnetic flux across the surface surrounded by the transmission lines and the underground depth at which magnetic flux is small enough. When we placed a transmission line on two different ground structures, GIC shows a strong influence from the electrical conductivity gradient of the ground especially near the coastal lines.

Global distribution of the GIE and GIC becomes clear in the system including air, ground (sea water) and a transmission line. All these results settle the argument about the generation of GIC. That is, GIC is generated by temporal variation of magnetic flux through a surface deep inside the Earth. The conductivity gradient gives rise to space charge, which also affect the GIC. Regarding influence of the presence of the transmission line on the natural GIE, further studies will be needed.

ABSTRACTS (MASTER THESIS)

Simulation study on the growth of whistler mode chorus wave in the magnetosphere in disturbed conditions

**(Graduate School of Engineering,
Laboratory of Computer Simulation for Humanospheric Sciences,
RISH, Kyoto University)**

Takuya Ikeda

The radiation belt in the Earth's magnetosphere is composed of energetic electrons and protons. In order to understand risks for satellite launch, we need to understand the processes that govern the variation of the radiation belt. It is suggested that non-adiabatic acceleration of electrons interacting with electromagnetic waves called whistler mode chorus waves is effective for an abrupt increase in the radiation belt electrons. By coupling global MHD simulation and advection simulation (CIMI model), we calculated the growth rate of whistler mode waves and investigated spatiotemporal regions where the whistler mode waves can be excited. In the MHD simulation, the solar wind was changed under two kinds of conditions and the responses of the magnetosphere was reproduced. The results were used for advection simulation to reproduce the evolution of the phase space density of electrons in the magnetosphere. In Case 1, the dynamic pressure of the solar wind was multiplied by 6, and the z component of the interplanetary magnetic field (IMF) was changed from north to south. In Case 2, we changed the z component of the IMF from north to south without changing solar wind dynamic pressure. In Case 1, the interplanetary (IP) shock propagates anti-sunward. Just after the arrival of IP shock at the magnetosphere, the linear growth rate increased in the dayside magnetosphere, but there was no significant increase in the nonlinear growth rate. Substorm occurred in Case 1 and Case 2. In Case 2, the linear growth rate increased in the dawn-midnight region about 40 minutes after the substorm onset, and the nonlinear growth rate also increased in the same region. The nonlinear growth rate is much larger than the linear growth rate and it was found that nonlinear growth is extremely effective due to the excitation of whistler mode chorus waves. In Case 1, about 40 minutes after the substorm onset, the linear and nonlinear growth rate increased in the dawn-midnight region, too. The growth rate was larger and the increased area was wider that those in Case 2. This indicates that an increase in solar wind velocity has a great influence on the growth rate of the whistler mode waves. This is consistent with the idea that the radiation belt electrons are largely enhanced under the high speed solar wind.

ABSTRACTS (MASTER THESIS)

Development of microwave power transfer system with high efficiency for drone application

(Graduate School of Engineering, Laboratory of Applied Radio Engineering for Humanosphere, RISH, Kyoto University)

Nobuyuki Takabayashi

Drones, multicopter-typed unmanned aerial vehicles, gathering a lot of attention from various kinds of industries. In such a circumstance, we proposed to give those drones a function of wireless power transfer (WPT). Among WPT methods, microwave power transfer (MPT) has an advantage for long-range power transmission, that is suitable for flying drones. Therefore, for drone applications (Fig.1), we aim to enhance the overall efficiency of MPT system by array antenna beamformings and circuit technologies.

First of all, we tackle beamformings to synthesize at-topped beams mainly at 2.45 GHz. Then we design and practically produce a 32-element array for power transmission and a 37-element array for power absorption. Then we conduct simulations and experiments for the flat-topped beam's transmission between a 32-element transmitting and a 37-element receiving antenna by employing synthesized beams. These results indicate how much power is intercepted on the receiving plane. Subsequently, using the obtained illuminance distributions on the rectenna plane, we investigate the rectification efficiency of these flat-topped beams from viewpoints of simulations and experiments. Conventionally, rectifications of rectenna array have energy loss caused from multiple rectifiers' connection. Flat-topped beams have been expected to reduce such a connection loss, but that have never confirmed. Therefore, we compare the efficiencies for rectifications in detail between conventional beams and our designed flat-topped beams. Then we show the flat-topped beams have almost zero connection loss for the rectification by the rectenna array. Finally, we conduct overall experiments of MPT at 2.45 GHz, where the overall efficiency of MPT are measured and the advantage of flat-topped beam are confirmed (Fig.2 and Fig.3).

In this thesis, we mainly evaluate the MPT efficiencies of flat-topped beams at 2.45 GHz. These results show the flat-topped beams have a potential to achieve MPT with extremely high efficiency where the overall efficiency exceeds 60% .

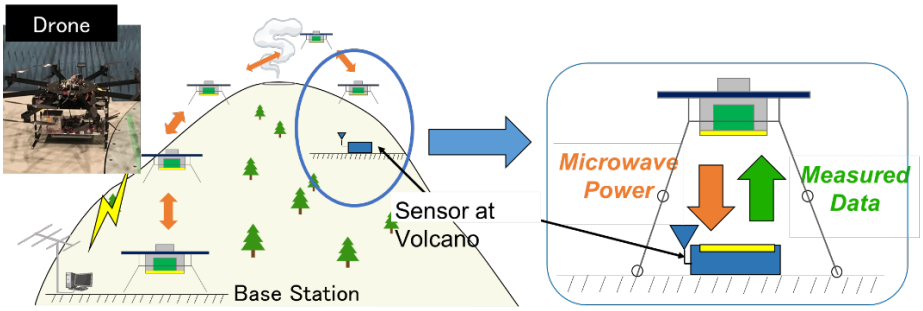

Fig. 1 Proposed MPT-aided sensor system with drone

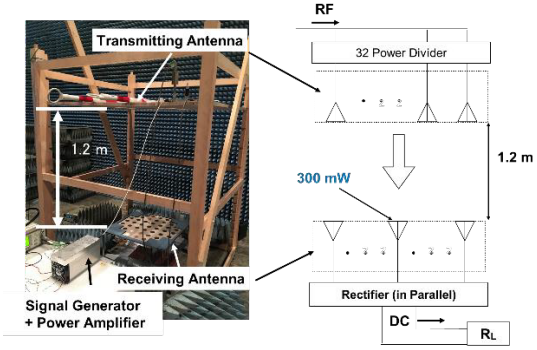

Fig.2 Experimental setup

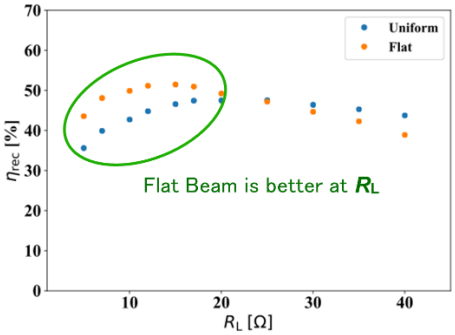

Fig.3 Total efficiency by flat beam and conventional beam

ABSTRACTS (MASTER THESIS)

Development of a compact microwave rectifier with the multilayer substrate filter

**(Graduate School of Engineering,
Laboratory of Applied Radio Engineering for Humanosphere, RISH, Kyoto University)**

Kouta Okazaki

These days, Internet of Things (IoT) is the focus of attention for the realization of more convenient world. Microwave power transfer (MPT) is expected to be a method of power supply to the IoT devices. In order to apply MPT techniques to the IoT devices, microwave receiving components are required. Hence, the size of the components for MPT should be reduced because of limited size of IoT devices. The objective of the present study is to develop more compact microwave rectifier. In the previous study, the multilayer substrate filters have been proposed as a new compact microwave filter and demonstrates its effectiveness for circuit size reduction. However, their proper operation principle have not been studied.

At first, the principle of the multilayer substrate filter (Fig.1) is analyzed so as to provide a more simple and flexible method for filter design. With the equivalent circuit and electromagnetic analysis the filter operation is clarified. In addition, a four-layer substrate filter for the microwave rectifier is designed by electromagnetic simulation. A single shunt class-F load-type rectifier is generally chosen as a microwave rectifier. It requires input and output filters (Fig.2) in order to obtain high rf-dc conversion efficiency. Hence, the multilayer substrate filter is designed, fabricated and measured to satisfy the required characteristic for the rectifier's filters. The good measurement results are obtained compared with the simulation results. Finally, a multilayer substrate rectifier with the multilayer substrate filter is designed by circuit simulation. As a result of the simulations, higher efficiency and more compact circuit size of the rectifier with the multilayer substrate filter are achieved than one with the conventional filter. Additionally, the designed rectifier is fabricated (Fig.3) . However, its measured rf-dc conversion efficiency is low, compared with simulated results (Fig.4). The efficiency reduction of the fabricated multilayer rectifier is discussed.

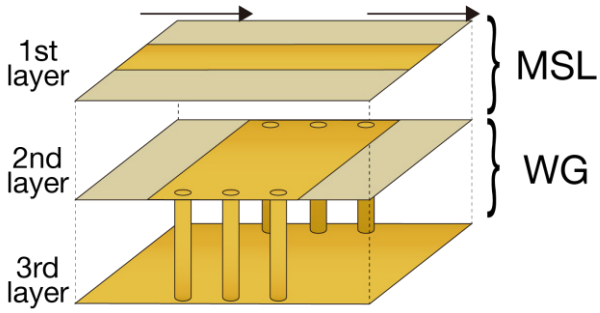

Fig. 1 Proposed new microwave filter (MSL : Microstrip antenna, WG : Waveguide)

Fig. 2 Developed output filter

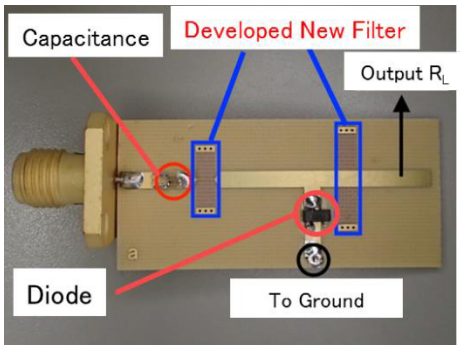

Fig. 3 Developed rectifier

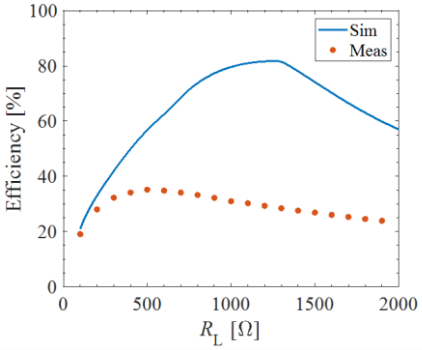

Fig.4 rf-dc conversion efficiency

ABSTRACTS (MASTER THESIS)

Study on Beltrami field in microwaves

**(Graduate School of Engineering,
Laboratory of Applied Radio Engineering for Humanosphere, RISH, Kyoto University)**

Ryo Mochizuki

Beltrami field is a vector field parallel to its curl. Beltrami field in an electromagnetic field has some interesting properties; however, there are very few applications using Beltrami field. This is because there is no established theory about Beltrami field. The first objective of this study is to obtain the general mathematical expression and the boundary condition of Beltrami fields, establishing basic theory about Beltrami field. The second objective is to develop applications exploiting the properties of Beltrami fields. The mathematical expression of a general Beltrami field was derived by an angular spectrum method. The mathematical representation of a general electromagnetic field with electric and magnetic field in parallel, **E** || **B** field, was obtained. It was shown that for any Beltrami field B^+ there exists another Beltrami field B^- such that, the superposition $B^+ + B^-$ becomes **E** || **B** field. It was also shown that any **E** || **B** field is expressed in the superposition of two Beltrami fields (Fig.1). The method of obtaining the Beltrami field using a familiar expression of an electromagnetic field was proposed. By using the method the mathematical expression of the Beltrami field in the rectangular waveguide was derived. The boundary condition of the Beltrami field in the waveguide was obtained. The use of a grating was proposed to achieve the boundary condition. The rectangular waveguide with a grating is designed to generate the Beltrami field. Full wave simulations were carried out and the Beltrami field and **E** || **B** field were generated in the waveguide. In this study, the application exploiting Beltrami field was investigated to achieve the second purpose. A novel length independent resonator with two corrugated reflectors was proposed. The operating principle and resonant condition of the resonator was theoretically obtained. Full wave simulations were carried out to verify the theory. It was confirmed that the length independency of the proposed resonator and the generation of one-dimensional Beltrami standing wave in the resonator (Fig.2).

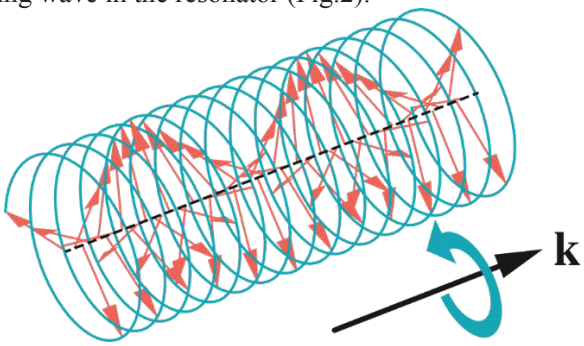

Fig.1 Beltrami field created by created front two circular electromagnetic waves

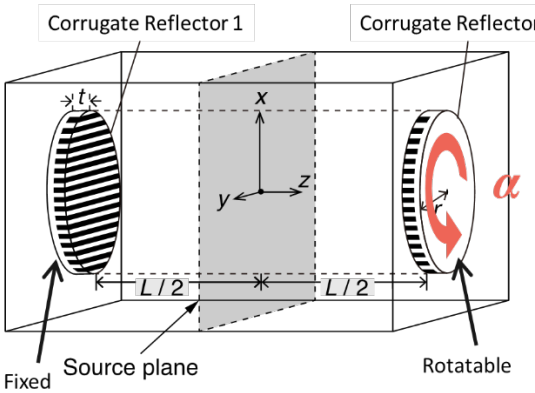

f	**10 GHz**
r	75 mm
t	10 mm
E_{source}	1 V/m

Fig.2 Proposed resonator and the generation of one-dimensional Beltrami standing wave and its simulation parameters

ABSTRACTS (MASTER THESIS)

Study on thrust performance evaluation of magneto plasma sail with magnetic nozzle

**(Graduate School of Engineering,
Laboratory of Space Electromagnetic Environment Exploration,
RISH, Kyoto University)**

Tatsumasa Hagiwara

The development of new propulsion system for exploring other planets in the solar system or deep space is necessary to enable short travelling term missions and large payload ratios. Magneto plasma sail (MPS) has been focused on as a candidate system to attain above objectives. The MPS is a propulsion system, which generates its force by the interaction between the charged particles from the sun (solar wind) and magnetic fields inflated by a plasma injection. In the previous studies, the thrust of the MPS was reduced by injecting plasma into the opposite direction of the thrust. The new propulsion system which is called "MPS with magnetic nozzle" is proposed. This proposed system combines the MPS and a magnetic nozzle. The magnetic nozzle itself is a propulsion system, which generates its force by converting the thermal energy of plasma injected into the nozzle magnetic field. In order to demonstrate the mechanism of thrust increase and evaluate the thrust performance, we conducted the laboratory experiments with two types of plasma sources. In the first experiment, we used an MPD arcjet as a plasma source, which produces plasma with arc discharge. The thrust of the MPS with the magnetic nozzle is 12 times larger than that of magnetic sail, and 2 times larger than that of the magnetic nozzle. We succeeded in evaluating the thrust increase experimentally. However, compared with an ion engine, the thrust performance is very low due to high electric power consumption of the MPD arcjet. In the second experiment, therefore, we developed the new low power plasma source consists of a LaB6 cathode, which is widely utilized for thermionic emission source. The thrust of the MPS with the magnetic nozzle is also 17 times larger than that of magnetic sail, and 1.3 times larger than that of magnetic nozzle. Hence, compared the first experiment, thrust performance is improved. We confirmed the usefulness of the LaB6 plasma source as a plasma source of the MPS with the magnetic nozzle.

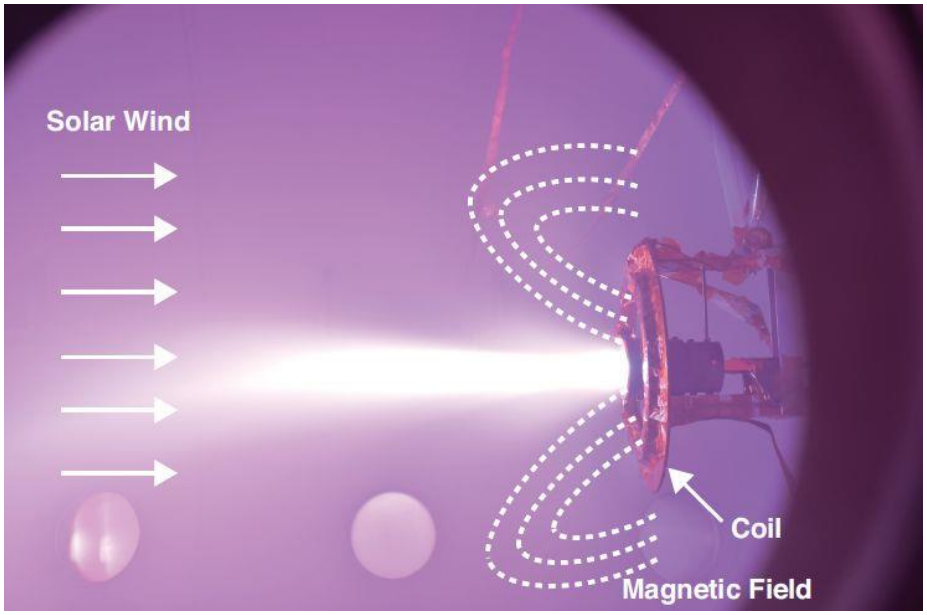

Figure 1. Experiment of the MPS with magnetic nozzle in the plasma chamber.

ABSTRACTS (MASTER THESIS)

Study on the integration of waveform capture-type plasma wave receivers

**(Graduate School of Engineering,
Laboratory of Space Electromagnetic Environment Exploration,
RISH, Kyoto University)**

Shunsuke Kamata

The Waveform capture(WFC) type plasma wave receiver is commonly used in recent space missions, because it can acquire all properties of plasma waves except their wave numbers. The size of a plasma wave receiver on board satellites is generally large to satisfy the desired scientific requirements. The miniaturization of the WFC-type plasma wave receiver as a chip is meaningful in the future nano-/micro-satellite missions. In this study, we miniaturized the WFC-type receiver using the Application Specific Integrated Circuit (ASIC) technology. We improved the switched capacitor filter (SC filter) for an anti-aliasing filter. We modified the circuit not only to reduce the noise level, but also to expand the observation frequency range of the SC filter. We experimentally demonstrated by the prototype chip of SC Filter that optimizing parameters of circuit elements in WFC receiver has significant effects on noise suppression and wider bandwidth. We implemented interferometry functions on the WFC chip. The interferometry function allows us to identify phase velocities of plasma waves. The implementation of this function on the WFC chip is very reasonable, because it consumes lots of resources when we realize that function using discrete parts. With a parallel circuit, we achieved small and lightweight interferometry circuits for WFC receiver. Implementing digital filter used for data compression of the WFC receiver with ASIC, we achieved miniaturization of the digital filters with the same performance as that of existing circuit with FPGA. We connect the improved analogue parts and the newly developed digital part as the unit system of the small WFC receiver. We obtained desired responses from the new system, which suggests the interference of noise between individual modules are negligible. The developed miniaturized WFC receiver appears promising for future space missions.

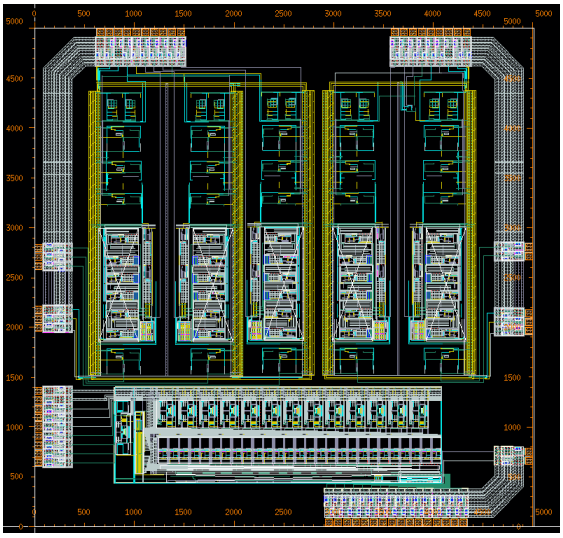

Figure 1. Developed WFC chip. The size is 5mm x 5mm. The chip contains 4 waveform receivers that have the capability of the interferometry mode.

ABSTRACTS (MASTER THESIS)

Study on the improvement of the identification techniques for space debris orbits by the MU radar

**(Graduate School of Engineering,
Laboratory of Space Electromagnetic Environment Exploration,
RISH, Kyoto University)**

Takuya Torii

Recently, the amount of space debris has been rapidly increasing, and this is becoming an obstacle for space developments. The organizations in the world are tracing space debris and sharing their orbit information. However, the present surveillance network is not sufficient to completely avoid space accidents due to collisions with space debris, and we need to improve and expand the observation network. In our study, it is the objective to develop the orbit determination method through the observation by the MU radar held by RISH, Kyoto University. The MU radar is an atmospheric radar. The development of orbit determination methods of space debris by the atmospheric radar leads to the enhancement of tracing system over the world, because the global network of atmospheric radars are already established. In the previous our study, the orbit determination of the known debris was discussed. However, it is difficult to re-observe the same debris consulting the orbit elements which were identified by the MU radar because the accuracy for the orbit identification is not sufficient. We performed the simulation to examine the relation between the accuracy of the orbit determination method and measurement errors. From the simulation results, we confirmed the following relations. The orbit elements in the relation to geometries are influenced by the range error. The orbit elements for the location on the orbit are influenced by the Zenith error. The orbit elements for the orbital plane is influenced by the azimuth error. We found that the accuracy was not sufficient to re-observe through the MU radar observation data using the previous methods. We stress that it is important to determine the Mean motion correctly for the re-observation. It is necessary to improve the range determination accuracy for improving the determination accuracy of the Mean motion. We succeeded in improving the determination accuracy of the range by using the new proposed method based on Range Weighting Function.

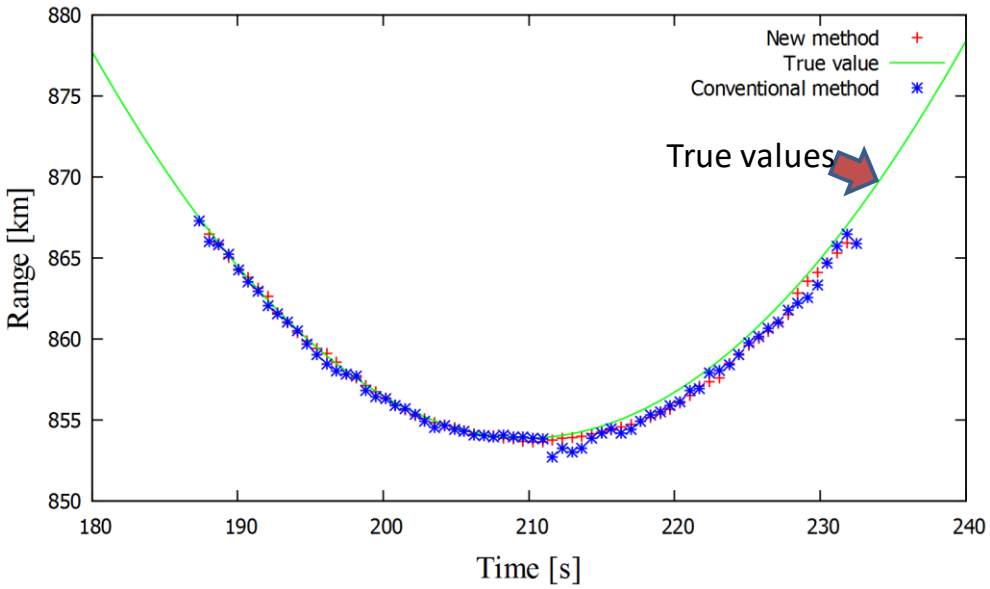

Figure 1. Estimated range distances of the space debris (ID: 23088). The values obtained by the new method are distributed well along the true value curve over the observation period.

ABSTRACTS (MASTER THESIS)

Study on the accuracy improvement of 3D shape estimation of space debris

**(Graduate School of Engineering,
Laboratory of Space Electromagnetic Environment Exploration,
RISH, Kyoto University)**

Takuto Ueno

Up to 2016, 20,000 debris have been found in the orbit around the earth. The number of space debris is still growing year by year. Since space debris threaten space infrastructures such as satellites and space stations, identifying their orbits and locations is very important in the meanings of avoiding collisions and removing them. It is necessary to expand the observation network for detecting debris and improve the accuracy of debris observation. We utilized an atmospheric radar to know the existence of debris to be removed in the present research. Atmospheric radars have the advantage that the global network has be already established. The atmospheric radar we used is the MU radar (Middle and Upper atmosphere radar) held by RISH, Kyoto University. Debris on low orbits can be sufficiently observed by lengthening the pulse and enlarging the transmission power of the MU radar. In the present thesis, we focused on studying the improvement of the accuracy of 3D shape estimation of space debris. In previous research, by combining the RCS (Radar Cross Section) method and the SRDI (Single-Range Doppler Interferometry) method, 3D shape estimation of space debris was roughly enabled. However, in this combined method, only one certain cross-section was estimated along an observation direction. This point should be improved to make estimation accuracy higher. To address this issue, we attempted to observe space debris by using multi-directional radar beams. The results showed the estimation of overall debris' size is close to the real size. On the other hand, we also examined the accuracy of the RCS values. Shape estimation errors come from the errors in calculating RCS values from radar echoes. We examined the limit in the precision of the RCS values by observing the small satellite called DIWATA-2b, which is 50 cm square satellite. We confirmed the echo signal from it. Calculated RCS value from it is 1 m^2. This calculated value is 50 times larger than expected value. Therefore, we think that RCS value is not correct for less than 1 m^2 . Moreover, with FDTD method, we performed computer simulations on the time variation of the RCS value to evaluate the observation results.

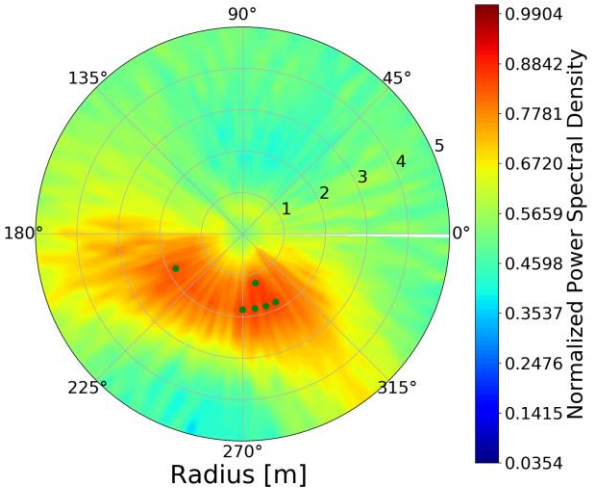

Figure 1. Estimated shape of the space debris (SL16RB) based on the MU radar echoes.

PUBLICATIONS

Publications in FY2018 (April 2018 - March 2019)
(Articles in English published in refereed journals)

Abe K. (2019) Novel fabrication of high-modulus cellulose-based films by nanofibrillation under alkaline conditions. Carbohydrate Polymers 205:488-491.
[online] URL: http://dx.doi.org/10.1016/j.carbpol.2018.10.069

Abe K., Morita M., Yano H. (2018) Fabrication of optically transparent cotton fiber composite. Journal of Materials Science 53:10872-10878. [online] URL: http://dx.doi.org/10.1007/s10853-018-2309-1

Ajith K.K., Tulasi Ram S., Carter B.A., Sathish Kumar S., Yamamoto M., Yokoyama T., Gurubaran S., Sripathi S., Hozumi K., Groves K., Caton R.G. (2018) Unseasonal development of post-sunset F-region irregularities over Southeast Asia on 28 July 2014: 2. Forcing from below? Progress in Earth and Planetary Science 5 [online] URL: http://dx.doi.org/10.1186/s40645-018-0218-1

Biswas S.K., Tanpichai S., Witayakran S., Yang X., Shams M.I., Yano H. (2019) Thermally Superstable Cellulosic-Nanorod-Reinforced Transparent Substrates Featuring Microscale Surface Patterns. ACS Nano [online] URL: http://dx.doi.org/10.1021/acsnano.8b08477

Bong L.-J., Neoh K.-B., Yoshimura T. (2018) Comparison of Water Relation in Two Powderpost Beetles Relative to Body Size and Ontogenetic and Behavioral Traits. Environmental Entomology 47:990-996. [online] URL: http://dx.doi.org/10.1093/ee/nvy062

Bong L.-J., Neoh K.-B., Yoshimura T. (2018) Developmental Irregularity and Abnormal Elytra Formation in the Oriental Wood Borer Induced by Physical Disturbance. Journal of Insect Science 18. [online] URL: http://dx.doi.org/10.1093/jisesa/iey001

Chen C., Li D., Abe K., Yano H. (2018) Formation of high strength double-network gels from cellulose nanofiber/polyacrylamide via NaOH gelation treatment. Cellulose 25:5089-5097. [online] URL: http://dx.doi.org/10.1007/s10570-018-1938-5

Chen C., Li D., Yano H., Abe K. (2019) Bioinspired hydrogels: Quinone crosslinking reaction for chitin nanofibers with enhanced mechanical strength via surface deacetylation. Carbohydrate Polymers 207:411-417. [online] URL: http://dx.doi.org/10.1016/j.carbpol.2018.12.007

Chen J.-S., Wang C.-Y., Chu Y.-H., Su C.-L., Hashiguchi H. (2018) 3-D Radar Imaging of E-Region Field-Aligned Plasma Irregularities by Using Multireceiver and Multifrequency Techniques. IEEE Transactions on Geoscience and Remote Sensing 56:5591-5599.
[online] URL: http://dx.doi.org/10.1109/TGRS.2018.2818331

Cui S., Wada S., Tobimatsu Y., Takeda Y., Saucet S.B., Takano T., Umezawa T., Shirasu K., Yoshida S. (2018) Host lignin composition affects haustorium induction in the parasitic plants Phtheirospermum japonicum and Striga hermonthica. New Phytologist 218:710-723.
[online] URL: http://dx.doi.org/10.1111/nph.15033"

Do T.V., Trung P.D., Yamamoto M., Kozan O., Thang N.T., Thuyet D.V., Thang H.V., Phuong N.T.T., Khuong N.V., Cam N.V. (2017) Aboveground biomass increment and stand dynamics in tropical evergreen broadleaved forest. Journal of Sustainable Forestry 37:1-14. [online] URL: http://dx.doi.org/10.1080/10549811.2017.1375959

Dutta B., Kalita B.R., Bhuyan P.K., Sharma S., Tiwari R.C., Wang K., Hozumi K., Tsugawa T., Yokoyama T., Le Huy M., Pham T.T.H. (2018) Spatial Features of L-Band Equinoctial Scintillations From Equator to Low Midlatitude at Around 95°E During 2015-2016. Journal of Geophysical Research: Space Physics 123:7767-7788. [online] URL: http://dx.doi.org/10.1029/2018JA025533

Ebihara Y. (2019) Simulation study of near-Earth space disturbances: 1. magnetic storms. Progress in Earth and Planetary Science 6. [online] URL: http://dx.doi.org/10.1186/s40645-019-0264-3

Ebihara Y. (2019) Simulation study of near-Earth space disturbances: 2. Auroral substorms. Progress in Earth and Planetary Science 6. [online] URL: http://dx.doi.org/10.1186/s40645-019-0273-2

PUBLICATIONS

Ebihara Y., Tanaka T., Kamiyoshikawa N. (2019) New Diagnosis for Energy Flow From Solar Wind to Ionosphere During Substorm: Global MHD Simulation. Journal of Geophysical Research: Space Physics 124:360-378. [online] URL: http://dx.doi.org/10.1029/2018JA026177

Fujisawa, M., Hanasaki, N., Takikawa, Y., Yanagawa, A., Matsukawa, T., Akino, T., Kajiyama, S., Arai, S. (2019) A Questionnaire-based Investigation Indicated Mental Relaxation Effects in the Scent of the Sacred Flower of the Saikusa Festival, Lilium japonicum, Japanese Journal of Pharmacology 73(2), 1-6. (in Japanese with English summary)

Grabber J.H., Davidson C., Tobimatsu Y., Kim H., Lu F., Zhu Y., Opietnik M., Santoro N., Foster C.E., Yue F., Ress D., Pan X., Ralph J. (2019) Structural features of alternative lignin monomers associated with improved digestibility of artificially lignified maize cell walls. Plant Science. [online] URL: http://dx.doi.org/10.1016/j.plantsci.2019.02.004

Guswenrivo I., Sato H., Fujimoto I., Yoshimura T. (2018) First record of the termite ectoparasite Laboulbeniopsis termitarius thaxter in Japan. Mycoscience 59:247-251.
[online] URL: http://dx.doi.org/10.1016/j.myc.2018.01.001

Guswenrivo I., Tseng S.P., Scotty Yang C.C., Yoshimura T. (2018) Development of Multiplex Nested PCR for Simultaneous Detection of Ectoparasitic Fungi Laboulbeniopsis termitarius and Antennopsis gallica on Reticulitermes speratus (Blattodea: Rhinotermitidae). Journal of Economic Entomology 111:1330-1336. [online] URL: http://dx.doi.org/10.1093/jee/toy091

Hara K., Osada K., Yabuki M., Takashima H., Theys N., Yamanouchi T. (2018) Important contributions of sea-salt aerosols to atmospheric bromine cycle in the Antarctic coasts. Scientific Reports 8. [online] URL: http://dx.doi.org/10.1038/s41598-018-32287-4

Hasebe F., Aoki S., Morimoto S., Inai Y., Nakazawa T., Sugawara S., Ikeda C., Honda H., Yamazaki H., Halimurrahman, Komala N., Putri F.A., Budiyono A., Soedjarwo M., Ishidoya S., Toyoda S., Shibata T., Hayashi M., Eguchi N., Nishi N., Fujiwara M., Ogino S.-Y., Shiotani M., Sugidachi T. (2018) Coordinated Upper-Troposphere-to-Stratosphere Balloon Experiment in Biak. Bulletin of the American Meteorological Society 99:1213-1230. [online] URL: http://dx.doi.org/10.1175/BAMS-D-16-0289.1

Hashiguchi H., Manjo T., Yamamoto M. (2018) Development of Middle and Upper Atmosphere Radar Real-Time Processing System With Adaptive Clutter Rejection. Radio Science 53:83-92. [online] URL: http://dx.doi.org/10.1002/2017RS006417

Hayakawa H., Ebihara Y., Cliver E.W., Hattori K., Toriumi S., Love J.J., Umemura N., Namekata K., Sakaue T., Takahashi T., Shibata K. (2018) The extreme space weather event in September 1909. Monthly Notices of the Royal Astronomical Society 484:4083-4099.
[online] URL: http://dx.doi.org/10.1093/mnras/sty3196

Hayakawa H., Ebihara Y., Hand D.P., Hayakawa S., Kumar S., Mukherjee S., Veenadhari B. (2018) Low-latitude Aurorae during the Extreme Space Weather Events in 1859. The Astrophysical Journal 869:57. [online] URL: http://dx.doi.org/10.3847/1538-4357/aae47c

Hayakawa H., Ebihara Y., Vaquero J.M., Hattori K., Carrasco V.M.S., de la Cruz Gallego M., Hayakawa S., Watanabe Y., Iwahashi K., Tamazawa H., Kawamura A.D., Isobe H. (2018) A great space weather event in February 1730. Astronomy & Astrophysics 616:A177.
[online] URL: http://dx.doi.org/10.1051/0004-6361/201832735

Hayakawa H., Ebihara Y., Willis D.M., Hattori K., Giunta A.S., Wild M.N., Hayakawa S., Toriumi S., Mitsuma Y., Macdonald L.T., Shibata K., Silverman S.M. (2018) The Great Space Weather Event during 1872 February Recorded in East Asia. The Astrophysical Journal 862:15. [online] URL: http://dx.doi.org/10.3847/1538-4357/aaca40

Hayakawa H., Vaquero J.M., Ebihara Y. (2018) Sporadic auroras near the geomagnetic equator: in the Philippines, on 27 October 1856. Annales Geophysicae 36:1153-1160.
[online] URL: http://dx.doi.org/10.5194/angeo-36-1153-2018

Hayakawa, H., F. R. Stephenson, Y. Uchikawa, Y. Ebihara, C. J. Scott, M. N. Wild, J. Wilkinson, and D.

PUBLICATIONS

M. Willis, The Celestial Sign in the Anglo-Saxon Chronicle in the 770s: Insights on Contemporary Solar Activity, Solar Physics, 294:42. [online] URL: https://doi.org/10.1007/s11207-019-1424-8

Hikishima M., Kojima H., Katoh Y., Kasahara Y., Kasahara S., Mitani T., Higashio N., Matsuoka A., Miyoshi Y., Asamura K., Takashima T., Yokota S., Kitahara M., Matsuda S. (2018) Data processing in Software-type Wave-Particle Interaction Analyzer onboard the Arase satellite. Earth, Planets and Space 70. [online] URL: http://dx.doi.org/10.1186/s40623-018-0856-y

Hisamochi R., Watanabe Y., Sano M., Nakatsuka T., Kurita N., Matsuo-Ueda M., Yamamoto H., Tazuru S., Sugiyama J., Subiyanto B., Marsoem S.N., Tsuda T., Tagami T. (2018) Cellulose oxygen isotopic composition of teak (Tectona grandis) collected from Java Island: a tool for dendrochronological and dendroclimatological analysis. Dendrochronologia 52:80-86.
[online] URL: http://dx.doi.org/10.1016/j.dendro.2018.09.010

Horikawa Y., Hirano S., Mihashi A., Kobayashi Y., Zhai S., Sugiyama J. (2019) Prediction of Lignin Contents from Infrared Spectroscopy: Chemical Digestion and Lignin/Biomass Ratios of Cryptomeria japonica. Applied Biochemistry and Biotechnology.
[online] URL: http://dx.doi.org/10.1007/s12010-019-02965-8

Horikawa Y., Shimizu M., Saito T., Isogai A., Imai T., Sugiyama J. (2018) Influence of drying of chara cellulose on length/length distribution of microfibrils after acid hydrolysis. International Journal of Biological Macromolecules 109:569-575.
[online] URL: http://dx.doi.org/10.1016/j.ijbiomac.2017.12.051

Horký M., Omura Y. (2019) Novel nonlinear mechanism of the generation of non-thermal continuum radiation. Physics of Plasmas 26:022904. [online] URL: http://dx.doi.org/10.1063/1.5077094

Horký M., Omura Y., Santolík O. (2018) Particle simulation of electromagnetic emissions from electrostatic instability driven by an electron ring beam on the density gradient. Physics of Plasmas 25:042905. [online] URL: http://dx.doi.org/10.1063/1.5025912

Hsieh Y.-K., Omura Y. (2018) Nonlinear Damping of Oblique Whistler Mode Waves Via Landau Resonance. Journal of Geophysical Research: Space Physics 123:7462-7472. [online] URL: http://dx.doi.org/10.1029/2018JA025848

Hsu H.-W., Chiu M.-C., Shih C.-J., Matsuura K., Yang C.-C.S. (2019) Apoptosis as a primary defense mechanism in response to viral infection in invasive fire ant Solenopsis invicta. Virology 531:255-259.
[online] URL: http://dx.doi.org/10.1016/j.virol.2019.03.015

Hsu H.-W., Chiu M.-C., Shoemaker D., Yang C.-C.S. (2018) Viral infections in fire ants lead to reduced foraging activity and dietary changes. Scientific Reports 8.
[online] URL: http://dx.doi.org/10.1038/s41598-018-31969-3

Hwang S.-W., Kobayashi K., Zhai S., Sugiyama J. (2017) Automated identification of Lauraceae by scale-invariant feature transform. Journal of Wood Science 64:69-77.
[online] URL: http://dx.doi.org/10.1007/s10086-017-1680-x

Igarashi Y., Sato A., Okumura H., Nakatsubo F., Yano H. (2018) Manufacturing process centered on dry-pulp direct kneading method opens a door for commercialization of cellulose nanofiber reinforced composites. Chemical Engineering Journal 354:563-568.
[online] URL: http://dx.doi.org/10.1016/j.cej.2018.08.020

Imai M., Mihashi A., Imai T., Kimura S., Matsuzawa T., Yaoi K., Shibata N., Kakeshita H., Igarashi K., Kobayashi Y., Sugiyama J. (2019) Selective fluorescence labeling: time-lapse enzyme visualization during sugarcane hydrolysis. Journal of Wood Science 65.
[online] URL: http://dx.doi.org/10.1186/s10086-019-1798-0

Imamura T., Miyamoto M., Ando H., Häusler B., Pätzold M., Tellmann S., Tsuda T., Aoyama Y., Murata Y., Takeuchi H., Yamazaki A., Toda T., Tomiki A. (2018) Fine Vertical Structures at the Cloud Heights of Venus Revealed by Radio Holographic Analysis of Venus Express and Akatsuki Radio Occultation Data. Journal of Geophysical Research: Planets 123:2151-2161.

PUBLICATIONS

[online] URL: http://dx.doi.org/10.1029/2018JE005627

Isozaki K., Shimoaka T., Oshiro S., Yamaguchi A., Pincella F., Ueno R., Hasegawa T., Watanabe T., Takaya H., Nakamura M. (2018) Robust Surface Plasmon Resonance Chips for Repetitive and Accurate Analysis of Lignin-Peptide Interactions. ACS Omega 3:7483-7493.
[online] URL: http://dx.doi.org/10.1021/acsomega.8b01161

Iwata H., Mano M., Ono K., Tokida T., Kawazoe T., Kosugi Y., Sakabe A., Takahashi K., Miyata A. (2018) Exploring sub-daily to seasonal variations in methane exchange in a single-crop rice paddy in central Japan. Atmospheric Environment 179:156-165.
[online] URL: http://dx.doi.org/10.1016/j.atmosenv.2018.02.015

Juaeni I., Tabata H., Noersomadi, Halimurrahman, Hashiguchi H., Tsuda T. (2018) Retrieval of temperature profiles using radio acoustic sounding system (RASS) with the equatorial atmosphere radar (EAR) in West Sumatra, Indonesia. Earth, Planets and Space 70.
[online] URL: http://dx.doi.org/10.1186/s40623-018-0784-x

Kakad A., Kakad B., Omura Y., Sinha A.K., Upadhyay A., Rawat R. (2019) Modulation of Electromagnetic Ion Cyclotron Waves by Pc5 ULF Waves and Energetic Ring Current Ions. Journal of Geophysical Research: Space Physics 124:1992-2009.
[online] URL: http://dx.doi.org/10.1029/2017JA024930

Kakad B., Omura Y., Kakad A., Upadhyay A., Sinha A.K. (2018) Characteristics of Subpacket Structures in Ground EMIC Wave Observations. Journal of Geophysical Research: Space Physics 123:8358-8376. [online] URL: http://dx.doi.org/10.1029/2018JA025473

Kamitakahara H., Okayama T., Praptiwi, Agusta A., Tobimatsu Y., Takano T. (2018) Two-dimensional NMR analysis of Angiopteris evecta rhizome and improved extraction method for angiopteroside. Phytochemical Analysis 30:95-100. [online] URL: http://dx.doi.org/10.1002/pca.2794"

Kantha L., Lawrence D., Luce H., Hashiguchi H., Tsuda T., Wilson R., Mixa T., Yabuki M. (2018) Correction to: Shigaraki UAV-Radar Experiment (ShUREX): overview of the campaign with some preliminary results. Progress in Earth and Planetary Science 5.
[online] URL: http://dx.doi.org/10.1186/s40645-018-0210-9

Kantha L., Luce H., Hashiguchi H. (2018) On a numerical model for extracting TKE dissipation rate from very high frequency (VHF) radar spectral width. Earth, Planets and Space 70. [online] URL: http://dx.doi.org/10.1186/s40623-018-0957-7

Kantha L., Luce H., Hashiguchi H. (2019) Midlevel Cloud-Base Turbulence: Radar Observations and Models. Journal of Geophysical Research: Atmospheres 124:3223-3245. [online] URL: http://dx.doi.org/10.1029/2018JD029479

Karim M.R., Yanagawa A., Ohinata K. (2018) Soy undecapeptide induces Drosophila hind leg grooming via dopamine receptor. Biochemical and Biophysical Research Communications 499:454-458. [online] URL: http://dx.doi.org/10.1016/j.bbrc.2018.03.162

Kasahara Y., Kasaba Y., Kojima H., Yagitani S., Ishisaka K., Kumamoto A., Tsuchiya F., Ozaki M., Matsuda S., Imachi T., Miyoshi Y., Hikishima M., Katoh Y., Ota M., Shoji M., Matsuoka A., Shinohara I. (2018) The Plasma Wave Experiment (PWE) on board the Arase (ERG) satellite. Earth, Planets and Space 70. [online] URL: http://dx.doi.org/10.1186/s40623-018-0842-4

Kataoka R., Nishiyama T., Tanaka Y., Kadokura A., Uchida H.A., Ebihara Y., Ejiri M.K., Tomikawa Y., Tsutsumi M., Sato K., Miyoshi Y., Shiokawa K., Kurita S., Kasahara Y., Ozaki M., Hosokawa K., Matsuda S., Shinohara I., Takashima T., Sato T., Mitani T., Hori T., Higashio N. (2019) Transient ionization of the mesosphere during auroral breakup: Arase satellite and ground-based conjugate observations at Syowa Station. Earth, Planets and Space 71. [online] URL: http://dx.doi.org/10.1186/s40623-019-0989-7

Katoh Y., Kojima H., Hikishima M., Takashima T., Asamura K., Miyoshi Y., Kasahara Y., Kasahara S., Mitani T., Higashio N., Matsuoka A., Ozaki M., Yagitani S., Yokota S., Matsuda S., Kitahara M.,

PUBLICATIONS

Shinohara I. (2018) Software-type Wave-Particle Interaction Analyzer on board the Arase satellite. Earth, Planets and Space 70. [online] URL: http://dx.doi.org/10.1186/s40623-017-0771-7

Katoh Y., Omura Y., Miyake Y., Usui H., Nakashima H. (2018) Dependence of Generation of Whistler Mode Chorus Emissions on the Temperature Anisotropy and Density of Energetic Electrons in the Earth's Inner Magnetosphere. Journal of Geophysical Research: Space Physics 123:1165-1177. [online] URL: http://dx.doi.org/10.1002/2017JA024801

Kazama Y., Kojima H., Miyoshi Y., Kasahara Y., Usui H., Wang B. -J., Wang S. -Y., Tam S.W.Y., Chang T. -F., Ho P.T.P., Asamura K., Kumamoto A., Tsuchiya F., Kasaba Y., Matsuda S., Shoji M., Matsuoka A., Teramoto M., Takashima T., Shinohara I. (2018) Density Depletions Associated With Enhancements of Electron Cyclotron Harmonic Emissions: An ERG Observation. Geophysical Research Letters 45:10,075-10,083. [online] URL: http://dx.doi.org/10.1029/2018GL080117

Kimura N., Watanabe T., Suenaga H., Fujihara H., Futagami T., Goto M., Hanada S., Hirose J. (2018) Pseudomonas furukawaii sp. nov., a polychlorinated biphenyl-degrading bacterium isolated from biphenyl-contaminated soil in Japan. International Journal of Systematic and Evolutionary Microbiology 68:1429-1435. [online] URL: http://dx.doi.org/10.1099/ijsem.0.002670

Kitajima S., Aoki W., Shibata D., Nakajima D., Sakurai N., Yazaki K., Munakata R., Taira T., Kobayashi M., Aburaya S., Savadogo E.H., Hibino S., Yano H. (2018) Comparative multi-omics analysis reveals diverse latex-based defense strategies against pests among latex-producing organs of the fig tree (Ficus carica). Planta 247:1423-1438. [online] URL: http://dx.doi.org/10.1007/s00425-018-2880-3

Kitamori A., Inayama M., Gotou M., Isoda H. (2018) Bending performance of traditional shear keyed column to beam joints. Journal of Structural and Construction Engineering (Transactions of AIJ) 83:859-867. [online] URL: http://dx.doi.org/10.3130/aijs.83.859

Kobayashi K., Hwang S.-W., Okochi T., Lee W.-H., Sugiyama J. (2019) Non-destructive method for wood identification using conventional X-ray computed tomography data. Journal of Cultural Heritage. [online] URL: http://dx.doi.org/10.1016/j.culher.2019.02.001

Koeduka T., Hatada M., Suzuki H., Suzuki S., Matsui K. (2019) Molecular cloning and functional characterization of an O-methyltransferase catalyzing 4′ -O-methylation of resveratrol in Acorus calamus. Journal of Bioscience and Bioengineering 127:539-543.
[online] URL: http://dx.doi.org/10.1016/j.jbiosc.2018.10.011

Komatsu K., Teng Q., Li Z., Zhang X., Que Z. (2019) Experimental and analytical investigation on the nonlinear behaviors of glulam moment-resisting joints composed of inclined self-tapping screws with steel side plates. Advances in Structural Engineering:136943321985872. [online] URL: http://dx.doi.org/10.1177/1369433219858722

Komatsu K., Teng Q., Li Z., Zhang X., Cai W., Que Z. (2018) Experimental and numerical analyses on nonlinear behaviour of wooden parallel chord trusses composed of self-tapping screws. Journal of Wood Science 64:776–793. [online] URL: http://dx.doi.org/10.1007/s10086-018-1774-0

Kubota Y., Omura Y. (2018) Nonlinear Dynamics of Radiation Belt Electrons Interacting With Chorus Emissions Localized in Longitude. Journal of Geophysical Research: Space Physics 123:4835-4857. [online] URL: http://dx.doi.org/10.1029/2017JA025050

Kubota Y., Omura Y., Kletzing C., Reeves G. (2018) Generation Process of Large-Amplitude Upper-Band Chorus Emissions Observed by Van Allen Probes. Journal of Geophysical Research: Space Physics 123:3704-3713. [online] URL: http://dx.doi.org/10.1029/2017JA024782

Kumamoto A., Tsuchiya F., Kasahara Y., Kasaba Y., Kojima H., Yagitani S., Ishisaka K., Imachi T., Ozaki M., Matsuda S., Shoji M., Matsuoka A., Katoh Y., Miyoshi Y., Obara T. (2018) High Frequency Analyzer (HFA) of Plasma Wave Experiment (PWE) onboard the Arase spacecraft. Earth, Planets and Space 70. [online] URL: http://dx.doi.org/10.1186/s40623-018-0854-0

Kusano H., Ohnuma M., Mutsuro-Aoki H., Asahi T., Ichinosawa D., Onodera H., Asano K., Noda T.,

PUBLICATIONS

Horie T., Fukumoto K., Kihira M., Teramura H., Yazaki K., Umemoto N., Muranaka T., Shimada H. (2018) Establishment of a modified CRISPR/Cas9 system with increased mutagenesis frequency using the translational enhancer dMac3 and multiple guide RNAs in potato. Scientific Reports 8. [online] URL: http://dx.doi.org/10.1038/s41598-018-32049-2

Lam P.Y., Lui A.C.W., Yamamura M., Wang L., Takeda Y., Suzuki S., Liu H., Zhu F., Chen M., Zhang J., Umezawa T., Tobimatsu Y., Lo C. (2019) Recruitment of specific flavonoid B-ring hydroxylases for two independent biosynthesis pathways of flavone-derived metabolites in grasses. New Phytologist. [online] URL: http://dx.doi.org/10.1111/nph.15795

Lee C.-C., Wang J., Matsuura K., Yang C.-C.S. (2018) The complete mitochondrial genome of yellow crazy ant, Anoplolepis gracilipes (Hymenoptera: Formicidae). Mitochondrial DNA Part B 3:622-623. [online] URL: http://dx.doi.org/10.1080/23802359.2018.1467739

Li L., Zhou X.-Z., Omura Y., Wang Z.-H., Zong Q.-G., Liu Y., Hao Y.-X., Fu S.-Y., Kivelson M.G., Rankin R., Claudepierre S.G., Wygant J.R. (2018) Nonlinear Drift Resonance Between Charged Particles and Ultralow Frequency Waves: Theory and Observations. Geophysical Research Letters 45:8773-8782. [online] URL: http://dx.doi.org/10.1029/2018GL079038

Li R., Narita R., Ouda R., Kimura C., Nishimura H., Yatagai M., Fujita T., Watanabe T. (2018) Structure-dependent antiviral activity of catechol derivatives in pyroligneous acid against the encephalomycarditis virus. RSC Advances 8:35888-35896.
[online] URL: http://dx.doi.org/10.1039/c8ra07096b

Li Y., Shuai L., Kim H., Motagamwala A.H., Mobley J.K., Yue F., Tobimatsu Y., Havkin-Frenkel D., Chen F., Dixon R.A., Luterbacher J.S., Dumesic J.A., Ralph J. (2018) An “ideal lignin” facilitates full biomass utilization. Science Advances 4:eaau2968.
[online] URL: http://dx.doi.org/10.1126/sciadv.aau2968

López-Puertas M., García-Comas M., Funke B., Gardini A., Stiller G.P., von Clarmann T., Glatthor N., Laeng A., Kaufmann M., Sofieva V.F., Froidevaux L., Walker K.A., Shiotani M. (2018) MIPAS observations of ozone in the middle atmosphere. Atmospheric Measurement Techniques 11:2187-2212. [online] URL: http://dx.doi.org/10.5194/amt-11-2187-2018

Luce H., Kantha L., Hashiguchi H., Lawrence D., Doddi A. (2018) Turbulence kinetic energy dissipation rates estimated from concurrent UAV and MU radar measurements. Earth, Planets and Space 70. [online] URL: http://dx.doi.org/10.1186/s40623-018-0979-1

Luce H., Kantha L., Hashiguchi H., Lawrence D., Mixa T., Yabuki M., Tsuda T. (2018) Vertical structure of the lower troposphere derived from MU radar, unmanned aerial vehicle, and balloon measurements during ShUREX 2015. Progress in Earth and Planetary Science 5. [online] URL: http://dx.doi.org/10.1186/s40645-018-0187-4

Luce H., Kantha L., Yabuki M., Hashiguchi H. (2018) Atmospheric Kelvin-Helmholtz billows captured by the MU radar, lidars and a fish-eye camera. Earth, Planets and Space 70. [online] URL: http://dx.doi.org/10.1186/s40623-018-0935-0

Luo B., Imai T., Sugiyama J., Qiu J. (2019) The occurrence and development of intraxylary phloem in young Aquilaria sinensis shoots. IAWA Journal 40:23-42.
[online] URL: http://dx.doi.org/10.1163/22941932-40190221

Marzuki, Hashiguchi H., Vonnisa M., Harmadi, Katsumata M. (2018) Determination of Intraseasonal Variation of Precipitation Microphysics in the Southern Indian Ocean from Joss-Waldvogel Disdrometer Observation during the CINDY Field Campaign. Advances in Atmospheric Sciences 35:1415-1427. [online] URL: http://dx.doi.org/10.1007/s00376-018-8026-5

Matsubara D., Wakashima Y., Fujisawa Y., Shimizu H., Kitamori A., Ishikawa K. (2017) Effects of tightening speed on torque coefficient in lag screw timber joints with steel side plates. Journal of Wood Science 64:112-118. [online] URL: http://dx.doi.org/10.1007/s10086-017-1679-3

Matsuda S., Kasahara Y., Kojima H., Kasaba Y., Yagitani S., Ozaki M., Imachi T., Ishisaka K., Kumamoto

PUBLICATIONS

A., Tsuchiya F., Ota M., Kurita S., Miyoshi Y., Hikishima M., Matsuoka A., Shinohara I. (2018) Onboard software of Plasma Wave Experiment aboard Arase: instrument management and signal processing of Waveform Capture/Onboard Frequency Analyzer. Earth, Planets and Space 70. [online] URL: http://dx.doi.org/10.1186/s40623-018-0838-0

Mitani T., Nakajima R., Shinohara N., Nozaki Y., Chikata T., Watanabe T. (2019) Development of a Microwave Irradiation Probe for a Cylindrical Applicator. Processes 7:143. [online] URL: http://dx.doi.org/10.3390/pr7030143

Miyamoto T., Mihashi A., Yamamura M., Tobimatsu Y., Suzuki S., Takada R., Kobayashi Y., Umezawa T. (2018) Comparative analysis of lignin chemical structures of sugarcane bagasse pretreated by alkaline, hydrothermal, and dilute sulfuric acid methods. Industrial Crops and Products 121:124-131. [online] URL: http://dx.doi.org/10.1016/j.indcrop.2018.04.077

Miyamoto T., Takada R., Tobimatsu Y., Takeda Y., Suzuki S., Yamamura M., Osakabe K., Osakabe Y., Sakamoto M., Umezawa T. (2019) Os MYB 108 loss-of-function enriches p-coumaroylated and tricin lignin units in rice cell walls. The Plant Journal. [online] URL: http://dx.doi.org/10.1111/tpj.14290

Miyamoto T., Yamamura M., Tobimatsu Y., Suzuki S., Kojima M., Takabe K., Terajima Y., Mihashi A., Kobayashi Y., Umezawa T. (2018) A comparative study of the biomass properties of Erianthus and sugarcane: lignocellulose structure, alkaline delignification rate, and enzymatic saccharification efficiency. Bioscience, Biotechnology, and Biochemistry 82:1143-1152. [online] URL: http://dx.doi.org/10.1080/09168451.2018.1447358

Miyoshi Y., Shinohara I., Takashima T., Asamura K., Higashio N., Mitani T., Kasahara S., Yokota S., Kazama Y., Wang S.-Y., Tam S.W.Y., Ho P.T.P., Kasahara Y., Kasaba Y., Yagitani S., Matsuoka A., Kojima H., Katoh Y., Shiokawa K., Seki K. (2018) Geospace exploration project ERG. Earth, Planets and Space 70. [online] URL: http://dx.doi.org/10.1186/s40623-018-0862-0

Mori S., Hamada J.-I., Hattori M., Wu P.-M., Katsumata M., Endo N., Ichiyanagi K., Hashiguchi H., Arbain A.A., Sulistyowati R., Lestari S., Syamsudin F., Manik T., Yamanaka M.D. (2018) Meridional march of diurnal rainfall over Jakarta, Indonesia, observed with a C-band Doppler radar: an overview of the HARIMAU2010 campaign. Progress in Earth and Planetary Science 5. [online] URL: http://dx.doi.org/10.1186/s40645-018-0202-9

Motoba T., Ebihara Y., Ogawa Y., Kadokura A., Engebretson M.J., Angelopoulos V., Gerrard A.J., Weatherwax A.T. (2019) On the Driver of Daytime Pc3 Auroral Pulsations. Geophysical Research Letters 46:553-561. [online] URL: http://dx.doi.org/10.1029/2018GL080842

Mutuku J.M., Cui S., Hori C., Takeda Y., Tobimatsu Y., Nakabayashi R., Mori T., Saito K., Demura T., Umezawa T., Yoshida S., Shirasu K. (2019) The Structural Integrity of Lignin Is Crucial for Resistance against Striga hermonthica Parasitism in Rice. Plant Physiology 179:1796-1809. [online] URL: http://dx.doi.org/10.1104/pp.18.01133

Nakagawa M., Kimura A., Umemura K., Kawai S. (2018) Evaluation of NO2 sorption of cedar wood (Cryptomeria Japonica) with difference of the specimen size and contact condition between NO2 gas and specimen using new test system. Journal of Wood Science 64:318-325. [online] URL: http://dx.doi.org/10.1007/s10086-017-1685-5

Nakamura S., Ebihara Y., Fujita S., Goto T., Yamada N., Watari S., Omura Y. (2018) Time Domain Simulation of Geomagnetically Induced Current (GIC) Flowing in 500-kV Power Grid in Japan Including a Three-Dimensional Ground Inhomogeneity. Space Weather 16:1946-1959. [online] URL: http://dx.doi.org/10.1029/2018SW002004

Nakamura S., Omura Y., Summers D. (2018) Fine Structure of Whistler Mode Hiss in Plasmaspheric Plumes Observed by the Van Allen Probes. Journal of Geophysical Research: Space Physics 123:9055-9064. [online] URL: http://dx.doi.org/10.1029/2018JA025803

Nakanishi-Masuno T., Shitan N., Sugiyama A., Takanashi K., Inaba S., Kaneko S., Yazaki K. (2018) The Crotalaria juncea metal transporter CjNRAMP1 has a high Fe uptake activity, even in an environment

PUBLICATIONS

with high Cd contamination. International Journal of Phytoremediation 20:1427-1437. [online] URL: http://dx.doi.org/10.1080/15226514.2018.1501333

Neoh K.-B., Nguyen M.T., Nguyen V.T., Itoh M., Kozan O., Yoshimura T. (2018) Intermediate disturbance promotes termite functional diversity in intensively managed Vietnamese coffee agroecosystems. Journal of Insect Conservation 22:197-208. [online] URL: http://dx.doi.org/10.1007/s10841-018-0053-0

Nge T.T., Tobimatsu Y., Takahashi S., Takata E., Yamamura M., Miyagawa Y., Ikeda T., Umezawa T., Yamada T. (2018) Isolation and Characterization of Polyethylene Glycol (PEG)-Modified Glycol Lignin via PEG Solvolysis of Softwood Biomass in a Large-Scale Batch Reactor. ACS Sustainable Chemistry & Engineering 6:7841-7848. [online] URL: http://dx.doi.org/10.1021/acssuschemeng.8b00965

Nguyen T.D., Kohdzuma Y., Endo R., Sugiyama J. (2018) Evaluation of chemical treatments on dimensional stabilization of archeological waterlogged hardwoods obtained from the Thang Long Imperial Citadel site, Vietnam. Journal of Wood Science 64:436-443. [online] URL: http://dx.doi.org/10.1007/s10086-018-1719-7

Nguyen T.D., Nishimura H., Imai T., Watanabe T., Kohdzuma Y., Sugiyama J. (2018) Natural durability of the culturally and historically important timber: Erythrophleum fordii wood against white-rot fungi. Journal of Wood Science 64:301-310. [online] URL: http://dx.doi.org/10.1007/s10086-018-1704-1

Nishida M., Tanaka T., Miki T., Ito T., Kanayama K. (2018) Instrumental analyses of nanostructures and interactions with bound water of superheated steam treated plant materials. Industrial Crops and Products 114:1-13. [online] URL: http://dx.doi.org/10.1016/j.indcrop.2018.01.072

Nishimura H., Kamiya A., Nagata T., Katahira M., Watanabe T. (2018) Direct evidence for α ether linkage between lignin and carbohydrates in wood cell walls. Scientific Reports 8. [online] URL: http://dx.doi.org/10.1038/s41598-018-24328-9

Ohashi, Y., & Watanabe, T. (2018). Catalytic Performance of Food Additives Alum, Flocculating Agent, Al (SO4)3, AlCl3, and Other Lewis Acids in Microwave Solvolysis of Hardwoods and Recalcitrant Softwood for Biorefinery. ACS Omega, 3(11), 16271-16280. [online] URL: https://doi.org/10.1021/acsomega.8b01454

Oigawa M., Tsuda T., Seko H., Shoji Y., Realini E. (2018) Data assimilation experiment of precipitable water vapor observed by a hyper-dense GNSS receiver network using a nested NHM-LETKF system. Earth, Planets and Space 70. [online] URL: http://dx.doi.org/10.1186/s40623-018-0851-3

Oki H., Kawahara K., Maruno T., Imai T., Muroga Y., Fukakusa S., Iwashita T., Kobayashi Y., Matsuda S., Kodama T., Iida T., Yoshida T., Ohkubo T., Nakamura S. (2018) Interplay of a secreted protein with type IVb pilus for efficient enterotoxigenic Escherichia coli colonization. Proceedings of the National Academy of Sciences 115:7422-7427. [online] URL: http://dx.doi.org/10.1073/pnas.1805671115

Ono E., Murata J., Toyonaga H., Nakayasu M., Mizutani M., Yamamoto M.P., Umezawa T., Horikawa M. (2018) Formation of a Methylenedioxy Bridge in (+)-Epipinoresinol by CYP81Q3 Corroborates with Diastereomeric Specialization in Sesame Lignans. Plant and Cell Physiology. [online] URL: http://dx.doi.org/10.1093/pcp/pcy150

Oramahi H.A., Yoshimura T., Diba F., Setyawati D., Nurhaida (2018) Antifungal and antitermitic activities of wood vinegar from oil palm trunk. Journal of Wood Science 64:311-317. [online] URL: http://dx.doi.org/10.1007/s10086-018-1703-2

Ozaki M., Miyoshi Y., Shiokawa K., Hosokawa K., Oyama S., Kataoka R., Ebihara Y., Ogawa Y., Kasahara Y., Yagitani S., Kasaba Y., Kumamoto A., Tsuchiya F., Matsuda S., Katoh Y., Hikishima M., Kurita S., Otsuka Y., Moore R.C., Tanaka Y., Nosé M., Nagatsuma T., Nishitani N., Kadokura A., Connors M., Inoue T., Matsuoka A., Shinohara I. (2019) Visualization of rapid electron precipitation via chorus element wave-particle interactions. Nature Communications 10. [online] URL: http://dx.doi.org/10.1038/s41467-018-07996-z

Ozaki M., Shiokawa K., Miyoshi Y., Hosokawa K., Oyama S., Yagitani S., Kasahara Y., Kasaba Y.,

PUBLICATIONS

Matsuda S., Kataoka R., Ebihara Y., Ogawa Y., Otsuka Y., Kurita S., Moore R.C., Tanaka Y. -M., Nosé M., Nagatsuma T., Connors M., Nishitani N., Katoh Y., Hikishima M., Kumamoto A., Tsuchiya F., Kadokura A., Nishiyama T., Inoue T., Imamura K., Matsuoka A., Shinohara I. (2018) Microscopic Observations of Pulsating Aurora Associated With Chorus Element Structures: Coordinated Arase Satellite-PWING Observations. Geophysical Research Letters 45:12,125-12,134. [online] URL: http://dx.doi.org/10.1029/2018GL079812

Pavan Chaitanya P., Patra A.K., Otsuka Y., Yokoyama T., Yamamoto M. (2018) On the Solstice Maxima and Azimuth-Dependent Characteristics of the 150-km Echoes Observed Using the Equatorial Atmosphere Radar. Journal of Geophysical Research: Space Physics 123:6752-6759. [online] URL: http://dx.doi.org/10.1029/2018JA025491

Penttilä P.A., Imai T., Capron M., Mizuno M., Amano Y., Schweins R., Sugiyama J. (2018) Multimethod approach to understand the assembly of cellulose fibrils in the biosynthesis of bacterial cellulose. Cellulose 25:2771-2783. [online] URL: http://dx.doi.org/10.1007/s10570-018-1755-x

Penttilä P.A., Imai T., Hemming J., Willför S., Sugiyama J. (2018) Enzymatic hydrolysis of biomimetic bacterial cellulose-hemicellulose composites. Carbohydrate Polymers 190:95-102. [online] URL: http://dx.doi.org/10.1016/j.carbpol.2018.02.051

Penttilä P.A., Imai T., Sugiyama J., Schweins R. (2018) Biomimetic composites of deuterated bacterial cellulose and hemicelluloses studied with small-angle neutron scattering. European Polymer Journal 104:177-183. [online] URL: http://dx.doi.org/10.1016/j.eurpolymj.2018.05.015

Rino C., Carrano C., Groves K., Yokoyama T. (2018) A Configuration Space Model for Intermediate-Scale Ionospheric Structure. Radio Science 53:1472-1480.
[online] URL: http://dx.doi.org/10.1029/2018RS006678

Rino C., Yokoyama T., Carrano C. (2018) Dynamic spectral characteristics of high-resolution simulated equatorial plasma bubbles. Progress in Earth and Planetary Science 5.
[online] URL: http://dx.doi.org/10.1186/s40645-018-0243-0

Saeki H., Hara R., Takahashi H., Iijima M., Munakata R., Kenmoku H., Fuku K., Sekihara A., Yasuno Y., Shinada T., Ueda D., Nishi T., Sato T., Asakawa Y., Kurosaki F., Yazaki K., Taura F. (2018) An Aromatic Farnesyltransferase Functions in Biosynthesis of the Anti-HIV Meroterpenoid Daurichromenic Acid. Plant Physiology 178:535-551. [online] URL: http://dx.doi.org/10.1104/pp.18.00655

Saito S., Yamamoto M., Maruyama T. (2018) Arrival Angle and Travel Time Measurements of HF Transequatorial Propagation for Plasma Bubble Monitoring. Radio Science 53:1304-1315. [online] URL: http://dx.doi.org/10.1029/2017RS006518

Saito Y., Endo T., Ando D., Nakatsubo F., Yano H. (2018) Influence of drying process on reactivity of cellulose and xylan in acetylation of willow (Salix schwerinii E. L. Wolf) kraft pulp monitored by HSQC-NMR spectroscopy. Cellulose 25:6319-6331.
[online] URL: http://dx.doi.org/10.1007/s10570-018-2034-6

Sakai S., Seki K., Terada N., Shinagawa H., Tanaka T., Ebihara Y. (2018) Effects of a Weak Intrinsic Magnetic Field on Atmospheric Escape From Mars. Geophysical Research Letters 45:9336-9343. [online] URL: http://dx.doi.org/10.1029/2018GL079972

Sarr P.S., Sugiyama A., Begoude A.D.B., Yazaki K., Araki S., Nawata E. (2019) Diversity and distribution of Arbuscular Mycorrhizal Fungi in cassava (Manihot esculenta Crantz) croplands in Cameroon as revealed by Illumina MiSeq. Rhizosphere 10:100147.
[online] URL: http://dx.doi.org/10.1016/j.rhisph.2019.100147

Sato M., Isoda H., Araki Y., Nakagawa T., Kawai N., Miyake T. (2019) A seismic behavior and numerical model of narrow paneled cross-laminated timber building. Engineering Structures 179:9-22. [online] URL: http://dx.doi.org/10.1016/j.engstruct.2018.09.054

Shiomitsu M., Sakai Y., Isoda H., Araki Y., Matsumori T. (2018) Development of hysteresis characteristics model for existing wooden houses. Journal of Structural and Construction Engineering (Transactions of

PUBLICATIONS

AIJ) 83:717-726. [online] URL: http://dx.doi.org/10.3130/aijs.83.717

Shoji M., Miyoshi Y., Omura Y., Kasaba Y., Ishisaka K., Matsuda S., Kasahara Y., Yagitani S., Matsuoka A., Teramoto M., Takashima T., Shinohara I. (2018) Instantaneous Frequency Analysis on Nonlinear EMIC Emissions: Arase Observation. 2018 2nd URSI Atlantic Radio Science Meeting (AT-RASC). [online] URL: http://dx.doi.org/10.23919/URSI-AT-RASC.2018.8471543

Shoji M., Miyoshi Y., Omura Y., Kistler L.M., Kasaba Y., Matsuda S., Kasahara Y., Matsuoka A., Nomura R., Ishisaka K., Kumamoto A., Tsuchiya F., Yagitani S., Teramoto M., Asamura K., Takashima T., Shinohara I. (2018) Instantaneous Frequency Analysis on Nonlinear EMIC Emissions: Arase Observation. Geophysical Research Letters 45:13,199-13,205.
[online] URL: http://dx.doi.org/10.1029/2018GL079765

Sinha S., Regeena M.L., Sarma T.V.C., Hashiguchi H., Tuckley K.R. (2018) Doppler Profile Tracing Using MPCF on MU Radar and Sodar: Performance Analysis. IEEE Geoscience and Remote Sensing Letters 15:508-511. [online] URL: http://dx.doi.org/10.1109/LGRS.2018.2797071

Stephenson, F. R., D. M., Willis, H. Hayakawa, Y. Ebihara, M. N. Wild, C. J. Scott, and J. Wilkinson, Do the Chinese Astronomical Records Dated A.D. 776 January 12/13 Describe an Auroral Display or a Lunar Halo? A Critical Re-examination, Solar Physics Solar Physics, 294:36. [online] URL: https://doi.org/10.1007/s11207-019-1425-7

Suzuki S., Suzuki H., Tanaka K., Yamamura M., Shibata D., Umezawa T. (2019) De novo transcriptome analysis of needles of Thujopsis dolabrata var. hondae. Plant Biotechnology 36:113-118. [online] URL: http://dx.doi.org/10.5511/plantbiotechnology.19.0220a

Tabata Y., Kamano Y., Uji H., Imai T., Kimura S. (2019) Electronic Properties of Cyclic β-Peptide Nanotube Bundles Reflecting Structural Arrangement. Chemistry Letters 48:322-324. [online] URL: http://dx.doi.org/10.1246/cl.181007

Tabata Y., Mitani S., Uji H., Imai T., Kimura S. (2019) The effect of macrodipole orientation on the piezoelectric response of cyclic β-peptide nanotube bundles on gold substrates. Polymer Journal 51:601-609. [online] URL: http://dx.doi.org/10.1038/s41428-019-0169-4

Tabata Y., Uji H., Imai T., Kimura S. (2018) Two one-dimensional arrays of naphthyl and anthryl groups along peptide nanotubes prepared from cyclic peptides comprising α- and β-amino acids. Soft Matter 14:7597-7604. [online] URL: http://dx.doi.org/10.1039/c8sm01627e

Takanashi K., Nakagawa Y., Aburaya S., Kaminade K., Aoki W., Saida-Munakata Y., Sugiyama A., Ueda M., Yazaki K. (2018) Comparative Proteomic Analysis of Lithospermum erythrorhizon Reveals Regulation of a Variety of Metabolic Enzymes Leading to Comprehensive Understanding of the Shikonin Biosynthetic Pathway. Plant and Cell Physiology 60:19-28. [online] URL: http://dx.doi.org/10.1093/pcp/pcy183

Takeda Y., Suzuki S., Tobimatsu Y., Osakabe K., Osakabe Y., Ragamustari S.K., Sakamoto M., Umezawa T. (2018) Lignin characterization of rice CONIFERALDEHYDE 5-HYDROXYLASE loss-of-function mutants generated with the CRISPR/Cas9 system. The Plant Journal 97:543-554. [online] URL: http://dx.doi.org/10.1111/tpj.14141

Takeda Y., Tobimatsu Y., Karlen S.D., Koshiba T., Suzuki S., Yamamura M., Murakami S., Mukai M., Hattori T., Osakabe K., Ralph J., Sakamoto M., Umezawa T. (2018) Downregulation of p-COUMAROYL ESTER 3-HYDROXYLASE in rice leads to altered cell wall structures and improves biomass saccharification. The Plant Journal 95:796-811.
[online] URL: http://dx.doi.org/10.1111/tpj.13988

Takeda Y., Tobimatsu Y., Yamamura M., Takano T., Sakamoto M., Umezawa T. (2019) Comparative evaluations of lignocellulose reactivity and usability in transgenic rice plants with altered lignin composition. Journal of Wood Science 65. [online] URL: http://dx.doi.org/10.1186/s10086-019-1784-6

Tamura K., Nakajima S., Nakagawa T., Nakajima S. (2019) Creep rupture behavior of steel plate insertion type drift pin joint. AIJ Journal of Technology and Design 25:151-154. [online] URL:

PUBLICATIONS

http://dx.doi.org/10.3130/aijt.25.151

Tanaka T., Obara T., Watanabe M., Fujita S., Ebihara Y., Kataoka R., Den M. (2018) Cooperatives Roles of Dynamics and Topology in Generating the Magnetosphere-Ionosphere Disturbances: Case of the Theta Aurora. Journal of Geophysical Research: Space Physics 123:9991-10,008. [online] URL: http://dx.doi.org/10.1029/2018JA025514

Tarmadi D., Tobimatsu Y., Yamamura M., Miyamoto T., Miyagawa Y., Umezawa T., Yoshimura T. (2018) NMR studies on lignocellulose deconstructions in the digestive system of the lower termite Coptotermes formosanus Shiraki. Scientific Reports 8.
[online] URL: http://dx.doi.org/10.1038/s41598-018-19562-0

Tascioglu C., Umemura K., Yoshimura T. (2018) Seventh-year durability evaluation of zinc borate incorporated wood-plastic composites and particleboard. Composites Part B: Engineering 137:123-128. [online] URL: http://dx.doi.org/10.1016/j.compositesb.2017.11.011

Tazuru-Mizuno S., Sugiyama J. (2019) Wood Identification of Western School “Janes’</sup> Mansion in Kumamoto Prefecture Collapsed by the Kumamoto Earthquake.” Mokuzai Gakkaishi 65:33-38. [online] URL: http://dx.doi.org/10.2488/jwrs.65.33

Terzi E., Nami Kartal S., Yoshimura T. (2018) Efficacy of NaF and DOT against drywood and subterranean termites. Proceedings of the 5th International Conference on Processing Technologies for the Forest and Bio-based Products Iindustries (PTF BPI 2018), Freising/Munich, Germany, 20180000

Thanh N.D., Wakiya S., Matsuda K., Ngoc B.D., Sugiyama J., Kohdzuma Y. (2018) Diffusion of chemicals into archaeological waterlogged hardwoods obtained from the Thang Long Imperial Citadel site, Vietnam. Journal of Wood Science 64:836-844.
[online] URL: http://dx.doi.org/10.1007/s10086-018-1754-4

Thonglek V., Yoshikawa K., Tokuda Y., Ueda Y. (2018) Identification of High Concentration Ultra-Fine Bubbles in the Water. International Journal of Plasma Environmental Science and Technology, 20181200

Tobimatsu Y., Schuetz M. (2019) Lignin polymerization: how do plants manage the chemistry so well? Current Opinion in Biotechnology 56:75-81.
[online] URL: http://dx.doi.org/10.1016/j.copbio.2018.10.001

Tokunaga Y., Nagata T., Suetomi T., Oshiro S., Kondo K., Katahira M., Watanabe T. (2019) NMR Analysis on Molecular Interaction of Lignin with Amino Acid Residues of Carbohydrate-Binding Module from Trichoderma reesei Cel7A. Scientific Reports 9.
[online] URL: http://dx.doi.org/10.1038/s41598-018-38410-9

Tsubaki S., Hayakawa S., Ueda T., Mitani T., Suzuki E., Fujii S., Wada Y. (2018) Proton-Enhanced Dielectric Properties of Polyoxometalates in Water under Radio-Frequency Electromagnetic Waves. Materials 11:1202. [online] URL: http://dx.doi.org/10.3390/ma11071202

Tsuchiya S., Shiokawa K., Fujinami H., Otsuka Y., Nakamura T., Yamamoto M. (2018) Statistical Analysis of the Phase Velocity Distribution of Mesospheric and Ionospheric Waves Observed in Airglow Images Over a 16-Year Period: Comparison Between Rikubetsu and Shigaraki, Japan. Journal of Geophysical Research: Space Physics 123:6930-6947.
[online] URL: http://dx.doi.org/10.1029/2018JA025585

Ueda S., Osada K., Hara K., Yabuki M., Hashihama F., Kanda J. (2018) Morphological features and mixing states of soot-containing particles in the marine boundary layer over the Indian and Southern oceans. Atmospheric Chemistry and Physics 18:9207-9224.
[online] URL: http://dx.doi.org/10.5194/acp-18-9207-2018

Uji H., Ogawa J., Itabashi K., Imai T., Kimura S. (2018) Compartmentalized host spaces accommodating guest aromatic molecules in a chiral way in a helix-peptide-aromatic framework. Chemical Communications 54:12483-12486. [online] URL: http://dx.doi.org/10.1039/c8cc07380e

PUBLICATIONS

Umezawa T. (2018) Lignin modification in planta for valorization. Phytochemistry Reviews 17:1305-1327. [online] URL: http://dx.doi.org/10.1007/s11101-017-9545-x

Utsumi M., Murata K., Umemura K., Yoshimura T., Hattori K., Nakamura M. (2019) Mechanical Properties and Biological Performance of Particle Board Made of Sendan (Melia azedarach). BioResources, 14(2), 4100-4109

Van Do T., Kozan O., Yamamoto M., Hai V.D., Trung P.D., Thang N.T., Van Thang H., Manh T.D., Lam V.T., Thinh N.H. (2018) A Natural Forest of Commercial Timber Species: Logging or Not Logging. Small-scale Forestry 17:555-568. [online] URL: http://dx.doi.org/10.1007/s11842-018-9403-8

Wang B., Nishimura Y., Hietala H., Lyons L., Angelopoulos V., Plaschke F., Ebihara Y., Weatherwax A. (2018) Impacts of Magnetosheath High-Speed Jets on the Magnetosphere and Ionosphere Measured by Optical Imaging and Satellite Observations. Journal of Geophysical Research: Space Physics 123:4879-4894. [online] URL: http://dx.doi.org/10.1029/2017JA024954

Wang C., Okubayashi S. (2019) 3D aerogel of cellulose triacetate with supercritical antisolvent process for drug delivery. The Journal of Supercritical Fluids 148:33-41. [online] URL: http://dx.doi.org/10.1016/j.supflu.2019.02.026

Wang L., Hikima Y., Ohshima M., Sekiguchi T., Yano H. (2018) Evolution of cellular morphologies and crystalline structures in high-expansion isotactic polypropylene/cellulose nanofiber nanocomposite foams. RSC Advances 8:15405-15416. [online] URL: http://dx.doi.org/10.1039/c8ra01833b

Wang L., Okada K., Hikima Y., Ohshima M., Sekiguchi T., Yano H. (2019) Effect of Cellulose Nanofiber (CNF) Surface Treatment on Cellular Structures and Mechanical Properties of Polypropylene/CNF Nanocomposite Foams via Core-Back Foam Injection Molding. Polymers 11:249. [online] URL: http://dx.doi.org/10.3390/polym11020249

Wang L., Okada K., Sodenaga M., Hikima Y., Ohshima M., Sekiguchi T., Yano H. (2018) Effect of surface modification on the dispersion, rheological behavior, crystallization kinetics, and foaming ability of polypropylene/cellulose nanofiber nanocomposites. Composites Science and Technology 168:412-419. [online] URL: http://dx.doi.org/10.1016/j.compscitech.2018.10.023

Wang, B., Nishimura, Y., Hietala, H., Shen, X.-C., Shi, Q., Zhang, H., … Weatherwax, A. (2018). Dayside Magnetospheric and Ionospheric Responses to a Foreshock Transient on 25 June 2008: 2. 2-D Evolution Based on Dayside Auroral Imaging. Journal of Geophysical Research: Space Physics, 123(8), 6347-6359. [online] URL: https://doi.org/10.1029/2017ja024846

Widyorini R., Umemura K., Kemalasari Soraya D., Kusuma Dewi G., Dwi Nugroho W. (2019) Effect of Citric Acid Content and Extractives Treatment on the Manufacturing Process and Properties of Citric Acid-bonded Salacca Frond Particleboard. BioResources, 14(2), 4171-4180

Widyorini R., Umemura K., Septiano A., Soraya D.K., Dewi G.K., Nugroho W.D. (2018) Manufacture and Properties of Citric Acid-Bonded Composite Board made from Salacca Frond: Effects of Maltodextrin Addition, Pressing Temperature, and Pressing Method. BioResources 13. [online] URL: http://dx.doi.org/10.15376/biores.13.4.8662-8676

Wilson R., Hashiguchi H., Yabuki M. (2018) Vertical Spectra of Temperature in the Free Troposphere at Meso-and-Small Scales According to the Flow Regime: Observations and Interpretation. Atmosphere 9:415. [online] URL: http://dx.doi.org/10.3390/atmos9110415

Yamamoto M., Otsuka Y., Jin H., Miyoshi Y. (2018) Relationship between day-to-day variability of equatorial plasma bubble activity from GPS scintillation and atmospheric properties from Ground-to-topside model of Atmosphere and Ionosphere for Aeronomy (GAIA) assimilation. Progress in Earth and Planetary Science 5. [online] URL: http://dx.doi.org/10.1186/s40645-018-0184-7

Yanagawa A., Couto A., Sandoz J.-C., Hata T., Mitra A., Ali Agha M., Marion-Poll F. (2019) LPS perception through taste-induced reflex in Drosophila melanogaster. Journal of Insect Physiology 112:39-47. [online] URL: http://dx.doi.org/10.1016/j.jinsphys.2018.12.001

PUBLICATIONS

Yang B., Mitani T., Shinohara N. (2019) Evaluation of the Modulation Performance of Injection-Locked Continuous-Wave Magnetrons. IEEE Transactions on Electron Devices 66:709-715. [online] URL: http://dx.doi.org/10.1109/TED.2018.2877204

Yang X., Abe K., Biswas S.K., Yano H. (2018) Extremely stiff and strong nanocomposite hydrogels with stretchable cellulose nanofiber/poly (vinyl alcohol) networks. Cellulose 25:6571-6580. [online] URL: http://dx.doi.org/10.1007/s10570-018-2030-x

Yano H., Omura H., Honma Y., Okumura H., Sano H., Nakatsubo F. (2018) Designing cellulose nanofiber surface for high density polyethylene reinforcement. Cellulose 25:3351-3362. [online] URL: http://dx.doi.org/10.1007/s10570-018-1787-2

Yeo S.-Y., Komatsu K., Hsu M.-F., Chung Y.-L., Chang W.-S. (2018) Structural behavior of traditional Dieh-Dou timber main frame. International Journal of Architectural Heritage 12:555-577. [online] URL: http://dx.doi.org/10.1080/15583058.2018.1442518

Zhao Z., Hayashi S., Xu W., Wu Z., Tanaka S., Sun S., Zhang M., Kanayama K., Umemura K. (2018) A Novel Eco-Friendly Wood Adhesive Composed by Sucrose and Ammonium Dihydrogen Phosphate. Polymers 10:1251. [online] URL: http://dx.doi.org/10.3390/polym10111251

Zhao Z., Miao Y., Yang Z., Wang H., Sang R., Fu Y., Huang C., Wu Z., Zhang M., Sun S., Umemura K., Yong Q. (2018) Effects of Sulfuric Acid on the Curing Behavior and Bonding Performance of Tannin-Sucrose Adhesive. Polymers 10:651. [online] URL: http://dx.doi.org/10.3390/polym10060651

Zheng P., Aoki D., Seki M., Miki T., Tanaka S., Kanayama K., Matsushita Y., Fukushima K. (2018) Visualization of solute diffusion into cell walls in solution-impregnated wood under varying relative humidity using time-of-flight secondary ion mass spectrometry. Scientific Reports 8. [online] URL: http://dx.doi.org/10.1038/s41598-018-28230-2

Zushi T., Kojima H., Kasahara Y., Hamano T. (2019) Development of a miniaturized spectrum-type plasma wave receiver comprising an application-specific integrated circuit analog front end and a field-programmable gate array. Measurement Science and Technology 30:055901. [online] URL: http://dx.doi.org/10.1088/1361-6501/ab0821

Sustainable Humanosphere　第15号

発　行　日　令和元年９月30日
編集兼発行者　京都大学　生存圏研究所
京都府宇治市五ヶ庄
印　刷　所　株式会社　北斗プリント社
京都市左京区下鴨高木町38-2